Barts
Cancer Institute
Queen Mary, University of London

The Effects of Interleukin-6 on Angiogenesis

Ganga Gopinathan

A thesis submitted for the degree of Doctor of Philosophy

at Queen Mary, University of London

October 2014

Centre for Cancer and Inflammation

Barts and The London

Queen Mary's School of Medicine and Dentistry

3rd Floor, John Vane Science Centre

Charterhouse Square

London, EC1M 6BQ

Abstract

Elevated levels of the inflammatory cytokine interleukin-6, IL-6, have been linked with poor prognosis in ovarian cancer patients by influencing tumour growth, invasion, angiogenesis and chemo-resistance. A clinical trial conducted in parallel with pre-clinical studies showed an anti-IL-6 antibody to have some activity in ovarian cancer patients and in xenograft models, via reduction in pro-inflammatory and angiogenic factors such as TNF-α, IL-8 and VEGF. Anti-IL-6 treatment also showed significant reductions in vascular area with decreased expression of an angiogenic factor Jagged1.

The aim of my study was to investigate the effects of IL-6 on normal and tumour angiogenesis. I found that recombinant IL-6 stimulates angiogenesis in mouse and rat aortic ring assays and that it can also stimulate growth and migration of endothelial cells *in vitro*. IL-6 has similar potency as VEGF in inducing vessel sprouting. IL-6 itself does not induce VEGF in the endothelial cells I tested. Investigation of the effects of IL-6 on vessel maturation revealed a significant reduction in pericyte coverage of vessels treated with IL-6 compared with VEGF. Collectively, these data led to my hypothesis that 'IL-6 drives aberrant angiogenesis, independent of VEGF signalling'.

Investigating the mechanism by which IL-6 drives angiogenesis and leads to defective pericyte formation, I showed a link between IL-6 and the Notch ligands, Jagged1 and DLL*4*. My data suggested that IL-6 could stimulate Jagged1 in endothelial cells, whereas VEGF induces DLL*4*, the Notch ligand known to be involved in inducing stalk phenotype. Exploring previous findings to get a better understanding of the interaction of Notch ligands and pericyte recruitment also suggested a role of Angiopoeitin-2 in relation to IL-6 signalling. These observations were extended in IGROV-1 ovarian cancer xenografts treated with an anti-IL-6 antibody and by analysis of gene expression datasets from ovarian cancer biopsies. My results suggest therapeutic potential of combining inhibitors of IL-6 and VEGF in ovarian cancer.

Declaration

I, Ganga Gopinathan, hereby declare that the work on which this thesis is based is my original work and effort (except where acknowledgements indicate otherwise) and neither the whole work nor any part of it has been, is being, or is to be submitted for another degree in this or any other university.

Signature:…….

Date:…….

Acknowledgements

Throughout my PhD experience, many people have been instrumental directly or indirectly in shaping up my academic career. It would have been difficult for me to accomplish this study without the incredible support and encouragement of these individuals.

Fist and foremost, I would like to mainly thank my supervisor Prof Frances Balkwill for all the valuable guidance and motivation throughout my research. Her trust in my abilities and her constant championing has inspired and helped me to complete this research in a respectable manner. I would also like to thank my second supervisor Prof Thorsten Hagemann for his help and guidance.

I terms of research collaborations, I would like to thank Dr Carla Milagre and Richard Thomspon for performing the *in vivo* anti-IL-6 studies. Carla has also been of great help assisting me on a day to day basis. I would also like to thank Prof Kairbaan Hodivala-Dilke, Louise Reynolds and Dr Andrew Leinster for all their advice and help with my research. Dr James Whiteford has also given me a lot of encourgement and guidance and has helped me a great deal in setting up various experiments. Another person who has been fundamental to my research is Dr Hagen Kulbe who has greatly supported me and given me ideas in pursuing this line of research. I also want thank all the current and previous members of the Centre of Cancer and Inflammation, especially my thesis readers: Dr Chiara Berlato, Dr Anne Montfort and Dr Jackie McDermott for all their advice and help.

Last but not the least, my love and gratitude to my wonderful family and friends for their continuous moral support. I'm really grateful for the immense encouragement, care and support I received from my amazing parents without whom this would not have been possible. Special thanks to my husband for being patient, understanding and for putting up with all my mood swings. Finally, one person I'm hugely indebted to is my best friend, Angelin Ferns who stood by me through the toughest times. My frequent escape to your lovely home has kept my sanity in those difficult times.

Table of Contents

List of Figures

List of Tables

Abbreviations

ALL	Acute Lymphoblastic Leukaemia
AML	Acute Myeloid Leukaemia
ANG	Angiopoietin
APC	Adenomatous polyposis coli
ARID1A	AT – rich interactive domain-containing protein 1A
AOCS	Australian Ovarian Cancer Study
BCA	Bicinchoninic acid
BSA	Bovine serum albumine
CCC	Clear cell carcinoma
CAC	Colitis associated cancer
CoA	CoactivatorA
CEBPβ	CCAAT enhancer binding protein β
CNS	Central nervous system
CSC	Cancer stem cells
DLL	Delta like ligand
DNER	Delta and Notch like epidermal growth factor related receptor
EGF	Epidermal growth factor
EOC	Epithelial ovarian cancer
FAK	Focal adhesion kinase
FCS	Fetal calf serum
FDA	Food and Drug Administration
FGF	Fibroblast growth factor
FTSEC	Fallopian tube secretary epithelial cells
Gp130	Glycoprotein 130
GSI	γ-secretase inhibitors
HCC	Hepatocellular carcinoma

HGF	Hepatocyte growth factor
HGSC	High grade serous cancer
HIF-1α	Hypoxia-inducible factor-1α
HRP	Horseradish peroxidase
HRR	Homologous recombinant repair
HSPG	Heparan sulfate proteoglycans
IL-6	Interleukin-6
IL-6R	Interleukin-6 receptor
IL-8	Interleukin-8
IGF	Insulin growth factor
MAPK	Mitogen activated phosphate kinase
MDSC	Myeloid derived suppressor cell
MLEC	Mouse lung endothelial cell
MMP-9	Matrix metalloproteinase-9
MRE	Multiple response element
NCAM	Neural cell adhesion molecule
NICD	Notch intracellular domain
NECD	Notch extracellular domain
NFκB	Nuclear factor kappa beta
NF-IL6	Nuclear factor IL-6
NG2	Neural glial antigen 2
NSCLC	Non small cell lung cancer
OSE	Ovarian surface epithelium
PDGF	Platelet derived growth factor
PI3K	Phosphatidylinositol-3 kinase
PLGF	Placenta growth factor
PVDF	Polyvinylidine fluoride
SDS	Sodium dodecyl sulphate

SMC	Smooth muscle cell
STIC	Serous intraepithelial carcinomas
STAT3	Signal transducer and activator of transcription 3
TACE	TNF-α converting enzyme
TEM	Tie2 expressing macrophages
TCGA	The Cancer Genome Atlas
TGF-α	Transforming growth factor- alpha
TMA	Tissue microarrays
TNF-α	Tumour necrosis factor-alpha
VEGF	Vascular endothelial growth factor
VEGFR	Vascular endothelial growth factor receptor
VEGFRi	Vascular endothelial growth factor receptor inhibitor
VHL	Von-Hippel-Lindau
VCAM	Vascular cell adhesion molecule

1 Introduction

The aim of this thesis is to study the effects of IL-6 on normal and tumour angiogenesis with a focus on ovarian cancer.

1.1 Ovarian cancer

Ovarian cancer is the most lethal gynaecological malignancy and is the 4th most common cause of cancer-related death in women [1]. It is now clear that the term 'ovarian cancer' refers to a number of distinct diseases, with different genetic drivers that share a common anatomical location in the peritoneum [2]. 'Ovarian cancer' is normally categorised depending on its malignant potential. Low-grade malignancies are often characterised by RAS/RAF mutations and their tissue of origin is not entirely clear but may be the ovary [3]. Among the high-grade malignancies, there are two subtypes which probably arise from endometriosis via retrograde menstruation: endometrioid ovarian cancer and clear cell carcinoma (CCC). CCC is characterised by a common genetic mutation in ARID1A (AT – rich interactive domain-containing protein 1A) [4]. It is also characterised by a strong HIF-STAT3-IL-6 signature [5]. Another high-grade tumour is mucinous ovarian cancer, which is most likely metastases from intestinal or stomach malignancies. Finally, high-grade serous ovarian cancers (HGSC) are aggressive and have high invasive potential (Figure 1.1). These tumours may arise from the fallopian tube or mullerian epithelium rather than the ovary. They are known to disseminate early and spread extensively throughout the peritoneal space resulting in multiple lesions, which are difficult to treat [6, 7]. 96% of HGSC tumours have TP53 mutations and about 50% will also have abnormalities related to the homologous recombinant repair (HRR) pathway. Apart from this, HGSC exhibit a great deal of molecular heterogeneity. The cancer genome atlas project also identified seven other significantly mutated genes in 2-6% of HGSC samples, including mutations in CCNE1, RB, PI3K/RAS and the NOTCH pathway [8].

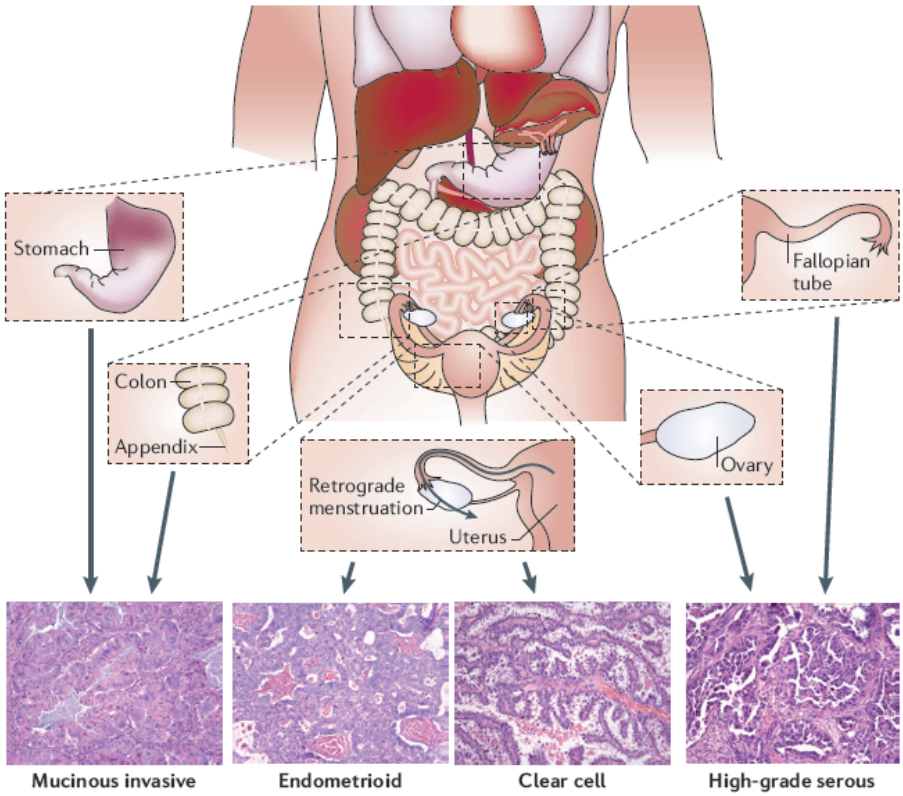

Figure 1.1 The pathogenesis of ovarian cancer.
Most of the invasive cancers that are termed 'ovarian' are derived from different tissues. Cancers that arise from the colon, stomach or appendix often metastasise and lead to invasive mucinous ovarian cancer. Endometriosis caused by retrograde menstruation has been shown to be the source of clear cell and endometrioid cancers. HGSC can arise from the surface of the ovaries or the fimbria of the fallopian tubes [2].

For the past 50 years treatment strategies for ovarian cancer have included radical surgery and platinum based chemotherapy with advances in the chemotherapy only leading to small improvements in outcome [9]. Due to the complexity of ovarian carcinogenesis there have been many flaws in understanding its nature, which has had an impact on the treatment of the disease [10].

Certain types of 'ovarian' cancer have more similarity with renal or breast cancer than other subtypes of ovarian cancer. Now that there is a clearer idea on the distinction between the different subtypes of 'ovarian' cancer and its pathogenesis, the focus is on developing and improving targeted therapies for each subtype of the disease [11].

1.2 Pathogenesis of HGSC

The earliest view of ovarian cancer asserts that all different subtypes of ovarian cancer arise from a common origin in the ovarian surface epithelium (OSE) [12]. This is a result of the physical trauma inflicted on the ovarian surface due to follicular rupture and oocyte release during the process of ovulation [13]. It was believed that the constant damage and repair of the OSE could facilitate tissue remodelling and lead to metaplastic change from an epithelial to mesenchymal phenotype. Ovulation-associated inflammatory cytokines and reactive oxygen species could also lead to DNA damage of the OSE cells and these DNA damaging processes also increased the risk of transformation of the OSE. Another theory associated with the ovarian surface origin is the development of numerous invaginations of the epithelial cells into the cortical stroma [6]. These invaginations were frequently found trapped within the stroma in circular structures called cortical inclusion cysts. There are several growth hormones acting upon the ovary that can induce proliferation of the epithelial cells within the cortical inclusion cysts. In cases where these epithelial cells undergo DNA damage, the theory suggested that they would be major targets for neoplastic transformation, which could ultimately give rise to ovarian carcinomas [13].

However this theory of the OSE and the cortical inclusion cysts was questioned due to the differences in the outcomes and genetic phenotype of the different ovarian tumours that arise from the cortical inclusion cysts within the ovaries [14].

Recent studies suggest that most HGSC malignancies may have a fallopian tube origin [15]. One of the earliest findings linking the fallopian tube pathway to HGSC malignancies came from the study carried out by Callahan *et al* in BRCA mutation carriers. In that study, primary fallopian tube malignancies were detected in BRCA-positive women undergoing surgery for ovarian cancer risk reduction [16]. The fimbria of the distal fallopian tube was found to be the dominant site of origin for early malignancies in BRCA carriers. Immunohistochemistry staining of these serous intraepithelial carcinomas (STIC) revealed p53 mutations in 80% of the cases [10]. The next major link was proposed from a study carried out by Crum *et al*, which indicated that 70% of sporadic (nonhereditary) HGSCs have tubal involvement

including STICs [17]. These studies suggest that at least some HGSC arise from fallopian tube/fimbria and subsequently metastasise to the ovaries.

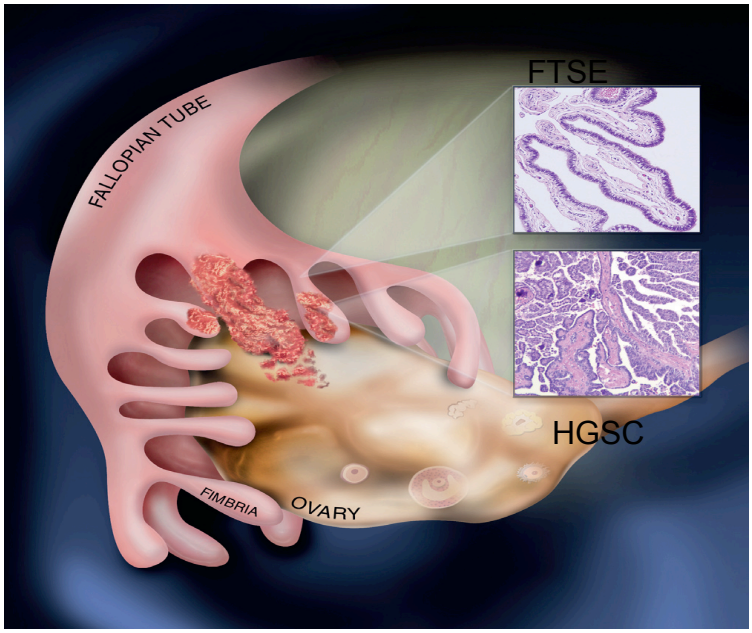

Figure 1.2 Emergence of HGSC from the fimbrinated end of the fallopian tube and spread to the ovarian surface epithelium.
Majority of HGSC (bottom inset) emerge from secretory cells (top inset) found in the fimbria of the fallopian tube and spread to the OSE where the bulk of the tumour resides [1].

There is a possible mechanism that would incorporate both theories; the ovarian cortical inclusion cysts and the fimbrial origin of ovarian cancer. According to this hypothesis, the fimbria come into close contact with the ovary and shed tubal epithelial cells on the disrupted ovarian surface to form a cortical inclusion cyst (Figure 1.2) [18]. This theory suggests that some 'ovarian cancers' may arise from ovarian inclusion cysts, but these cysts come from implanted fallopian tube fimbrial deposits. Follicular fluid containing reactive oxygen species can act on the OSE and further contribute to ovarian carcinogenesis [13].

Experiments using mouse models have shown that the fallopian tube can not only initiate but can also advance de novo to the full spectrum of the metastatic malignancy of HGSC. A recent study by Perets *et al*, generated a mouse model of HGSC using the PAX8 promoter to disrupt commonly altered genes such as

BRCA1/2, TP53 and PTEN selectively in the fallopian tube secretary epithelial cells (FTSEC) [19]. In this mouse model they observed precursor STIC lesions progress to advanced stage disease with ovarian and peritoneal metastasis. This study showed that HGSC could arise from FTSEC and lead to pre-invasive lesions, which then spread to the ovaries. Even though the majority of mice displayed STIC lesions, on gross inspection the fallopian tube appeared normal, whereas the ovary often showed visible signs of the disease. This observation is generally made in human disease and it explains the predisposition to term this disease as 'Ovarian cancer' [19].

1.3 Treatment for HGSC

The 5-year survival rate for HGSC patients is between 35% and 40% and this is strongly influenced by the stage of the disease at presentation. The current first line treatment for HGSC involves surgical debulking in combination with platinum with or without taxane chemotherapy [20]. Several clinical features such as tumour grade, size of the tumour after primary cytoreduction and general patient fitness are considered before implementing therapies of anticancer agents. The major challenge of the treatment is disease relapse of chemoresistant cells [21].

Women with germline mutations in HRR genes respond better to chemotherapy with longer progression free and overall survival compared with non-carriers [22, 23]. This is because the defect in HRR associated with loss of BRCA function increases the sensitivity of the ovarian cancer to platinum with or without taxane chemotherapy. These patients also benefit from treatment with PARP inhibitors [24].

Studies are also being carried out to understand the role of host cells in the growth and metastasis of the tumour cells. The tumour microenvironment has become an attractive target for the development of therapies, which will improve the standard treatment. This field of research is supported by the ongoing success witnessed in the clinical trials carried out with the anti-angiogenic agents to target the tumour vasculature [25]. A Phase III clinical trial with the angiogenic inhibitor bevacizumab, during and after treatment with chemotherapy, resulted in a significant increase in progression free survival in HGSC patients [21].

Another area which is of interest is the inflammatory cytokine and chemokine

networks in ovarian cancer [26]. Studies have identified a cytokine network within the ovarian cancer microenvironment, which has a profound effect on tumour growth, angiogenesis and leucocyte infiltrate. One of the earliest studied inflammatory cytokines in ovarian cancer is tumour necrosis factor-alpha (TNF-α) [27]. TNF-α is also involved in HGSC progression by acting as a principle mediator between other cytokines/chemokines. My lab has previously shown that the cytokines TNF-α, interleukin-6 (IL-6), the chemokine CXCL12 and its receptor CXCR4, were constitutively expressed and co-regulated in ovarian cancer cells *in vitro*. This was followed by the identification of the co-expression and co-regulation of this cytokine network in human ovarian cancer biopsies, which is now described as the 'TNF-network'. With the use of gene expression arrays they went on to show the involvement of TNF in angiogenesis, inflammation and NOTCH signalling in ovarian cancer tumour microenvironment [28, 29].

TNF-α was also involved in development of metastases and neo-vascularisation of tumours in HGSC xenograft models. The study also showed that the tumour growth and metastasis were significantly reduced with a stable knockdown of TNF-α in malignant cells [30]. This led to the use of anti-TNF-α antibodies in phase I trial for the treatment of recurrent ovarian cancer. The results from the trial showed disease stabilisation in six of the 18 patients who received treatment for minimum of twelve weeks. There was also a drop in levels of IL-6 and CCL2 in more than half of the patients. All these studies collectively showed the importance of inflammation/inflammatory cytokine and HGSC in the context of tumour progression.

1.4 Inflammation and Cancer

In the last decade inflammation has been shown to foster multiple hallmarks of cancer by providing 'bioactive molecules to the tumour microenvironment, including growth factors that sustain proliferative signalling, survival factors that limit cell death, pro-angiogenic factors and extracellular matrix-modifying enzymes that facilitate angiogenesis, invasion and metastasis' [31]. Epidemiological studies also revealed that 15-20% of cancer-related deaths are linked to infections and inflammatory responses. There are two pathways connecting cancer and inflammation; the intrinsic and extrinsic pathway [32]. The intrinsic pathway is activated by genetic events such as activation of oncogenes or by inactivation of tumour suppressor genes resulting in transformation of cells into a malignant phenotype. Cytokines and chemokines are produced by these malignant cells downstream of the oncogenic events. Hence, these transformed cells can trigger the production of inflammatory mediators, which can lead to the development of an inflammatory microenvironment in a tumour that did not have a predisposed inflammatory condition [33].

In the extrinsic pathway, infections or inflammatory conditions such as pancreatitis or colitis can predispose to cancers such as pancreatic or colorectal cancer. Both the intrinsic and extrinsic pathways lead to activation of transcription factors such as nuclear factor kappa beta (NFκB), signal transducer and activator of transcription 3 (STAT3) and hypoxia-inducible factor-1α (HIF-1α) in tumour cells which then lead to production of inflammatory mediators such as cytokines and chemokines (Figure 1.3). These cytokines can lead to activation of the same key transcription factors in inflammatory cells and stromal cells resulting in further induction of inflammatory mediators leading to a cancer-related inflammatory microenvironment. This microenvironment can then enhance tumour proliferation, cell survival, migration and invasion [34].

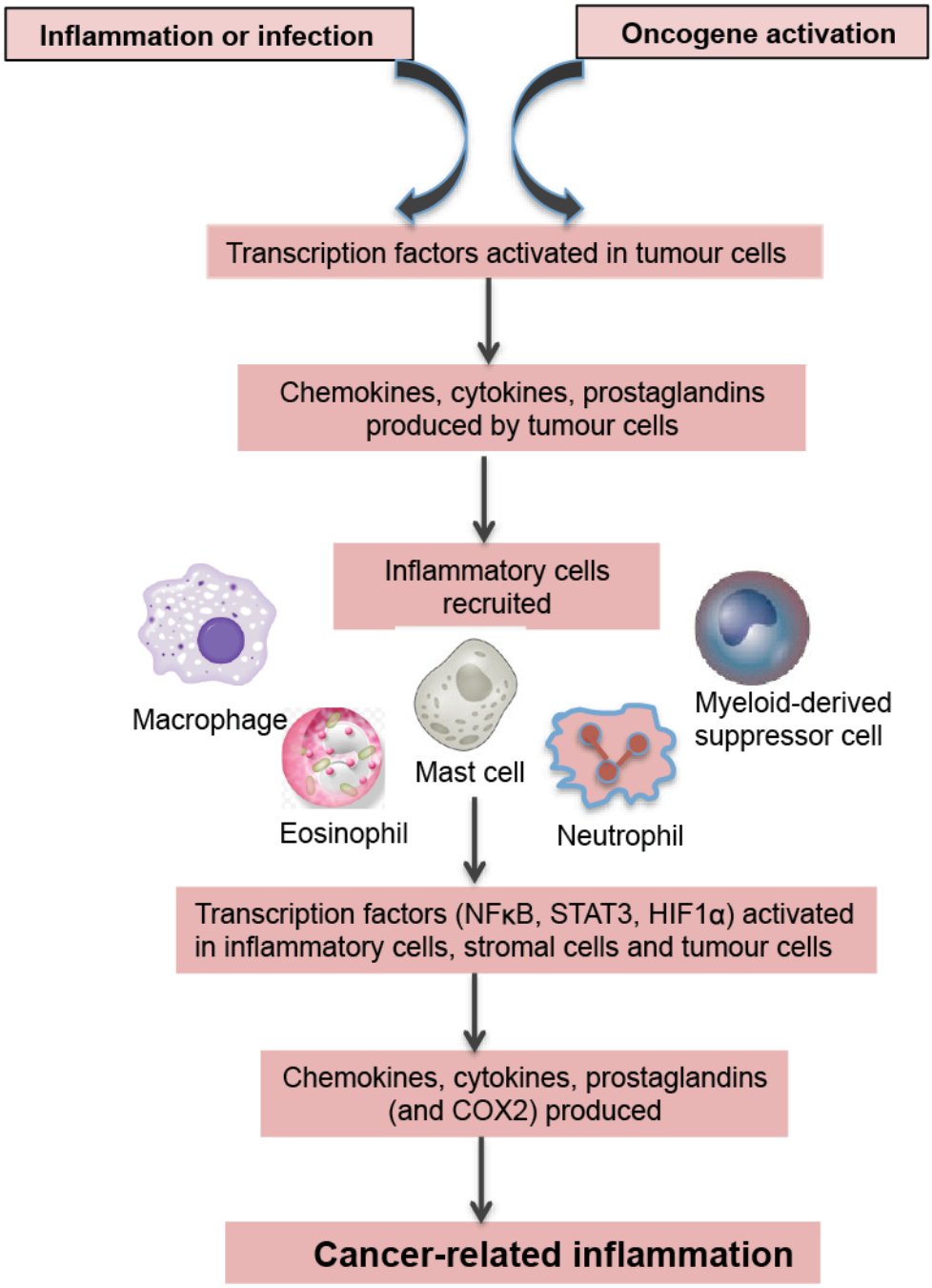

Figure 1.3 The intrinsic and extrinsic pathway that connect cancer and inflammation.
The intrinsic pathway is activated by genetic events that cause malignant transformation and the extrinsic pathway is activated by inflammatory or infectious conditions. Both of the pathways lead to the activation of transcription factors involved in growth, survival and invasion of cancer cells [34].

Pro-inflammatory cytokines and chemokines mediate interactions between the malignant and stromal cells in the ovarian cancer microenvironment. IL-6 is one of the most important cytokine in HGSC [35]. This cytokine is involved in HGSC

progression and invasion as demonstrated in various animal models and in human ovarian biopsy tissue [28, 29].

1.5 IL-6

IL-6 is a cytokine involved in various biological functions including the immune response and haematopoiesis. A number of cell types, including T cells, macrophages and endothelial cells, produce IL-6 (Figure 1.4) [36]. Activation of the IL-6 gene is mediated through the interaction of a number of transcription factors, including NF-κB, AP-1, CCAAT enhancer binding protein β (CEBPβ; formerly known as nuclear factor IL-6 (NF-IL6)) and the multiple response element (MRE) [37].

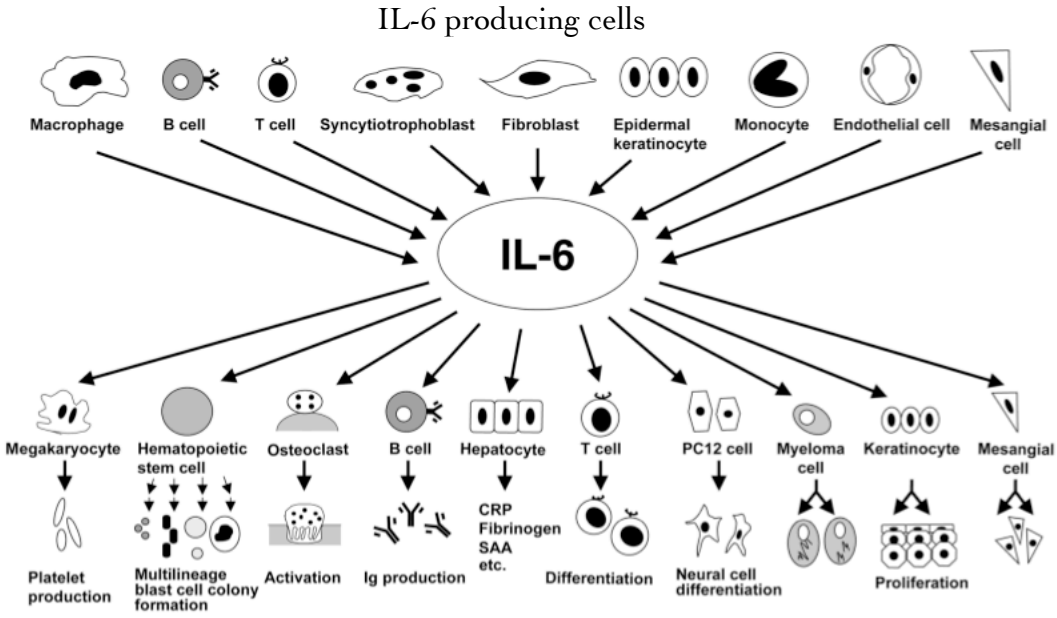

Figure 1.4 IL-6 producing cells and its target cells.
IL-6 is produced by lymphoid and non-lymphoid cells, such as T cells, B cells, monocytes, fibroblasts, keratinocytes, endothelial cells and mesangial cells. IL-6 has a wide range of biological activities on various target cells [38].

1.6 IL-6 signalling

IL-6 acts through the formation of a high affinity complex with its receptor, which has two components: the ligand binding 80kDa IL-6 receptor alpha (IL-6Rα) and its signal transducing glycoprotein 130 (gp130) [39]. IL-6Rα is predominantly restricted to cell types such as hepatocytes, leukocytes and some tumour cells, whereas the

signal transducing gp130 unit is ubiquitously expressed. Cells also express a soluble form of IL-6Rα (sIL-6Rα) which is produced by proteolysis of the membrane bound IL-6Rα [40].

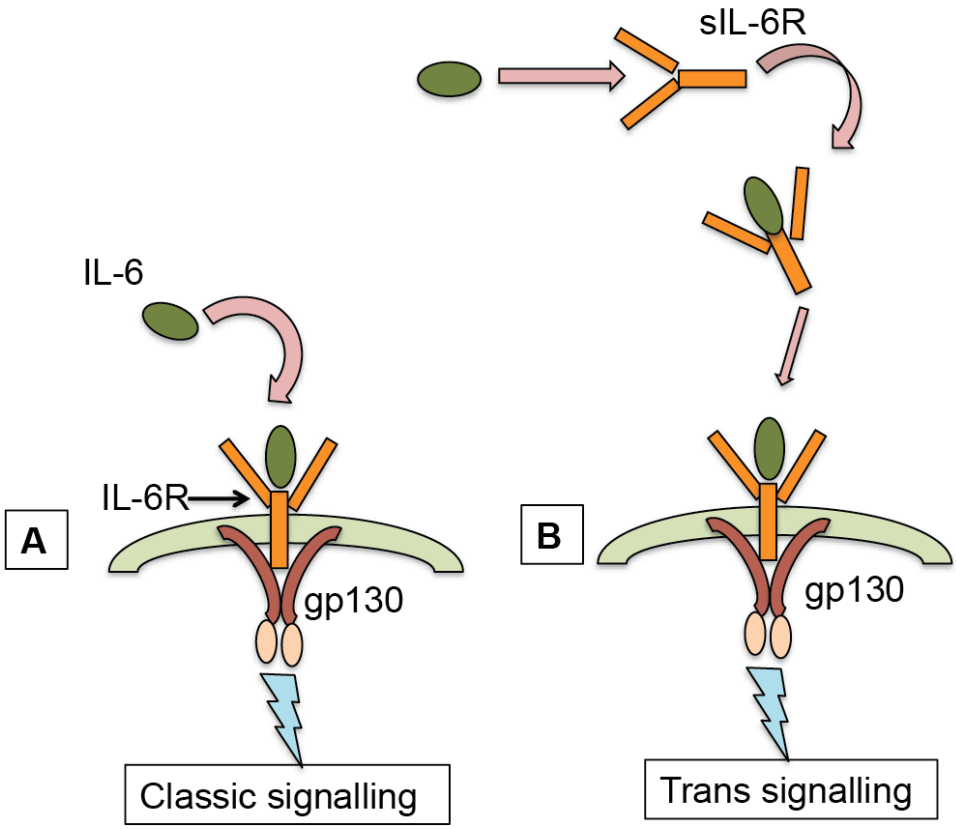

Figure 1.5 Schematic representations of two types of IL-6 signalling, Classic and Trans-signalling.
Classic signalling **(A)** in which IL-6 binds to IL-6Rα, which forms a complex with gp130 to initiate downstream signalling. Trans- signalling (**B)** in which IL-6 signalling is mediated through binding of IL-6 to sIL-6Rα and subsequent interaction of this complex with the membrane associated gp130.

As represented in Figure 1.5A, in the classic signalling pathway, IL-6 ligands bind with high affinity to cells that express membrane bound IL-6Rα. The IL-6/IL-6Rα then recruits the signal transducing gp130 unit, thereby activating IL-6 downstream signalling [41]. In trans-signalling (Figure 1.5B), IL-6 binds to the sIL-6Rα, which then associates with any cell that expresses the gp130 unit, thereby activating IL-6 signalling in cells, which do not express the membrane-bound IL-6Rα. Numerous studies have shown that a soluble version of the gp130 unit is capable of inhibiting the trans-signalling by binding to the IL-6/sIL-6Rα complex and blocking it from binding to the membrane bound form of gp130 [39].

1.7 Activation of the IL-6 receptor

The formation of a complex between the (IL-6)/(IL-6R) and signal transducing unit gp130 complex results in downstream activation of JAK1, JAK2, Tyk2 and in the phosphorylation of a specific tyrosine residue on the receptor. STAT3 then binds to this receptor and is phosphorylated by JAK [42]. Phosphorylated STAT3 (pSTAT3) dimerises and is recruited to the nucleus where it acts as a transcription factor (Figure 1.6). STAT3 regulates the transcription of genes such as Bcl2, Bcl-xl, cJun and cFos, which play a key role in cell growth and differentiation and in the inhibition of apoptosis. RAS is also activated in response to IL-6, and leads to hyper-phosphorylation and activation of mitogen activated phosphate kinase (MAPK) [43].

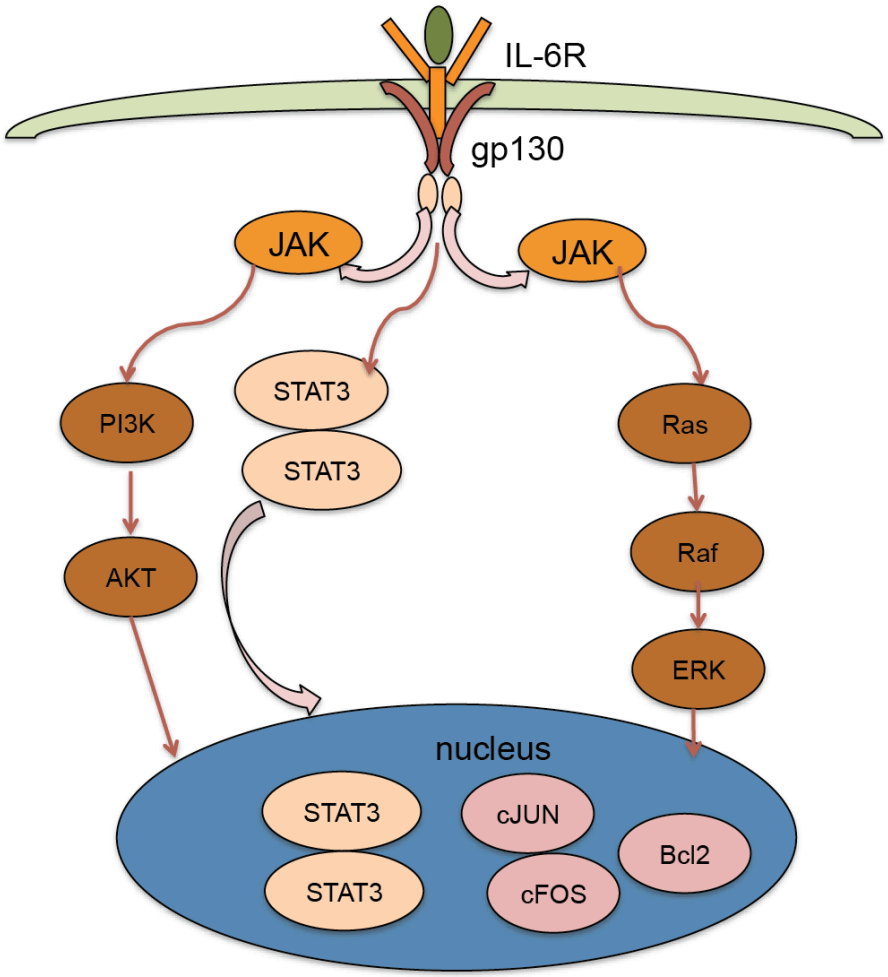

Figure 1.6 IL-6 and its downstream signalling targets.
Formation of the IL-6/IL-6Rα and gp130 complex leads to the activation of its direct downstream target STAT3. It can also activate the MAPK and PI3K pathway.

1.8 IL-6 and cancer

Various chronic conditions such as inflammatory bowel disease, rheumatoid arthritis and several malignancies, such as colon cancer, have been linked to inappropriate IL-6 trans-signalling [39, 44]. More than 50% of all cancers have aberrant STAT3 signalling which renders malignant cells resistant to apoptosis and increases their rate of proliferation, thereby enhancing tumourigenesis [45]. STAT3 regulates genes that are involved in proliferation, such as cyclin D1, c-myc and genes that suppress apoptosis, such as the Bcl-2 family members Mcl-1 and Bcl-xl. It can also promote angiogenesis and metastasis by up-regulating pro-angiogenic molecules like VEGF and matrix metalloproteinase-9 (MMP-9).

Other studies have also shown a role for IL-6 in increasing resistance to chemotherapy via the JAK/STAT signalling pathway [46, 47]. The tumour promoting actions of IL-6 are mediated by its role in cytokine networks found in several human malignancies such as serous and clear cell ovarian cancer [5, 29], multiple myeloma [48], Castleman's disease [49] and hepatocellular carcinoma [36].

Over the years, there have been several studies linking IL-6 with various cancers. Most of the findings from these studies have associated IL-6 with poor prognosis and disease progression as shown in Table 1.

Cancer type	Role of IL-6
Intestine	High serum IL-6 correlates with advanced stage and poor prognosis
Stomach	High levels of IL-6 in the serum is an independent predictor of poor prognosis
Liver	In hepatocellular carcinoma high serum levels of IL-6 correlate with poor prognosis
Pancreas	High levels of IL-6 in pancreatic cancer patient serum is linked to poor overall survival
Lung	High serum levels of IL-6 correlate with poor survival in non small cell lung cancer
Esophagus	Elevated serum levels of IL-6 are correlated with disease progression and poor prognosis
Breast	High systemic levels of IL-6 has been shown to correlate with poor prognosis and metastasis
Cervix	High serum levels of IL-6 correlates with disease progression
Ovary	High IL-6 level in serum and ascites correlates with poor prognosis
Prostate	High serum IL-6 is linked to poor prognosis and chemoresistance
Kidney	High serum IL-6 levels correlate with tumour size, stage and poor prognosis
Bladder	High IL-6 expression correlates with poor prognosis

Table 1 Clinical association data of IL-6 with various cancer types.
Data adapted from [50].

Due to this clinical association of IL-6 with disease progression or poor outcome, pre-clinical and *in vivo* studies have been carried out to understand the role of IL-6 in various cancer models [35, 51, 52].

IL-6 promotes proliferation and survival of colon cancer cells via induction of STAT3 [53]. The sIL-6Rα shedding within the tumour microenvironment can activate STAT3 in cells expressing gp130 but lacking the membrane bound IL-6Rα [54]. In addition to STAT3, there are other signalling molecules, which are activated by gp130 such as the Ras-MAPK and the PI3K-mTOR pathways that also play a role in tumour progression [55].

Mouse models of colitis associated cancer (CAC) have shown hematopoietic cells, especially macrophages and dendritic cells to be involved in production of IL-6 during early stages of tumour induction, followed by T cells during later stages of tumour progression. *In vivo* CAC studies with a neutralising antibody against IL-6Rα or a sgp130Fc fusion protein led to inhibition of tumour growth [54]. Deletion of STAT3 also resulted in the reduction of number of early adenomas in adenomatous polyposis coli (APC) mice [56].

Hepatocellular carcinoma (HCC) is another inflammation related cancer where IL-6 is linked with poor prognosis [56]. Kupffer cells and recruited macrophages are mainly responsible for IL-6 production in these tumour cells and hepatocytes also express high levels of IL-6Rα and gp130. The tumour promoting actions of IL-6 in HCC are mediated via STAT3 and targeting STAT3 in hepatocytes inhibits HCC development [57]. Studies investigating a liver specific knock out of SOCS3, an inhibitor of IL-6, led to enhanced HCC progression as a result of increased STAT3 and pERK activation [58]. *In vitro* IL-6 knockdown in HCC cell lines also resulted in inhibition of proliferation, migration and invasion confirming the importance of autocrine IL-6 signalling in this model of cancer.

Studies in Kras driven models of pancreatic ductal adenocarcinoma (PDAC) have shown the importance of STAT3 activation in the initiation and the progression of the disease [59]. In human esophageal cancer cells, IL-6 acts as an anti-apoptotic factor via induction of STAT3 and ERK signalling. Blocking IL-6 expression in these cell lines led to inhibition of aggressive tumour phenotype and overcame radiation

resistance *in vitro* and *in vivo* [60]. In breast cancer, IL-6 signalling plays a major role controlling cancer cell proliferation, cancer stem cell renewal and metastasis [61]. Cancer associated fibroblasts that stimulate angiogenesis and invasion also express high levels of IL-6. IL-6 induced Notch-3 dependent up-regulation of Jagged1 can also promote growth of breast cancer cells [62].

In prostate cancer, IL-6/STAT3 signalling results in transition from hormone sensitive to hormone resistant phenotype and it also leads to induction of myeloid derived suppressor cells (MDSCs). *In vivo* studies have indicated the activation of STAT3 in the development of castration resistant prostate cancer [63].

Pre-clinical studies exploring the regulation of IL-6 in ovarian cancer cell lines have established a link between high levels of IL-6 and p53 status. Wild-type p53 inhibits IL-6 promoter activity. 96% of the HGSC have a p53 mutation, which may increase IL-6 promoter activity [8, 37]. There have been studies showing that some of the ovarian cancer cell lines constitutively produce IL-6 and this production is enhanced when these cells are co-cultured with other cytokines/chemokines from the ovarian cancer microenvironment [29].

1.9 Clinical trials targeting IL-6

A neutralising anti-IL-6 antibody was initially tested in patients with prostate cancer. This was because the pre-clinical studies in prostate cancer showed IL-6 production to be associated with conversion of prostate cancer cells from an androgen-dependent to an androgen-independent phenotype, resulting in increased proliferation and decreased apoptosis [64]. These results led to a clinical trial with siltuximab in castrate resistant prostate cancer patients whose disease had progressed after docetaxel chemotherapy. The trial showed siltuximab to have biological activity in patients with decrease in c-reactive protein levels (CRP) in blood. High levels of CRP are linked to poor prognosis in prostate cancer patients. However, there was minimal clinical activity with siltuximab as a monotherapy. The paper suggested additional studies with siltuximab in combination with chemotherapy [65].

Another study investigated the role of IL-6 in paraneoplastic thrombocytosis; the raised platelet count seen in cancer patients, especially in HGSC. The study proposed that IL-6 made by the malignant cells stimulates thrombopoietin production in the liver, which increases platelet production in the bone marrow. Therefore countering paraneoplastic thrombocytosis by directly or indirectly targeting IL-6 was considered a potential therapeutic approach. Siltuximab treatment significantly reduced platelet count in tumour bearing mice and in patients with ovarian cancer. The study also indicated that treatment of tumour bearing mice with anti-platelet antibody resulted in decreased tumour growth and significantly diminished tumour vascular areas [66].

Currently there are several Phase II studies being carried with siltuximab in cancers such as transplant-refractory melanoma, castrate resistant prostate cancer and metastatic renal cell carcinoma. There are also other IL-6 targeting antibodies such as sirukumab, olokizukmab, elsilimomab, clazakizumab and MEDI5117, which are being tested in Phase I/II clinical trials in rheumatoid arthritis, inflammatory bowel diseases and in some cancer types [50].

Another approach undertaken to target the IL-6 signalling is by using antibodies such as Tocilizumab, which blocks the IL-6Rα. These antibodies have been successful and are approved for the treatment of rheumatoid arthritis and Castleman's disease in Japan [67]. Also another emerging class of drugs, which are now used in clinical trials to target the downstream IL-6 signalling, are JAK inhibitors. There are several of these inhibitors in Phase I/II clinical trials in rheumatoid arthritis, haematological malignancies and various solid tumours [50]. Among all the pre-clinical and clinical studies carried out with IL-6 targeting agents, the one that is of interest to me are the studies carried out in ovarian cancer using the siltuximab antibody.

1.10 Siltuximab clinical trial conducted in the Centre for Cancer and Inflammation

The clinical trial of siltuximab in ovarian cancer was based on several pre-clinical studies with cell lines, animal models and patient samples. These pre-clinical studies in my lab started by investigating the source of IL-6 in HGSC by staining patient tissue microarrays (TMAs), for IL-6 and its receptor. Significantly higher levels of IL-6 staining were present in the malignant cells compared to the stroma. This high level of IL-6 staining in malignant cells was also associated with shorter progression free and overall survival [35]. These results led the group to assess the therapeutic activity of an anti-human IL-6 antibody in human ovarian cancer. They combined pre-clinical and *in silico* experiments with a phase II clinical trial of siltuximab in ovarian cancer patients with platinum resistant disease.

Out of the 18 platinum resistant ovarian cancer patients in the trial described above, one patient had partial response. Stable disease was achieved in eight of the patients for a period of time and from these patients, four received anti-IL-6 treatment for 6 months or more. By the six-month time point all four of these patients had a significant reduction in the cytokine plasma levels of IL-6-regulated CCL2, CXCL12 and VEGF. The study concluded that the mechanism of action of anti-IL-6 in ovarian cancer is by inhibition of autocrine production of cytokines and chemokines that has paracrine effects on angiogenesis via inhibition of VEGF, Jagged1 and interleukin-8 (IL-8) and on the macrophage infiltrate via inhibition of chemoattractant CCL2 [35]. However, as the weeks progressed there was an increase in plasma cytokine levels, in particular IL-8, which correlated with disease progression.

The above discussed pre-clinical studies from our lab on anti-IL-6 antibody treated HGSC xenografts showed a significant reduction in tumour vascular areas. Immunohistochemistry and qRT-PCR results showing decreased expression of an angiogenic factor, Jagged1, which is a ligand of Notch signalling and in this way forms part of the autocrine cytokine network in ovarian cancer [29]. High Jagged1 levels were found in IL-6 secreting malignant cells and these levels were inhibited by the anti-IL-6 antibody siltuximab in xenograft models.

In the studies described above there was evidence that IL-6 might also be contributing to tumour angiogenesis. This observation was mainly based on the clinical and pre-clinical results, which showed decrease in VEGF levels in HGSC patients after treatment with siltuximab and the reduction in vascular areas with a decrease in Jagged1 expression noted in siltuximab treated HGSC xenografts. These data indicated a potential role of IL-6 in angiogenesis and led to the hypothesis to be investigated in this thesis.

1.11 Angiogenesis

Blood vessel formation is the first process in embryonic development and blood vessels form the largest network in our body. However, dysregulation of the vascular system can be a contributing factor to numerous malignant, ischemic and inflammatory disorders [68]. The formation of the vascular network either starts with an assembly process called vasculogenesis or through coordinated expansion of a pre-existing vasculature. Vasculogenesis refers to the formation of blood vessels by differentiation of the mesodermal derived angioblast into endothelial cells, which then forms a primitive network [69]. In contrast angiogenesis refers to the sprouting of pre-existing endothelial cells and the subsequent stabilisation and maturation of the sprouts by pericytes [70]. Angiogenesis is co-ordinated by a series of morphogenic events, which ultimately leads to formation of an extensive vascular network. As shown in Figure 1.7, pro-angiogenic molecules can activate endothelial cells in pre-existing vessels. These activated endothelial cells can then interact with pericytes to release proteases that degrade the basement membrane and extracellular matrix. This is followed by budding of activated endothelial cells migration and proliferation. Maturation proceeds with recruitment of pericytes to the endothelium [71].

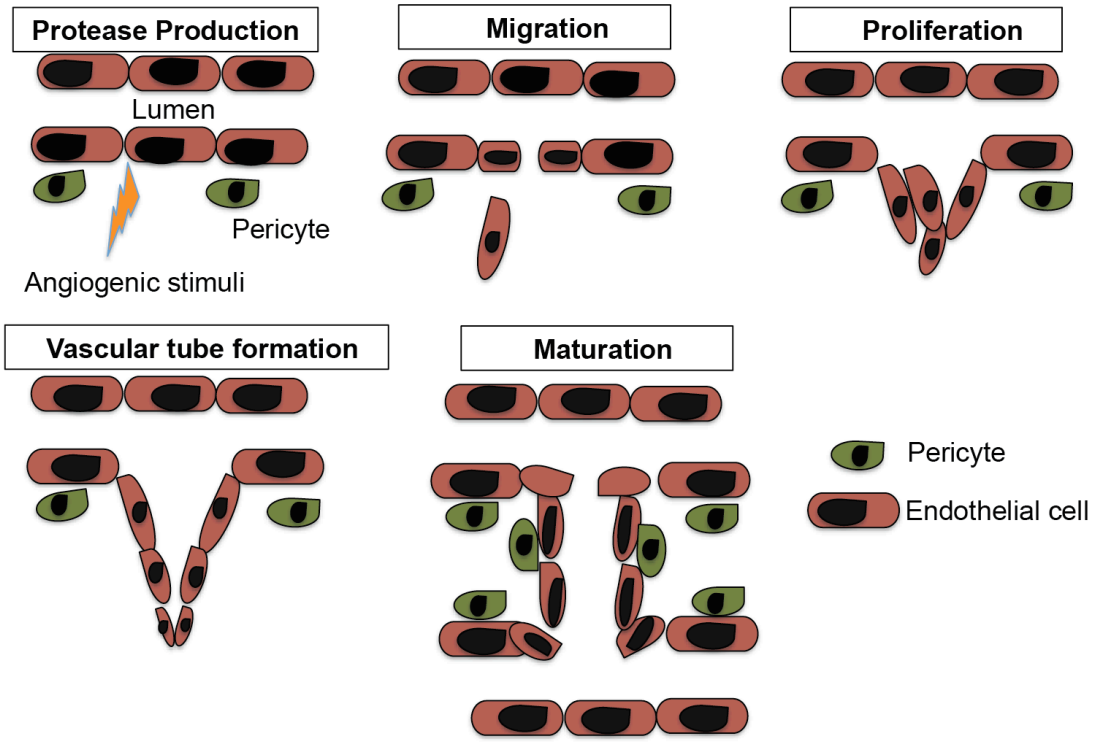

Figure 1.7 Key stages in the process of angiogenesis.
This process starts with a pro-angiogenic stimulus activating the endothelial cell, which then lead to release of proteases that degrade the extracellular matrix. This is followed by proliferation and migration of the endothelial cells and the subsequent stabilisation of the vessels by pericytes.

Excessive or aberrant angiogenesis contributes to various disorders like cancer, arthritis, blindness, obesity and asthma. There are also several disorders caused by insufficient vessel growth such as hypertension, neurodegeneration, respiratory disorders and also heart and brain ischemia [68]. The long-held view in tumours was that the development of the vasculature was through angiogenic process from pre-existing vessels. However, now studies have shown vasculogenesis as the contributor of at least 40% of the tumour vascularisation where the endothelial progenitor cells in the tumour are derived from the bone marrow [72].

Other modes of vessel formation such as the intussusception, co-option and vascular mimicry are now being investigated. Intussusception is where the pre-existing vessels split into daughter vessels; in vessel co-option the tumour cells hijack the existing vasculature and migrate along the host vessels. Vessel co-option is mainly observed in highly vascularised tissues such as the brain, lung and liver. Vascular mimicry is normally seen in highly aggressive tumours where the tumours cells themselves form vessel like structures [73]

1.12 Angiogenesis and Cancer

There have been several models developed to understand the process of tumourigenesis. These included exploring the initial events such as oncogene activation, which leads to genetic changes that affect the growth and transformation of certain cells [*74*, *75*]. The studies revealed in addition to the genetic changes that occur during transformation, there is another important step required for the tumour progression, and this is the establishment of the tumour vasculature. This process has been named as the 'angiogenic switch' [*76*, *77*]. This angiogenic switch can be turned on at different stages of tumour growth and is based on the nature and microenvironment of the tumour. The regulation of the angiogenic switch in tumours depends on the balance of the pro and anti-angiogenic agents. Stimuli such as hypoxia lead to increased expression of pro-angiogenic molecules such as VEGF, fibroblast growth factor (FGF), platelet derived growth factor (PDGF) and epidermal growth factor (EGF) that can lead to induction of the angiogenic switch [*77*].

Early studies showed that the tumour mass cannot exceed $1mm^3$ without a sufficient blood supply [*78*]. This is because, like normal cells, malignant cells require nutrients and oxygen in order to grow and these are supplied by new blood vessels [*79*]. However, there are several differences in the angiogenesis stimulated in tumours compared with normal physiological conditions. Physiological angiogenesis is a tightly regulated process involving a balanced level of pro and anti-angiogenic signals where the blood vessels rapidly mature and become stable [80]. However, in tumours the balance between pro and anti-angiogenic molecules is lost resulting in constant growth of new blood vessels.

Tumour blood vessels also appear irregularly shaped, dilated and torturous. They are chaotic and leaky as compared to the organised vasculature seen in normal angiogenesis. There is also a defective coverage or very loose attachment of pericytes to the tumour endothelium [81, 82].

Over the years, several molecules have been implicated as positive regulators of angiogenesis including FGF, transforming growth factor (TGF-α), (TGF-β), TNF-α, IL-8, angiopoietins and the Notch signalling pathway [83]. In depth investigation into the field of angiogenesis has identified VEGF as a key player in the regulation of angiogenesis in malignant diseases. The formation of new vessels involves highly co-ordinated and sequential activation of various angiogenic pathways and among these, VEGF signalling often represents a critical rate limiting step in the process of angiogenesis [84].

1.13 VEGF and its receptors

The VEGF family consist of five members, VEGFA, B, C, D and placenta growth factor (PLGF) (Figure 1.8). There are three main VEGF receptors (VEGFR); VEGFR1, VEGFR2 and VEGFR3. There are also two co-receptors for VEGF, heparan sulfate proteoglycans (HSPG) and neuropilins, which lack the VEGF induced catalytic domain [84]. The VEGF ligands have different affinity for different VEGF receptors. For example the VEGFA, B and PLGF ligands bind to the VEGFR1 receptor, VEGFA and E bind to VEGFR2, and VEGFC and D bind to VEGFR3. VEGFC and D can also bind to VEGFR2 with lower affinity after it has undergone proteolytic processing. There are also some isoforms of VEGFA i.e. VEGFA 121, VEGFA 145, VEGFA 165, VEGFA 189 and VEGFA 206. These VEGFA isoforms are known to interact with the VEGF co-receptors HSPG and neuropilins [83].

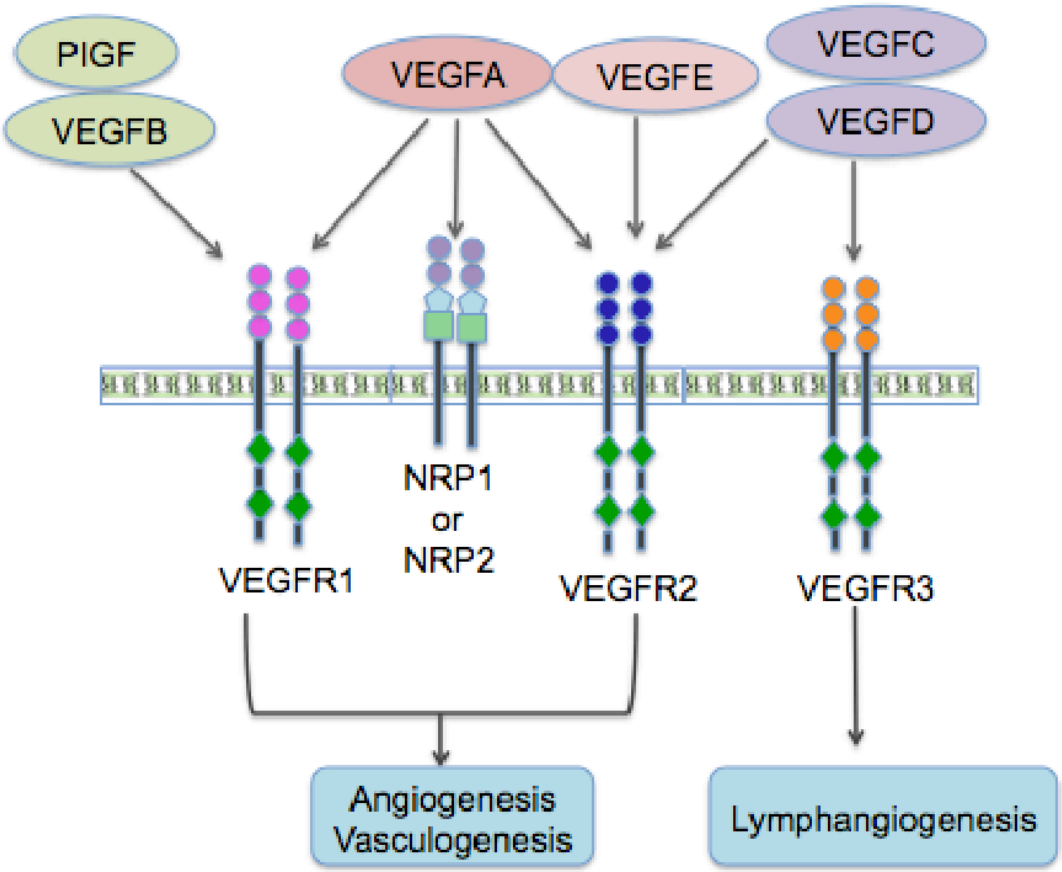

Figure 1.8 VEGF receptors and their ligands.
VEGFR1 and VEGFR2 functions via inducing angiogenesis and vasculogenesis and VEGFR3 plays a role in lymphangiogenesis.

The main VEGF receptors i.e. VEGFR1 and VEGFR2 and the ligand VEGFA are regulated under low oxygen tension. HIF-1 is activated as a result of mutations in the Von-Hippel-Lindau (VHL) tumour suppressor gene, a key regulator of hypoxic conditions. VHL functions by negatively regulating the levels of VEGF and other hypoxic genes. Therefore, HIF is constitutively activated in conditions where the VHL gene is mutated and this has been shown to increase the mRNA levels of VEGF [84]. There are also several growth factors that have been implicated in the up-regulation of VEGF mRNA and these include EGF, TGF-α, TGF-β, hepatocyte growth factor (HGF), insulin growth factor (IGF), FGF and PDGF[85].

Binding of the ligand to VEGF receptors leads to homo or hetero dimerisation of the receptors. Once the receptors are dimerised, this leads to activation of the tyrosine kinase, resulting in autophosphorylation of the receptors [86]. The phosphorylated receptors can then recruit interacting proteins and this leads to the activation of

downstream signalling pathways. The tyrosine kinase activity of the receptors can be inactivated by dephosphorylation of the receptors by tyrosine specific phosphatases. Downregulation of the receptor tyrosine kinase activity can also take place via proteasomal degradation or internalisation of the receptor and subsequent degradation in the lysosome [83].

VEGFR1 or Flt-1 was the first receptor tyrosine kinase to be identified as a VEGF receptor. VEGFR1 mainly functions as a positive regulator of monocyte and macrophage migration and it is not particularly required for normal vascular development. During embryogenesis, VEGFR1 can also negatively regulate the function of VEGFR2 by acting as a trap for VEGFA and reducing its accessibility to VEGFR2. VEGFR1 can also crosstalk with VEGFR2 and negatively regulate the functions of VEGFR2 [87]. Activation of VEGFR1 by PLGF has shown to positively regulate VEGFR2 and this is thought to be as the result of the displacement of VEGFA from VEGFR1 [88].

VEGFR2 or FLK-1 plays an important role in developmental angiogenesis and haematopoiesis. Mice lacking the VEGFR2 showed failure in forming organised blood vessels. Phosphorylation of these receptors results in activation of several pathways such as the PI3K (phosphatidylinositol-3 kinase), MAPK and the Src family. PI3K pathways activation is important in ensuring the pro-survival effects mediated by the VEGF signalling [85]. Downstream MAPK/ERK signalling is important in regulating the growth of the endothelial cells. VEGFR2 receptor activation increases the vascular permeability of the endothelial cells and this is mediated by the downstream activation of the p38 MAPK pathway. FAK (Focal adhesion kinase) is also implicated in the VEGF induced migration of the endothelial cells [87].

VEGFR3 is involved in the establishment and maintenance of the lymphatic vasculature. This receptor can form homodimers or heterodimers with VEGFR2 and bind to VEGFC or D. VEGFR3 induced signalling can also be modulated by co-receptors such as neuropilin-2. Neuropilin co-receptors were identified when studies into the VEGF binding sites on endothelial cell surface showed sites with distinct affinity and molecular mass from the two main VEGF receptors. Further investigations identified these receptors as neuropilin1, which are receptors that lack

the intrinsic catalytic activity and are known to be involved in neuronal guidance. When these neuropilin receptors are co-expressed with VEGFR2 they increase the binding affinity of the VEGFA isoform; 165 to the VEGFR2 thereby enhancing the downstream signal transduction [86].

1.14 VEGF targeted therapies

Understanding the role of VEGF in angiogenesis has led to the development of various VEGF targeted therapies. These agents include neutralising antibodies to VEGF or VEGFRs and inhibitors against the receptor tyrosine kinase that also target VEGFRs [89]. The first Food and Drug Administration (FDA) approval for anti-angiogenic agents was based on a phase III clinical trial in metastatic colorectal patients where promising results were observed with the treatment of bevacizumab (monoclonal antibody against VEGFA) alone or in combination with chemotherapy [90]. This was followed by observation of increased overall survival in patients with advanced non-small cell lung cancer when bevacizumab was combined with standard chemotherapy [91]. This led to the use of anti-angiogenic agents in various tumour types as summarised in Table 2.

VEGF targeting agent	Mode of Action	Cancer Types
Bevacizumab (Avastin)	Monoclonal anti-VEGF antibody	Breast, colorectal, non small cell lung, renal cell carcinoma, glioblastoma, ovarian, gastric, pancreatic and prostate cancer
Aflibercept (Zaltrap)	Chimeric VEGF/PIGF neutralising receptor	Colorectal, pancreatic, non small cell lung cancer
Sorafenib (Nexavar)	Small- molecule VEGFR TKI	Renal cell carcinoma, hepatocellular carcinoma, melanoma and non small cell lung cancer
Sunitinib (Sutent)	Small- molecule VEGFR TKI	Renal cell carcinoma, breast, hepatocelluar carcinoma, colorectal, pancreatic, non small cell lung cancer and prostate cancer
Pazopanib (Votrient)	Small- molecule VEGFR TKI	Renal cell carcinoma, non small cell lung cancer and soft tissue sarcomas
Vandetanib	Small- molecule VEGFR TKI	Non small cell lung cancer and medullary thyroid cancer
Vatalanib	Small- molecule VEGFR TKI	Colorectal cancer
Cediranib	Small- molecule VEGFR TKI	Colorectal, glioblastoma and ovarian cancer
Axitinib	Small- molecule VEGFR TKI	Renal cell carcinoma, pancreatic cancer

Table 2 The list of anti-VEGF agents tested in various cancer types.
Data adapted from [92]

Treatment with the majority of the above VEGF targeted therapies showed improvement in progression free survival in the various cancer types [92]. However, there are challenges or limitations with the use of these anti-angiogenic agents targeting VEGF signalling. Primarily, some cancers have shown resistance to these therapies and even in cases where an increase in progression free survival was observed it was by only a matter of few months [93]. There are several mechanisms involved in the induction of resistance to anti-VEGF therapies and these include up-regulation of other pro-angiogenic molecules such as PIGF, FGF, IL-8 and IL-6, which will be discussed in more detail later. Some cancers also acquire resistance to VEGF therapies by switching their mode of vascularisation. For example, it has been shown in metastatic melanoma and lung cancer that the tumour cells are capable of growing in an angiogenesis independent manner by co-opting or growing around the pre-existing vessels upon treatment with bevacizumab [94]. Some studies have also shown DLL4, a Notch ligand involved in inducing mature stalk cell phenotype to mediate anti-VEGF therapy resistance. This as a result of the large vessels induced by the DLL4-Notch signalling, which are insensitive to VEGF therapy [95]. Neuropilin1 has also been shown to play a role in resistance by acting independently of VEGF [96]. Anti-VEGF therapy has also shown to increase metastasis by up-regulation of c-MET in response to hypoxia [97]. Therefore, the combination of VEGF and c-MET inhibition has shown to reduce metastasis in pancreatic cancer [98, 99].

1.15 The Notch signalling pathway

As mentioned above, Notch signalling is another intrinsic signalling pathway that has also been shown to play a pivotal role in angiogenesis.

Notch signalling is involved in regulating cell fate, differentiation and proliferation. Notch receptors and ligands are transmembrane proteins. The communication between a signal sending cell and a signal-receiving cell is mediated by cell-to-cell contact. In mammals, there are four Notch cell surface receptors; Notch1, 2, 3 and 4, and five transmembrane ligands i.e. Jagged1, Jagged2, Delta like ligand (DLL) 1, 3 and 4 [100].

Notch signalling requires a series of proteolytic cleaving processes. The first proteolytic step is carried out by a furin molecule, which produces a ligand binding Notch extracellular domain (NECD) and a single pass transmembrane signalling domain i.e. the Notch intracellular domain (NICD) [101]. Binding of DLL ligand to the NECD leads to activation of the pathway. This leads to the second preoteolytic cleavage step where the NECD is removed from the outer surface of the membrane by TNF-α converting enzyme (TACE). In the ligand-expressing cell, the NECD is internalised through endocytosis and thereby undergoes lysosomal degradation. Following this, γ-secretase cleaves the rest of the receptor in the Notch expressing cell, producing a transcriptionally active NICD, which then translocates to the nucleus and forms a complex with the coactivatorA (CoA) and the transcription factor CSL. This then leads to activation of basic helix–loop–helix proteins i.e. HES and HEY, which are transcriptional repressor genes (Figure 1.9). Activation of these proteins leads to Notch dependent cell fate determination: proliferation, apoptosis and differentiation [102, 103].

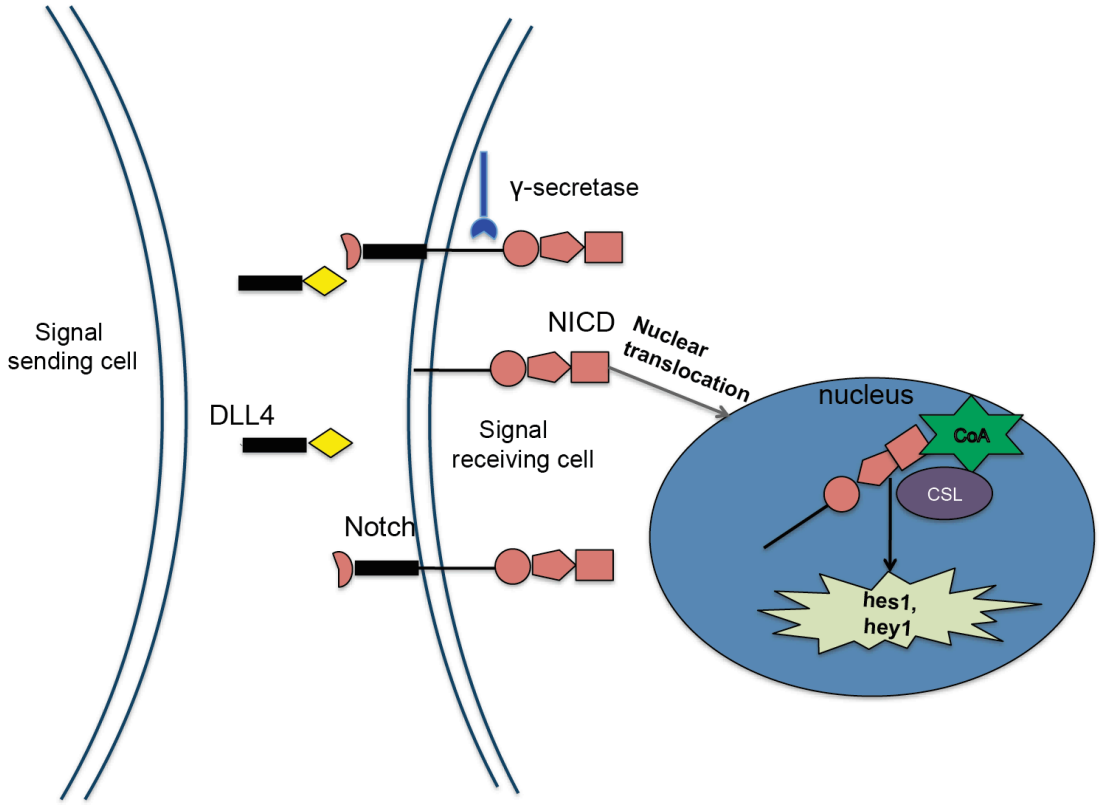

Figure 1.9 The Notch signalling pathway.
Ligand binding to the Notch receptor via cell to cell contact leads to cleavage of the NECD by TACE, which is then endocytosed and degraded via the lysosome in the signal sending cell. Subsequently, the γ-secretase cleaves the NICD and translocates it to the nucleus where it forms a complex with the transcription factor CSL and the coactivators to activate HES and HEY repressor genes.

Recently several studies have reported a non-canonical Notch signalling pathway, which is still not clearly understood [104]. This pathway is shown to be CSL independent and can be ligand dependent or independent. Various other ligands have been implicated in the induction of the Notch non-canonical pathway and these include Delta like 1 (DLK1), Delta and Notch like epidermal growth factor related receptor (DNER) and Jedi [101]. This non-canonical signalling interacts and activates pathways such as the NFκB, TGF-β and Wnt signalling [105]. Notch ligands can also inhibit the Notch signalling pathway. The activity of the Notch ligands can be regulated by post-transcriptional modifications or via cellular mechanisms such as endocytosis and proteolysis [106].

The Notch signalling pathway is important for cell-cell communication especially in vascular formation, in neuronal function and development. It is also required for the

selection of endothelial tip and stalk cells in sprouting angiogenesis. The receptors Notch1 and Notch 4 and the ligands Jagged1, DLL1 and DLL4 are mainly expressed in the endothelial cells and are known to play an important role in vascular formation [107]. DLL4, which is induced by VEGF, is highly expressed in the vascular endothelial cells [102, 108]. Higher expression of DLL4 is found on the tip of the sprouting vessels and it binds to Notch1 and 4 receptors that are expressed on the stalk of the adjacent vessel. This interaction of DLL4 with the Notch receptor promotes the stalk cell phenotype enabling vascular integrity and tissue perfusion and this is mediated partially by reducing the expression of VEGFR2. The DLL4-Notch interaction thereby maintains a balance between the tip cell and stalk cell, limiting the number of sprouting vessels [109]. Blocking DLL4-Notch signalling promoted excessive tip cell sprouting and angiogenesis. The vessels formed as a result of DLL4 inhibition were abnormal and poorly perfused with decreased pericyte coverage resulting in increased hypoxia [101].

Jagged1 antagonises DLL4, thereby blocking the positive Notch-DLL4 interaction leading to more of a tip phenotype. This is mediated through the fringe family members, which carry out post-transcriptional modifications on the Notch receptors. Fringe glycosylated Notch receptors shows strong activation of downstream targets HEY1 by DLL4 [108]. However, Jagged1, which normally has lower binding affinity than DLL4 to Notch receptors, works as an antagonist and can block DLL4-Notch interactions in fringe expressing cells [109]. There is an oscillatory effect reported with the regulation of the Notch signalling in the presence of VEGF. VEGF interaction in endothelial cells leads to induction of DLL4, which then binds to the Notch receptor resulting in the release of the NCID to the nucleus. This induces expression of HEY gene and the fringe gene. Fringe then glycosylates the Notch receptor thereby enhancing Notch-DLL4 interaction and decreasing Notch signalling in the presence of Jagged1 [110].

1.16 Role of Notch in tumorigenesis

The first evidence showing the involvement of Notch in cancer came from studies carried out in T-Acute Lymphoblastic Leukaemia (ALL), where an activating Notch1 mutation was found in 56% of the T-ALL patients [100]. Notch drives tumorigenesis in T-ALL by promoting cell-cycle progression and inhibiting apoptosis [111]. MYC, a driver of cell cycle progression, is also regulated by Notch in T-ALL (33, 34,23). In Acute Myeloid Leukaemia (AML), high levels of Notch1, Jagged1 and DLL1 were each found to be independent factors associated with poor prognosis [112].

Increased expression of Notch1 and Jagged1 is linked to poor prognosis in breast cancer. A recent study showed an up-regulation in the levels of IL-6 by the non-canonical Notch signalling in breast cancer cells. This Notch mediated up-regulation of IL-6 was controlled by the NFκB signalling cascade and by P53. This was shown to be CSL independent and resulted in the reduction of HEY expression [113].

Notch3 is overexpressed in 40% of the Non Small Cell Lung Cancer (NSCLC) patients and is involved in inhibiting apoptosis by activation of the EGFR/MAPK pathway [114]. High expression of Notch1 correlated with poor survival in lung adenocarcinoma patients and suggested inhibiting Notch1 to be a useful strategy for treating these patients [115].

In glioma patients, screening for overexpressed genes showed high levels of Notch1, DLL1 and Jagged1 [116]. Knockdown of these genes in mice resulted in increased apoptosis of glioma cells and increased survival of mice, indicating that Notch signalling drives glioma cell growth. Notch1 also correlated with glioma progression and poor outcome in patients [117].

Notch signalling plays a major role in prostate cancer development and metastasis. A study that included 154 prostate cancer samples showed overexpression of Jagged1 and Notch1 in metastatic prostate cancer patients compared to localised and benign tumours [118]. Knockdown of Notch1 inhibits proliferation and invasion of prostate cancer cells [119].

The Cancer Genome Atlas (TCGA) published data on most common abnormalities in 489 HGSC patients and the results showed dysregulated Notch signalling in 22% of the samples [8]. Studies in ovarian cancer stem cells (CSC) showed Notch3 to play a major role in chemoresistance to platinum based therapies [120]. Also, as previously reported, studies from my lab have shown Jagged1 to be involved in an autocrine cytokine network in ovarian cancer cells. Notch related drug resistance is also seen in colon cancer after treatment with oxaliplatin via activation of survival pathways such as PI3K/AKT [103].

Notch signalling is a 'double-edged sword' because Notch pathway members not only function as oncogenes but it can also act as tumour suppressors in certain cancer types [121]. For example, loss of Notch1 in skin epithelial cells leads to improper epidermal formation and impairs skin barrier integrity, which results in inflammation and tumorigenesis. Cervix development is also regulated by Notch and both an upregulation or downregulation of Notch have been associated with cervical cancer. Notch signalling has also been shown to activate p53 in some cervical cancer studies leading to growth arrest [103].

1.17 Targeting Notch in Cancer

Notch pathway targeting agents are in clinical development in many types of cancers (Table 3). For instance, γ-secretase inhibitors (GSI) for gain of function of Notch are being tested as possible anti-cancer agents [122]. Pre-clinical studies in lung, breast and pancreatic cancer have shown GSIs to suppress tumour growth [123-125]. However, there were numerous side effects witnessed in the *in vivo* studies with GSI treatment. These side effects included alteration of intestinal architecture, increased mucin secretion, epithelial erosion, leucocyte infiltration and abnormal changes in thymus and spleen [126]. At present, there are over 40 clinical trials either in progress or recently completed in T-ALL, breast, colorectal, lung, prostate and pancreatic cancer with GSI inhibitors alone or in combination with other drugs. A phase II clinical trial in metastatic colon cancer using a GSI inhibitor increased PFS by 1.8 months, indicating GSI single agent therapy is not effective [127].

Due to the high level of toxicity observed with the GSI inhibitors, antibodies against Notch receptors or ligands are now being developed. This approach is useful in cases like T-ALL where specific receptors like Notch1 are implicated in tumour growth. Preliminary *in vivo* studies with these specific Notch1/2 inhibitors show promising results, without causing major side effects as witnessed with the GSI treatment [128]. Similarly, pre-clinical *in vitro* and *in vivo* studies with antibodies against Notch ligands like DLL4 are being tested in various models. DLL4 inhibition led to formation of non-functional vessels with poor oxygen and nutrient supply [129]. A recent study using an anti-DLL4 antibody, MEDI0639 in an *in vivo* matrigel plug assay with human endothelial cells, resulted in excessive angiogenic sprouting with very poor α-smooth muscle cell coverage around the vessels, further indicating non-functional vessel formation [130]. MEDI0639 is currently being tested in a phase I trial in advanced solid cancers to test its safety and tolerability. Other DLL4 targeting antibodies are also being tested in combination with ionising radiation in colorectal cancer. The combination therapy resulted in impaired tumour growth by promoting non-functional tumour angiogenesis and extensive tumour necrosis [131].

Notch targeting Agents	Cancer type tested	Developmental Phase
Anti-Notch1 mAb	Breast cancer, colon cancer, T-cell leukemia, anaplastic carcinoma	Pre-clinical studies
Anti-Notch2 mAb	Breast cancer, colon cancer, anaplastic carcinoma	Pre-clinical studies
Anti-Notch2/3 mAb	Solid tumours	Phase 1 trial
Anti-DLL4 mAb	Colorectal cancer, small cell lung cancer, pancreatic cancer and other solid tumours	Phase 1 trial
Soluble forms of Notch1, DLL1 and Jagged1	Endothelial cells	Pre-clinical studies
γ-secretase inhibitors	Breast cancer, prostate cancer, non small cell lung cancer, pancreatic cancer, brain tumours, colorectal cancer, melanoma, T-cell leukemia	Phase 1 clinical trial

Table 3 List of Notch signalling targeting agents in various cancer types.
Data adapted from [132].

1.18 Pericytes

To maintain functional angiogenesis the vascular structure needs to be stabilised by supporting cells. These supporting cells are called pericytes; contractile cells that wrap around the endothelial cells and stabilise the vasculature, regulating micro-vascular blood flow [133].

Pericytes are embedded within the vascular basement membrane and they are known to play a major role in vascular development and homeostasis. Pericytes found on the blood microvessels make focal contact with the endothelium and extend primary cytoplasmic processes along the surface of the endothelium [134].

The interaction between the endothelial cell and the pericyte helps in the regulation of the vascular basement membrane. In most areas, endothelial cells and pericytes are separated by the vascular basement membrane. However, the two cell types come in contact at interfaces where there are holes in the endothelium. There are up to 1000 different contact points that have been described for a single endothelial cell [135]. Among these are areas called the peg pocket contacts in which the finger like cytoplasmic projections of the pericytes are inserted into the endothelial invaginations. Then there are adhesion plaques, which are areas that anchor the pericyte to the endothelial cell via N-cadherin connections. There are also direct connections such as gap junctions between the endothelial cell and pericyte that enable exchange of ions and small molecules [135].

The central nervous system (CNS) has the highest pericyte coverage around the microvessels. The exact role of these pericytes in the CNS is still not clear, however they are believed to play a role in the formation of the blood brain barrier [136]. *In vitro* co-culture studies have suggested that pericytes can improve blood brain barrier function [137]. Pericytes also function as sensors of hypoxia and it can mediate adaptive responses to protect the neurons of the CNS. Another tissue that is abundant with pericyte coverage is the retina. This is due to its high level of metabolic demands and this is also the most sensitive site for partial loss of pericytes [136].

There are several molecular markers used to identify pericytes and they include α-SMA, NG-2, desmin, platelet derived growth factor-beta (PDGFR-β), aminopeptidase A/N and RGS5. Since none of these markers are absolutely specific for pericytes, more than one marker is used or pericytes are identified by their location in relation to the endothelial cells [134].

1.19 Endothelial cell-pericyte interactions

As stated above, endothelial-pericyte communication is critical for blood vessel formation and function [135]. This interaction controls growth signals that inhibit endothelial proliferation. During vascular formation, pericytes are important for vascular pruning and for controlling the number of functional vessels, thereby enhancing tissue perfusion [136].

There are a host of different molecules that control the endothelial-pericyte interactions, regulating each step such as pericyte recruitment, attachment and detachment. TGF-β contributes to the differentiation of precursor cells into pericytes. Various studies have shown the importance of TGF-β in the de novo induction of vascular smooth muscle cells and defective TGF-β signalling leads to embryonic lethality [133]. TGF-β inhibits endothelial cells proliferation and migration. Inhibition of this pathway has shown to shift the balance from differentiation to endothelial proliferation thus resulting in more dilated and irregularly shaped vessels [133].

PDGF-B/PDGFRβ signalling plays a major role in endothelial-pericyte interactions. PDGF-B secreted from the endothelial cells binds to the pericyte PDGFRβ tyrosine kinase receptor. This interaction helps in the proliferation, migration and subsequent recruitment of pericytes to the newly formed vessels. Knockout for the PDGF ligand/receptor causes vascular dysfunction as a result of defective pericytes, which leads to endothelial hyperplasia and abnormal endothelial junctions [136].

Angiopoietin/Tie2 signalling is also implicated in endothelial-pericyte interactions. The two main ligands of this signalling pathway are Angiopoietin1 and 2 (Ang1 and Ang2). Ang1 is produced by the pericytes, Ang2 is expressed by endothelial cells and is located at the leading end of the proliferating vessels. Both these ligands bind to the

Tie2 receptors expressed on the endothelial cell and play a role in endothelial sprouting, vessel wall remodelling and pericyte recruitment (56). Loss and gain of function studies in Ang/Tie2 signalling have shown this pathway to be the gatekeeper of quiescent endothelial cell phenotype [133]. Studies in mice have shown the Ang1-Tie2 signalling to play a critical role in vessel maturation and stabilisation. Knock out of Ang1 or Tie2 in mice resulted in defective angiogenesis with poorly organised basement membrane [136]. The vessels formed in these mice also showed poor coverage and detachment of pericytes. Overexpression studies with Ang1 led to formation of a stabilised vasculature with leakage resistant vessels. Recombinant Ang1 was also able to partially restore the pericyte coverage and thereby rescue the vascular defects in the retina [136].

Ang2 acts as an antagonist of Ang1 and blocks the Ang1/Tie2 signalling resulting in dissociation of pericytes from vessels resulting in reduced pericyte coverage and destabilised vessels (Figure 1.10). Ang2 overexpression phenotype has shown to resemble that of the Ang1 or Tie2 knockout. Therefore, Ang1 and Ang2 expressed on different cell types have opposing effects on angiogenesis, with Ang1/Tie2 paracrine loop resulting in vessel stabilisation phenotype and Ang2/Tie2 autocrine loop in the endothelial cells resulting in a vessel destabilising phenotype [138].

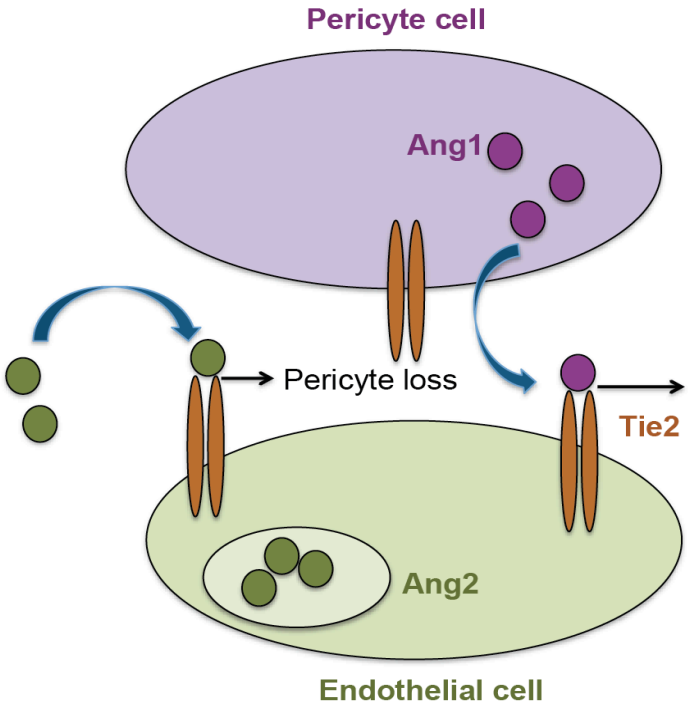

Figure 1.10 Angiopoietin/Tie signalling between the endothelial cells and pericytes.
Ang1 from the pericyte binds to the Tie receptor on the endothelial cell helping in the stabilisation of vessels. Ang2 released from the endothelial cell can act as an Ang1 antagonist and binds to Tie receptors on the endothelial cell resulting in pericyte loss.

N-cadherins found in the interface between endothelial cells and pericytes also play a major role in adhesion of pericytes to endothelial cells [139]. N-cadherins are not important for vasculogenesis, proliferation or migration of vessels but N-cadherin deficiency leads to impairment of pericytes covering the endothelium [140]. Then there are also other factors such as neural cell adhesion molecule (NCAM), vascular cell adhesion molecule (VCAM), EphrinB2 and integrin signalling that are involved in vessel maturation by regulating the adhesion of pericytes to endothelial cells.

Notch signalling is also implicated in vascular smooth muscle cell differentiation. Activation of Notch3 in the smooth muscle cells by Jagged1 initiates the formation of smooth muscle cells around the developing vessels [141]. In contrast, there are several findings showing positive correlation of the Notch ligand DLL4 with α-SMA staining. For example, a study carried out in bladder cancer showed that 98.7% of DLL4 positive tumour vessels were covered with α-SMA as opposed to 64.5% of DLL4 negative tumour vessels [142]. This finding was also supported by loss of function of DLL4 studies, which resulted in increased vascular proliferation with

decreased vessel maturation. The newly formed vessels showed decreased vascular lumen with defective pericyte coverage and reduced tissue perfusion [143].

1.20 Pericyte inhibitors in cancer treatment

As previously mentioned, compared to the normal tissue vasculature, tumour vessels are structurally and functionally abnormal. They are characterised by disorganised and highly dysfunctional vessels with leaky endothelial cell layer and loosely connected or abnormal pericyte coverage. Therefore, studies into understanding the role of pericytes in tumour vasculature have been explored.

Targeting the pericyte in tumour angiogenesis became of interest after anti-VEGF therapy resistance studies showed up-regulation of alternative pro-angiogenic pathways such as PDGF-B/PDGFRβ signalling. Vessels, which are sensitive to VEGF therapies, are mainly composed of immature vessels lacking pericyte coverage and the ones, which are resistant to VEGF therapies tend to be large mature vessels with good pericyte coverage [144]. Therefore, various strategies such as inhibiting especially the PDGF-B/PDGFRβ and Ang/Tie signalling are being tested pre-clinically and clinically to target the pericyte population that stabilises the tumour vasculature.

PDGF receptor kinase inhibitors such as imatinib, sunitinib, sorafenib, pazopanib and nilotanib are now tested in various cancer models. However, none of these inhibitors are specific and they also target other pathways such as c-kit, VEGF and FGF signalling. Imatinib treatment in tumour models resulted in reduced tumour interstitial fluid pressure thereby increasing the uptake of tumour seeking radio labelled antibody. This improved antibody uptake as a result of reduced interstitial fluid was identified as the primary reason for growth arrest in a colorectal cancer model [145]. Therefore, pre-clinical studies with PDGFRβ inhibitors in combination with chemo or radiotherapy displayed some beneficial effects. Similarly, PDGFRβ inhibition along with anti-VEGF therapy in the RIP Tag2 model of pancreatic cancer resulted in 80% reduction in pericyte numbers within the tumours. This correlated with increased cell death in endothelial and tumour cells thereby decreasing tumour growth [146]. However, clinical trial in renal cancer after treatment with VEGF and

PDGFR inhibitors showed no therapeutic benefit in the combination therapy group as compared to the single agent treatment with VEGF inhibition [147, 148].

Targeting Ang/Tie2 signalling in VEGF therapy resistant tumours is also considered an effective way to destabilise vessels by disrupting pericyte-endothelial cell interaction. Trebananib (AMG 386), a peptide tumour protein that interferes with Ang/Tie2 signalling was tested in combination with paclitaxel in a Phase II trial for patients with recurrent ovarian cancer. Even though the study did not result in statistically significant increase in progression free survival, the data suggested evidence of anti-tumour activity [149]. Phase III studies in recurrent ovarian cancer and Phase II studies in breast, colorectal, kidney, stomach and liver cancer are now being conducted [150].

However there have been studies showing no improvement in survival with the combination treatment of VEGF and pericyte inhibition. For example, a study carried out in T241 fibrosarcoma, B16 melanoma and Lewis lung carcinoma used a more specific pericyte depleting method using PDGFRβ deficient mice rather than a tyrosine kinase inhibitor. The study showed that pericyte depleted tumours and control tumours both showed same sensitivity to G6-31 VEGFA antibody. There was no additional decrease in tumour growth or vascular density in the pericyte deficient tumours as compared to the control tumours after treatment with the anti- VEGFA antibody [151].

Also some of these studies, especially the ones using the PDGFRβ inhibitor did not assess the effect of the inhibitor on metastasis. This is important because increasingly pericytes are being reported as the gatekeepers of tumour cell metastasis [138]. Studies in PDGFRβ deficient Rip1Tag2 mice with defective pericytes showed development of metastases in distant organs and local lymph nodes. This suggested that pericyte loss on tumour vessels could lead to escape and spread of tumour cells.

Another critical development in the benefits of restoring stabilised vasculature rather than disrupting the pericyte coverage came from Ang2 targeted studies in cancer treatment (Table 4). Ang2, as previously mentioned, is an antagonist of the Ang1/Tie signalling, and leads to detachment of pericytes from tumour vessels. Ang2 targeting approach was undertaken after studies in breast, gastric and metastatic melanoma

showed Ang2 to correlate with lymph node metastasis in patients [150]. Also, in prostate cancer studies there was higher expression of Ang2 staining in the malignant and metastatic tissue compared to Ang1, which was strongly expressed in non-malignant tissue [152].

More recent studies using recombinant humanised monoclonal antibody against Ang2 have shown promise in breast and colon cancer. There was a 50% reduction in Ang2 protein levels in tumours with a significant decrease in vessel number, density and pro inflammatory $Tie2^{+}$ expressing monocytes, which contribute to tumour progression [153]. Ang2 blocking also reduced tumour vasculature and inhibited progression of late stage metastatic mammary carcinomas and Rip1-Tag2 tumours [154].

Ang2 is also one of the main factors involved in inducing resistance to anti-angiogenic therapies [155]. Combination studies using Ang2 and VEGF blocking agents have been effective in targeting various tumours. This idea of targeting Ang2 and VEGF came from early studies carried out in advanced colorectal and epithelial ovarian cancer, where combined Ang2 and VEGF expression correlated with worse prognosis than either alone [156, 157]. Therefore, studies carried out with Ang2 and VEGF combination therapy in various tumour models have shown increased anti-tumour activity in the combination group as a result of potent inhibition of angiogenesis and tumour growth [158]. Ang2 inhibition has not only shown to inhibit tumour growth and tumour cell dissemination and metastasis but also suppressed the growth of established metastases [154]

The Ang2 receptor Tie2 is also weakly expressed by some circulating monocytes and is upregulated upon recruitment into tumours and differentiation into a subset of perivascular macrophages called Tie2 expressing macrophages (TEMs). These TEMs are similar to M2 polarised macrophages and they respond to Ang2 stimulation and drive tumour angiogenesis. They have also been shown to promote vascular regrowth following anti-angiogenic therapy induced vascular damage. Blocking Ang2 impedes the interaction of TEMs with blood vessels due to failure to upregulate Tie2. Therefore, inhibiting Ang2 cannot only inhibit tumour metastasis directly but also indirectly inhibit TEMs [154]. Hence, the combination therapy of VEGF and Ang2 inhibitors are of great interest now.

Agents	Targets	Tumour
AMG 386	Ang1, Ang2	Tested in Phase I to III trials in ovarian, breast, gastric, hepatocellular and renal cell carcinoma, endometrioid, colorectal cancer and glioblastoma
CVX-060	Ang2	Tested in Phase Ib/II trial in renal cell carcinoma
CVX-241	Ang2, VEGFA	Tested in Phase I trial in ovarian and primary peritoneal disease
MEDI-3617	Ang2	Tested in Phase I trial in advanced solid tumours
REGN910	Ang2	Tested in Phase I trial in advanced solid tumours
AMG-780	Ang2	Tested in Phase I trial in advanced solid tumours
CEP-1198	Tie2, VEGFR	Tested in Phase I trial in advanced solid tumours
MGCD265	Tie2, c-MET, VEGFR1-3	Tested in Phase I/II trials in advanced malignancies, non small cell lung cancer
Regorafenib	Tie2, VEGFR2	Tested in Phase III trials in gastrointestinal and renal cell carcinoma

Table 4 List of Ang/Tie2 targeting agents tested in different phases of clinical trials in tumours.
(Data adapted from [150]).

1.21 IL-6 as an angiogenic factor in Cancer

As previously described, IL-6 and its downstream signalling have also been implicated in resistance to anti-angiogenic therapies [159, 160]. However, in depth investigation into the role of IL-6 as an angiogenic factor in cancer have not yet been explored in detail.

The secretion of IL-6 from endothelial cells was observed a long time ago and over the years more studies have also supported the existence of IL-6Rα on endothelial cells [47, 161, 162]. These observations initiated investigations into the role of IL-6 in angiogenesis. This has led to studies showing the positive regulation of endothelial progenitor cell proliferation and migration by IL-6 in a dose dependent manner [163, 164]

Cohen *et al* investigated the effects of IL-6 on various tumour cell lines and found that IL-6 treatment led to upregulation of VEGF mRNA levels in those cells [165]. Since then, there have been several studies carried out in various cancers further demonstrating the link between IL-6 and VEGF via the common transcription factor NFκB [166]. IL-6 drives HIF-1α production and HIF-1α is a key regulator of VEGF, which further suggests the link between IL-6 and VEGF [167].

IL-6 induced expression and regulation of VEGF in tumours has been demonstrated in various pre-clinical and clinical studies [168-171]. For example, IL-6 is considered as a target in gliobastoma, where it is shown to drive tumour cell invasion and angiogenesis. High levels of IL-6 and VEGF have been reported in gliobastoma patients and monotherapy with either agent has not been that effective. Elevated levels of IL-6 were also found in glioma patients who failed bevacizumab therapy [159]. Therefore combination of IL-6 and VEGF inhibition has become a potential strategy in treating glioma patients.

Similarly, IL-6 was also shown to play a role in the development of resistance in sunitinib treated advanced renal cell carcinoma patients [172]. Elevated levels of IL-6 were also observed throughout the course of sunitinib treatment in hepatocellular carcinoma patients, which further supports, the role of IL-6 in relapse mechanism to anti-angiogenic therapies [160].

IL-6 has also been implicated in the regulation of other angiogenic signalling pathways, such as the Notch signalling pathway which is involved in numerous aspects of tumour angiogenesis including endothelial tip sprouting and vessel maturation [109]. The link between IL-6 and Notch was first reported in a study carried out by Sansone *et al,* in ductal breast carcinoma. According to the study IL-6 regulated a Notch-3 dependent signalling via Jagged1, which promoted self-renewal, hypoxia survival and invasive potential of normal and tumour mammospheres. Administration of anti-IL-6 to tumour mammospheres for 24 hours resulted in down regulation of Notch-3 mRNA and administration of IL-6 yielded Notch-3 mRNA. The data suggested that IL-6 might trigger a potential autocrine/paracrine Notch-3/Jagged1 loop to boost stem/progenitor cell self-renewal in the mammary gland [62]. Also studies from my lab have shown the decrease in expression of Jagged1 with a normalization and reduction in tumour vasculature after the treatment with an anti-IL-6 antibody [35].

Collectively, the involvement of IL-6 in other angiogenic signalling pathways along with the observations from various cancer models, including the findings from the HGSC clinical trial described above, indicate that IL-6 secreted from the malignant cell may effect tumour angiogenesis. This in conjunction with the results from the clinical studies showing IL-6 mediated anti-angiogenic therapy resistance and metastasis, suggests the possibility that IL-6 can act as driver of tumour angiogenesis in the absence of VEGF. Therefore, the hypothesis underlying the research in this study is 'IL-6 drives aberrant angiogenesis independent of VEGF signalling'.

In order to investigate this hypothesis the objectives of my study are as follows:

1. Establish experimental models to study the effects of IL-6 on normal endothelial cell angiogenesis.

2. Investigate the mechanisms of action of IL-6 on endothelial cells

3. Study the effects of IL-6 as an angiogenic factor in ovarian cancer

2 Materials and Methods

In the experiments described in this thesis, I have used VEGFA (VEGF), as this is the most commonly identified ligand in tumours.

2.1 Aortic Ring Assay

The aortic rings cultured in collagen with appropriate medium and angiogenic factors give rise to microvessel growth surrounded by pericytes. Angiogenic activators and inhibitors can be tested for their efficiency in inducing or inhibiting vessel growth using this model.

2.1.1 Extraction of Aorta

C57Black6 mice from 8 to 12 weeks old or Wistar rats weighing between 180-200g were used for this assay. The dead mouse/rat was first surface sterilised using 70% ethanol and then placed back down on a dissecting board in a laminar flow tissue culture hood. The skin was then cut from tail to neck. Once the sternum was located, the ribcage was cut along the middle and the heart and lungs were removed to expose the aorta, which is a deep red line running down the side of cavity. The aorta was then detached from the spine using a closed pair of forceps and closed scissors. 1cm of aorta was then cut and placed in a dish with PBS.

2.1.2 Cleaning

Under the dissecting microscope the extraneous fat, tissue and branching vessels were removed with forceps and a scalpel. Using a 27-G syringe fixed to a 1ml needle, the blood was flushed out of the aorta with OptiMEM (Gibco, cat. no. 51985-026). The aorta was then cut into small 0.5mm size rings and was transferred to a 10cm petri dish with 5ml of serum free OptiMEM + 1X penstrap (PS; PAA, P11-010, 100X). The rings were then incubated overnight at 37°C and 5% CO_2.

2.1.3 Embedding

The collagen mixture was prepared on ice. One-tenth volume of sterile 10X DMEM (Gibco, cat. no. 12800-017) was added to sterile water. Collagen (Millipore, cat. no. 08-115) was then added to a final concentration of 1mg/ml and thoroughly mixed. To this solution, 5N NaOH was added dropwise until the collagen mixture turned pink. 50µl of the collagen solution was distributed in each well of a 96 well plate. The serum starved rings were taken out of the incubator and dried before being placed onto the collagen containing wells. Once the rings were embedded in collagen, the plate was left to set for 1 hour at 37°C and 5% CO_2. The rings were then fed with 150µl of Optimen containing 1%FCS for the control. The concentration used for the other reagents are as follows 30ng/ml VEGF, 50ng/ml hIL-6, 30ng/ml mIL-6, 10ng/ml rIL-6 and 10nM VEGFRi. The medium was changed every 2 to 3 days. The rings were imaged once a week using phase contrast microscopy.

2.1.4 Staining of Aortic rings

The rat and mouse aortic rings we respectively cultured for 1 and 2 weeks before the staining. The rings were washed with PBS, fixed in 4% formaldehyde for 20 minutes. The wells were then washed once in PBS and the rings were permeabilised with 0.5% Triton X-100 in PBS for 30 minutes, before being washed twice in PBS. 100µl of BS-1 Lectin FITC (1 mg/ml; Sigma, cat. no. L9381/L5264) (1:200 in PBS) and anti-actin, α-SMA Cy3 (Sigma, cat. no. C6198) (1:500) was added and incubated overnight at 4°C. In case of the IL-6Rα staining on aortic rings, 100µl of the unconjugated (1 in 200) IL-6Rα antibody was left overnight at 4°C. The following day the rings were washed with PBS and incubated with goat anti-rabbit Alexa 488 antibody (Life Technologies, A-11034) for 2 hours at room temperature. The plates were washed twice in PBS and the rings were removed from the 96 well plate, using a syringe needle, placed on a microscope slide and mounted with Prolong Gold DAPI containing medium (Invitrogen, cat. no. P36931). The slides were left to dry and imaged using confocal microscopy.

2.1.5 Quantification of number, length of sprouts and pericyte coverage

The effect of medium, VEGF and IL6 on the sprout development was assessed by quantification of the average number of sprouts per condition. The length of sprouts was quantified using ImageJ software by drawing radial lines from the base of the aortic ring to the tip of the sprouting new vessel. Each measurement was then saved and the average length per aorta was calculated for each condition. Pericytes were quantified 250microns from the tip of the aortic ring vessel to avoid false positive quantification of activated fibroblast, which are normally found at the stalk of the vessel.

2.2 Tissue culture

2.2.1 Mouse Lung Endothelial cell line (MLEC)

MLEC, kindly given by Prof Kairbaan Hodivala-dilke, were used for most of the *in vitro* studies. Endothelial cells, immortalised with a temperature sensitive oncogene, were isolated as previously described [173]. This protocol used wild type mice crossed with H-2Kb-tsA58 (immorto gene) mice that express a temperature sensitive simian virus. The isolation was carried out by digesting the mouse lungs with collagenase. The digested cells were then further disaggregated in order to produce a single cell suspension. Since the initial suspension of cells contain a mixed population of endothelial cells, macrophages and fibroblasts, they were then subjected to a series of negative and positive sorts resulting in a >90% pure population of endothelial cells [174].

The MLEC medium was prepared as described below:

- 500ml of DMEM (Life Technologies, 10567-014) was mixed with 500ml Hams-F12 nutrient mix (Life Technologies, 31765-027)
- 50mg Heparin (Sigma-Aldrich, H3149) was dissolved in the above prepared medium
- 10 ml of 1X Pen-Strep (PS; PAA, P11-010, 100X) and 10ml of 200mM glutamine was added to the medium and then filtered with a 0.2 µm disposable bottle top filter.
- 25mg of endothelial mitogen (AbD seroTec, 4110-5004) and 100ml of FCS (FBS; PAA, A15-104) was added to the filtered medium and stored at 4°C.

2.2.2 IGROV-1

The human ovarian cancer cell line (IGROV-1) was seeded in endotoxin free RPMI-1640 with L-Glutamine (PAA, E15-840), 10% Fetal Bovine Serum (FBS; PAA, A15-104) and 1X Penicillin/Streptomycin (PS; PAA, P11-010, 100X), and grown under standard conditions (37°C, 5% CO_2). Cells were passaged every 2-3 days after washing in Dulbecco's PBS without Ca & Mg, (PAA, H15-002) and detached with 0.1%/0.04% Trypsin-EDTA in PBS, (PAA, L11-003, 0.5%/0.2%). The cell line was regularly checked for mycoplasma infection.

2.3 Proliferation Assay

70,000 MLEC cells were seeded in a 24 well plate. The following day cells were treated with either 50 or 100ng/ml of VEGF, hIL-6 or mIL-6. The plate was then incubated for 72 hours at 37°C and 5% CO_2. After incubation, the cells were trypsinised and counted using the Vi-cell counter (Beckman Coutler). Each condition was repeated in triplicate.

2.4 Scratch Assay

MLEC cells were cultured to a confluent monolayer in a 12 well plate. A scratch was made in the middle of each well using a p20 tip. The dislodged cells were then removed and cells were washed with PBS. The cells were then treated with 100ng/ml of VEGF or 100ng/ml of human/mouse IL-6 in serum free MLEC medium and placed under a time-lapse microscope. Images of the 'wound' were taken every hour for 16 hours. The wound closure percentage was determined by comparing the surface area of the defined wound area at 0 and 16 hours (% closure = migrated cell surface area / total surface area X 100).

2.5 Staining of MLEC

$2x10^5$ MLEC cells were plated on a coverslip in a 12 well plate. The coverslips were fixed with 4% formaldehyde for 30 min and washed with PBS (3 times for 5 min each). Following fixation the cells were permeablised with 0.1% Triton for 20 min and washed again in PBS. The cover slips were incubated with (1 in 200) rabbit IgG (R&D) or IL-6Rα antibody (1 in 200) (Santa Cruz C-20, Sc-661) overnight at 4°C. The following day the cover slips were incubated with secondary (1:2000) goat anti-rabbit Alexa 488 (Life Technologies, A-11034) for 2 hours at room temperature and then mounted on slides with Prolong Gold DAPI containing medium (Invitrogen, P36931). The images were taken using confocal microscopy. The same was repeated for pSTAT3 (1 in 100)(Cell signalling, D3A7) staining after treatment of the coverslips for 24 hours with human or mouse IL-6 (30ng/ml).

2.6 Drug Treatment for Protein extraction

$3 x10^5$ MLEC cells were plated in a 6 well plate with 2ml MLEC medium (10%FBS). The following day the supernatant was removed and the cells were treated with either VEGF (30ng/ml), hIL-6 (30ng/ml), mIL-6 (30ng/ml) or VEGFRi (100nM) in serum free MLEC medium. At 24 hours the cells were lysed for protein extraction by using a commercial Extraction Buffer (1% Triton (Sigma -Aldrich) in which we added 1X protease inhibitor cocktail (Complete Mini Protease Inhibitor Cocktail,

Roche, Burgess Hill, UK). Cells were then harvested using a cell scraper and the samples centrifuged at 4°C for 10 minutes. The cell pellet was discarded and the supernatant retained for protein quantification using the bicinchonic acid assay (BCA). Lysis was carried out at different time points depending on the protein analysed e.g. for pSTAT3 and pERK 5min, 30min, 2 hours, 6hours and 24hours were tested. For all the other ligands 6 hours and 24 hour time points were the standards time points analysed.

$3x10^5$ IGROV-1 cells were plated in a 6 well plate with 2ml RPMI (10% FBS) medium. The following day the medium was replaced with serum free RPMI and the cells were treated with IgG/diluent (control), anti-IL-6 antibody (20µg/ml), VEGFRi (100nM) or anti-IL-6 + VEGFRi. After 24 hours of treatment the above-mentioned protein extraction method was carried out to lyse the cells.

2.7 BCA assay

The BCA assay was used to measure protein concentration. BCA combined with copper sulphate is a highly alkaline solution, with a pH around 11. Protein peptide bonds react with Cu2+ ions in the solution, reducing the ions to Cu1+, resulting in a colour change from green to purple as Cu1+ ions accumulate. This colour change is directly proportional to the amount of protein present, enabling quantification of protein concentration upon measurement of colour intensity.

2.7.1 Procedure

A BSA (Bovine Serum Albumine) stock solution at 50mg/ml was prepared and diluted to make concentrations of 5mg/ml and 2mg/ml. Working standards were then prepared depending on the estimated protein concentration as shown in the Table 5.

Table 5 Standard dilution used for the BCA assay

BSA Solution	Vol. BSA (µL)	Vol. PBS (µL)	Protein Concentration (µg/µL)
2mg/mL	0	100	0
	10	90	0.2
	20	80	0.4
	30	70	0.6
	40	60	0.8
	50	50	1.0

Protein samples were diluted 1:10 or 1:5 with water, and 10µl of diluted sample were added to the 96 well plate in triplicates. 50 parts of bicinchoninic acid solution (Sigma, B9643-L) was combined with 1 part of copper (ii) solution (Sigma, C2284). 200µl of this solution was added to each well. The plate was incubated for 30 minutes at 37°C and the optical density was then read using the Opsys MR plate reader (Dynex Technologies) at 595nm.

2.8 Western blotting

There are three main steps involved in Western Blotting and they include (i) separating the proteins according to their polypeptide chains using SDS gel electrophoresis, (ii) transferring them to a polyvinylidine fluoride (PVDF) membrane and (iii) detecting the protein of interest using specific antibodies. SDS is negatively charged and it solubilises the proteins. The negative charge on Sodium Dodecyl Sulphate (SDS) neutralises any positive charge present on the protein. This results in proteins having identical charge per unit mass, which helps their fractionation by size. The list of western blotting antibodies used and its dilutions are shown in Table 6.

2.8.1 Procedure

10% acrylamide gels were made using AccuGel 19:1 (National Diagnostics, 10-10-07), 4x Protocol Resolving Buffer (National Diagnostics, 11-05-18), Protocol Stacking Buffer (National Diagnostics, 08-02-27), Ammonium persulfate (Sigma, 104H0456) and TEMED (Sigma, 116H1117). Laemmli Buffer (62.5mM Tris-HCL, 2% SDS, 25% Glycerol, 0.01% Bromophenol blue) was used as the loading buffer. It was added to each sample 1 in 6 according to the volume of protein solution then centrifuged briefly and incubated at 95°C for 5 minutes. The samples were then loaded onto the gel next to a protein molecular weight standard (Biolabs Cambridge, size varying between 230-10kDa). Running buffer was prepared using 25mM Tris Base, 250mM glycine, 0.1% SDS in H_2O (Invitrogen). The gel was run at 100V until the marker reached the bottom of the well. Using the Bio-Rad transfer system the resolved proteins were transferred onto the PVDF membrane (Perkin Elmer, Waltham, MA, US). In the transfer cassette, a sandwich was made between Scotch-Brite pads, Chromatography paper (Whatman, Maidstone, Kent), gel and the membrane. The cassette was then placed in the transfer tank with an ice pack and filled with transfer buffer (27mM Tris, 192mM Glycine, 20% methanol). The transfer was run at 100 Amps for 90 minutes.

In order to avoid non-specific binding, the membrane was blocked in blocking buffer (5% w/v skimmed milk powder (Marvel, Spanning, Lincolnshire) in TBST (50mM TrisHCL, 150mM NaCl, 0.1% Tween™-20) for one hour at room temperature. After incubation, the blocking solution was removed and the primary antibody diluted in the blocking buffer according to the dilution shown in the table below. The membrane was then incubated overnight on a roller at 4°C or incubated for 1 hour at room temperature. Following incubation with the primary antibody, the membrane was washed 3 times in TBST (5 minute each) and the secondary antibody horseradish peroxidase (HRP) conjugate was diluted 1:2000 and applied for 1 hour. This was followed by 3 washes (5 minute) in TBST at room temperature. The protein bands were visualised using ECL plus TM Western Blotting Detection Reagents (Amersham) and Hyperfilm ECL (Amersham). If required, membranes were

stripped using 1X Re-blot Plus Strong (Millipore) for 5 minutes before incubation in blocking buffer.

Table 6 Western blotting Antibodies and Dilution

Primary Antibody	Dilution	Secondary Antibody	Dilution
pSTAT3 (Cell signalling, D3A7)	1:1000	Rabbit	1:2000
STAT3 (Cell signalling, 4904)	1:1000	Rabbit	1:2000
pERK (Santa Cruz, sc-7383)	1:1000	Mouse	1:2000
ERK (Cell signalling, 137F5)	1:1000	Rabbit	1:2000
Jagged1 (Abcam, ab7771)	1:1000	Rabbit	1:2000
DLL4 (Abcam, ab7280)	1:1000	Rabbit	1:2000
Angiopoietin-2 (Abcam, ab8452)	1:500	Rabbit	1:2000
HEY (Abcam, ab22614)	1:500	Rabbit	1:2000
β-ACTIN (Sigma, A1978)	1:10000	Mouse	1:5000

2.9 *In vivo* injection of IGROV-1 cell lines and anti-IL-6 treatment

8 weeks old Balb/c nude female mice were injected i.p with $1x10^7$ IGROV-1-luc cells in 200µl of sterile, endotoxin free, PBS. After 24 hours, anti-IL-6 antibody (Med Immune) was prepared at a concentration of 20mg/kg in sterile, endotoxin free, PBS and mice were injected i.p with 200µl of this solution twice weekly for 4 weeks. Control mice were injected with 200µl of 20mg/kg IgG control antibody.

At 24 hours, 1 week, 2 weeks, 3 weeks and 4 weeks after tumour cell injection, mice were imaged in order to monitor tumour growth and spread by bioluminescent assay. For this purpose, mice were anaesthetised with isoflourane and injected with 100 µl luciferin i.p. (3 mg) 10 minutes before imaging (IVIS).

2.10 Visualisation and staining of tumour blood vessels

In order to visualise the architecture of blood vessels, 4 mice from each group were anaesthetised with isoflourane and injected with TRITC-conjugated *Bandeiraea simplicifolia* (lectin; 100µl, 2mg/ml; Sigma L5264) via the tail vein, 3 min before being perfused with 4% paraformaldehyde. Following fixation overnight the resected primary tumours were cryoprotected in 12%, 15%, and 18% sucrose for 1 hour each. Tumours were subsequently snap frozen in ornithine carbamyl transferase compound (Sankura Finetek, Torrance, CA) and sectioned at 10µm intervals.

The frozen sections from the lectin stained *in vivo* IGROV-1 xenograft study were then stained for pericyte markers by immunofluorescence. The slides were first washed in PBS X3 (5 min each) and a PAP pen was used to draw sections around the tumour areas. The slides were permeabilised with 0.1% Triton in PBS for 5 min at room temperature; washed again with PBS X2 (5 min each) and then blocked with blocking buffer (5% serum, 2.5% BSA in PBS) for 1 hour at room temperature. The primary antibodies were diluted in the blocking buffer i.e. 1 in 100 anti-α-SMA FITC (abcam, ab8211), 1 in 100 Mouse IgG2a (FITC) isotype control (ab81197), 1 in 50 or anti-NG2 (Millipore, ab5320) were incubated overnight at 4°C. The following day the sections were washed in PBS X3 (5 min each). Slides were then mounted with Prolong Gold DAPI containing medium (Invitrogen, P36931) and left to dry. Images were taken using confocal microscopy (Zeiss LSM S10 META).

2.11 Immunohistochemistry

Immunohistochemistry was performed on paraffin embedded sections of the remaining four mice from the two groups of the *in vivo* IGROV-1 tumours treated with the anti-IL-6 antibody (outlined in section 1.9). The antibodies and dilutions

used are summarised in Table 7. The streptavidin-peroxidase method used for immunostaining was performed on all tissue sections using the ABC kit (Vector Labs) with the following steps:

1) Tissue sections from the *in vivo* IGROV-1 xenografts were deparaffinised in xylene then rehydrated in graded ethanol as follows;

xylene	2 x 5 min
100% ethanol	2 x 2 min
95% ethanol	2 x 2 min
70% ethanol	2 x 2 min
50% ethanol	1 x 2 min
ddH_20	2 x 2 min

2) Antigen retrieval was carried out by immersing tissue sections in citrate buffer consisting of 2.5 ml Vector Antigen Unmasking solution (Vector laboratories, Peterborough, UK) in 250 ml ddH_20 and microwaving at 700W in a chamber for 10 min; followed by incubation at RT for 15 min.

3) Sections were washed in PBS X3 (5 min each).

4) PAP pen (Vector Labs) was used to draw around the tumour areas.

5) Sections were incubated in blocking buffer (rabbit or goat serum depending on species of antibody) for 45 min and drained.

6) The primary antibodies diluted in blocking buffer was added to the slides and incubated overnight at 4°C.

7) The primary antibody was aspirated the next day and washed in 3X PBS (5 min each).

8) The slides were incubated with biotinylated secondary antibody diluted 1:200 in blocking buffer at RT for 2 hours.

9) Sections were washed in 3XPBS (5 min each).

10) Avidin-Biotinylated enzyme Complex (ABC, Vectastain Standard Kit, Vector Laboratories, Peterborough, UK) was prepared and left on ice for at least 30 min.

11) Endogenous peroxide activity was blocked using 5ml of 30% H_2O_2 in 250 ml methanol at RT for 20 min.

12) The slides were washed 3 times in PBS (5 min each).

13) This was followed by incubation of the slides with Avidin-Biotinylated enzyme Complex in a covered humidified chamber at RT for 30 min. Sections were washed 3 times in PBS (5 min each).

14) Peroxidase substrate was prepared by vortexing one diaminobenzidine (DAB) tablet with one Tris/peroxide tablet in 15ml dH_2O (Sigma Aldrich, Gillingham, UK, D4418). The DAB solution was applied through a 0.45µm filter and sections were incubated for 3-20 min.

15) The sections were then briefly washed in water and counterstained in haematoxylin for 1 min, then immersed in differentiating solution (750µl ammonium hydroxide in 250 ml dH_2O).

16) Slides were dehydrated as follows;

100% isobutanol	20 dips
100% isobutanol	2 x 2 min
xylene	2 x 2 min

17) Sections were cleared and mounted whilst moist with DPX (Fisher, Loughborough, UK); coverslips were placed and slides left to air dry.

Table 7 Summary of Primary Antibodies for IHC analysis

Primary antibody	Dilution	Secondary antibody species
DLL4 (R&D Systems, af1389)	1:100	Goat
Jagged-1 (R&D Systems, af1277)	1:100	Rabbit
Angiopoietin 2 (Abcam, ab8452)	1:50	Rabbit

3 Actions of IL-6 in a model of angiogenesis

3.1 Aortic ring assay

Many experimental models have been developed to study the mechanism of angiogenesis and to test the efficacy of the anti-angiogenic agents [175]. These experimental models include *in vitro* cell based assays such as the endothelial tube formation or chemo-attractant induced endothelial cell migration assays. Then there are *in vivo* models of tumour angiogenesis or subcutaneously implanted sponges or matrigel plug assays [176].

There are several advantages and disadvantages to these methods. The *in vivo* angiogenesis techniques involve various cell types with a complex balance of pro and anti-inflammatory factors that work together to regulate blood vessel formation. This helps to fully understand the process of neovascularisation. The *in vivo* tumour models also have disadvantages e.g. they are relatively expensive and they also involve inflammatory and other stromal components which make it difficult to understand the direct effect of the malignant or stromal cells on angiogenesis. The implantation of the sponge or matrigel plugs may also stimulate inflammation and thereby further affect the process of angiogenesis [176].

These problems can be avoided in the *in vitro* endothelial cell assays, which are comparatively less expensive and growth factor stimulation can be studied directly without any interference from other cell types. However this system lacks sprouting of blood vessels and there is also absence of pericytes, which are important in the stabilisation of the vessels. These problems can be avoided by using the aortic ring model which is an *ex vivo* assay that bridges the gap between existing *in vivo* and *in vitro* assays [177].

Aortic ring cultures are composed of mixed populations of endothelial cells, pericytes, fibroblasts, macrophages and dendritic cells. The first cells to migrate out of the aortic rings after 1-2 days are fibroblasts and macrophages. Endothelial sprouts appear after 2-3 days of culture. The neovessel tips are made of highly migratory cells, which probe the surrounding matrix with filopodia-like processes. Staining for

cell proliferation markers such as Ki-67 show that the endothelial tip cells migrate without diverting whilst trailing endothelial cells actively proliferate. Over time neovessels become surrounded by pericytes, which migrate and proliferate along the endothelium. After sprouting, branching and forming networks for approximately 1-2 weeks, vessels stop growing and begin to regress [177].

I decided to use the aortic assay to test the angiogenic potential of IL-6 and to ask if IL-6 alone could stimulate microvessel outgrowths.

3.2 Setting up the Aortic ring Assay

I wanted to first establish this model of angiogenesis in my lab by optimising various conditions. The first series of aortic ring experiments were set up to establish sprout formation in my positive control group using VEGF, which has been long studied for its angiogenic effects on endothelial cells [176].

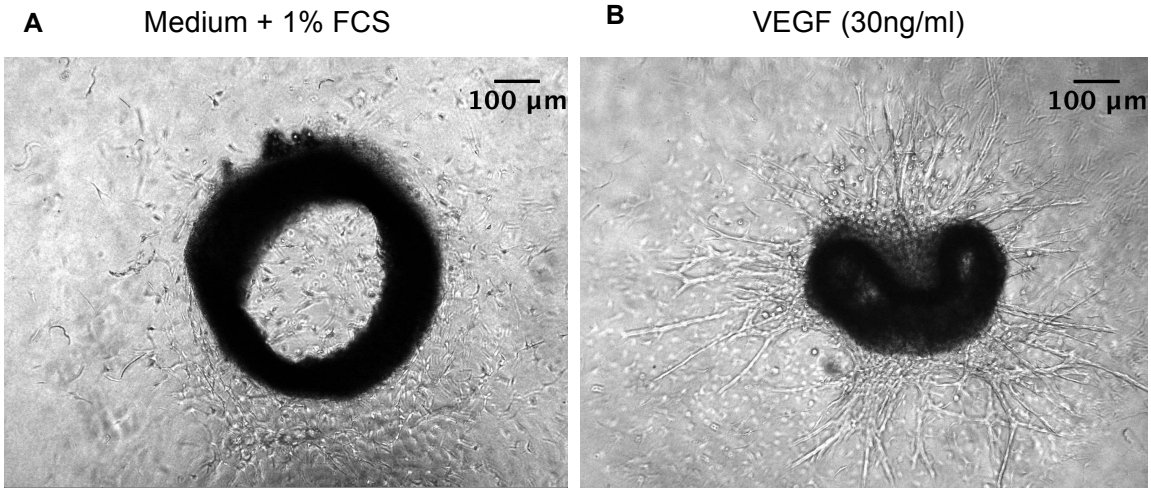

Figure 3.1 Phase-contrast images of aortic rings embedded in type I collagen showing microvessel outgrowth.
Aortas removed following cervical dislocation of 8-12 week old mice were treated with optimem medium containing 1% FCS (**A**) or recombinant VEGF (R&D) at 30ng/ml (**B**) for 2 weeks. The medium was changed every 3 days and the rings were imaged using phase contrast microscopy.

Figure 3.1A shows the growth of fibroblasts from an aortic ring grown in medium containing 1% FCS. This ring did not however produce any microvessel growth and was used as a negative control. In case of the positive control there were extensive sprouting vessels visible in the aorta treated with recombinant VEGF (30ng/ml)

(Figure 3.1B). I was able to overcome the difficulty of optimising VEGF concentration, since other departments in my Institute have already studied the effects of VEGF on the aortic ring assay. Therefore, I only attempted a small optimisation experiment testing 20, 30 and 40ng/ml, which suggested there was not much difference between the 30 and 40ng/ml of VEGF on sprouting. VEGF optimisation studies in other labs have also shown that higher concentrations of VEGF inhibited vessel growth. I carried out a small experiment to test the effects of high concentration of VEGF on blood vessel formation in the aortic ring assay.

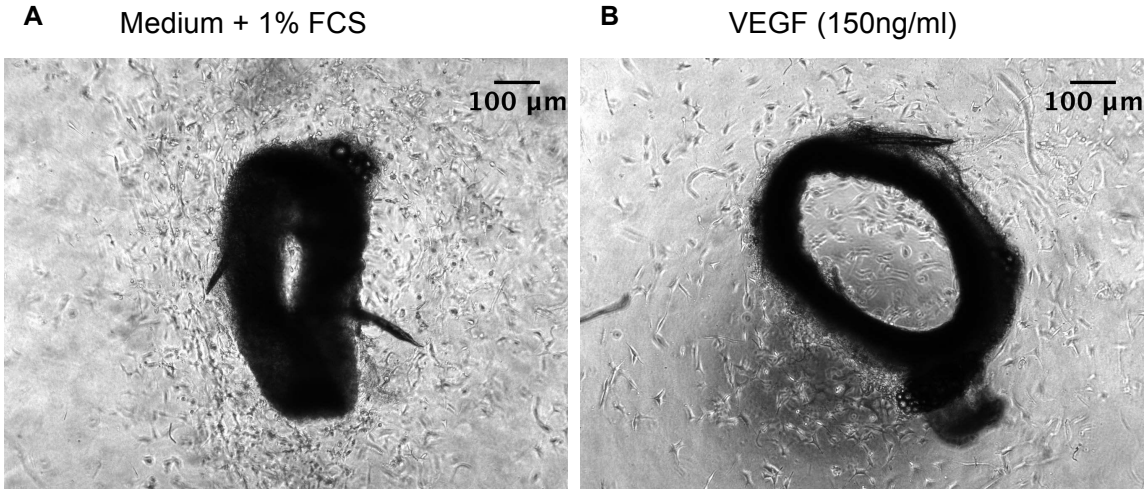

Figure 3.2 Phase-contrast images of aortic rings embedded in type I collagen for a period of two weeks.
Aortas removed following cervical dislocation of 8-12 week old mice were treated with optimem medium containing 1% FCS (**A**) or recombinant VEGF (R&D) at 150ng/ml (**B**) for 2 weeks. The medium was changed every 3 days and the rings were imaged using phase contrast microscopy.

Figure 3.2B shows that at concentrations of 150ng/ml and above VEGF can have an inhibitory effect on sprout formation and this agreed with the findings of other labs in our centre. Some studies have indicated that the extension and maintenance of the tip cell is dependent on VEGF signalling via the receptor VEGFR2 [178]. It was reported that high concentrations of VEGF can trigger high levels of DLL4 which in turn can inhibit VEGFR2 and thereby dampen the responsiveness of VEGF to its receptor [179]. This could be a possible explanation for the inhibitory effect observed with high levels of VEGF on sprout formation in the aortic ring assay.

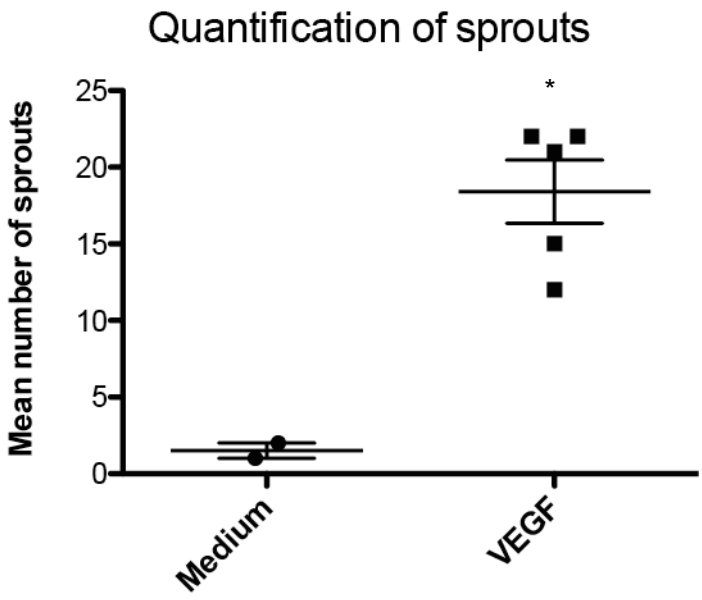

Figure 3.3 Mean number of sprouts in aortic rings treated with Medium and VEGF.

Aortas removed following cervical dislocation of 8-12 week old mice were treated with optimem medium containing 1% FCS or 30ng/ml VEGF (R&D) for 2 weeks. The medium was changed every 3 days. The rings were imaged using phase contrast microscopy and microvessel outgrowth was counted and quantified. Combines results from 2 independent experiments. * Represents statistical significance (p value < 0.005).

One of the angiogenic parameters that can be measured using the aortic ring assay is quantification of the number of microvessel sprouts to determine the potency of the angiogenic agent. This was usually carried out towards the end of the experiment by counting the number of branching vessels under the microscope then calculating the mean per condition. There were significantly more sprouts in the VEGF treated aortic rings compared to the medium treated aortic rings as shown in Figure 3.3. This experiment was repeated in order to optimise various experimental conditions and to obtain consistent results.

3.3 To study the effects of human IL-6 in the mouse aortic ring assay

Next, I wanted to investigate the effect of IL-6 on angiogenesis using the aortic ring assay. A human anti-IL-6 (hIL-6) antibody was effective in reducing the tumour vasculature in IGROV-1 xenograft, suggesting that the hIL-6 produced by the malignant cells had a paracrine effect on mouse endothelial cells [35]. Hence, I wanted to ask if a recombinant hIL-6 could stimulate microvessel formation in the mouse aortic ring assay. Initially, I set up an aortic ring assay with 30ng/ml of hIL-6, the same concentration used for VEGF and the study showed fibroblast production without any microvessel growth. I therefore, carried out a dose response experiment with increased concentrations of hIL-6.

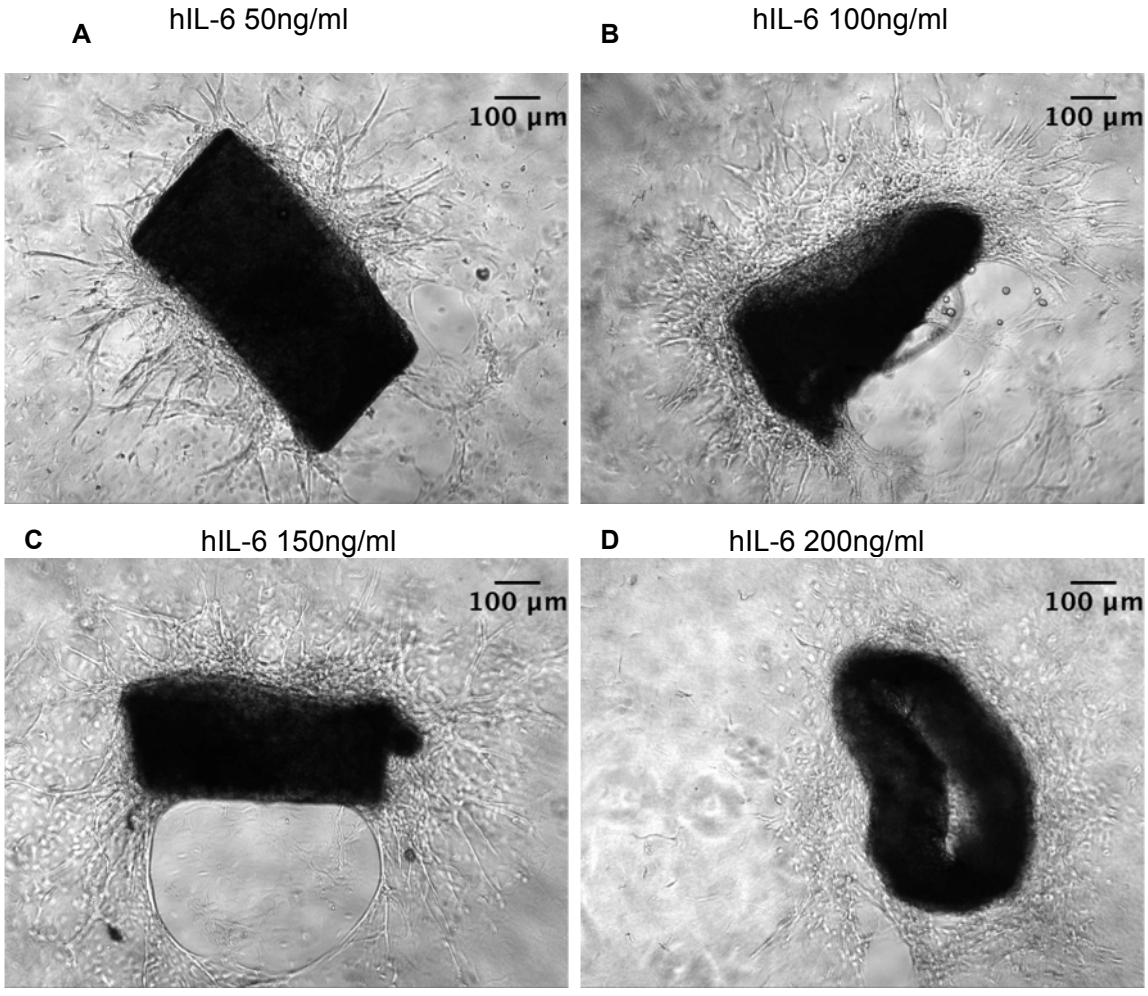

Figure 3.4 Phase-contrast images of aortic rings embedded in type I collagen showing microvessel outgrowth.

Aortas removed following cervical dislocation of 8-12 week old mice were treated with optimem medium containing 1% FCS (**A**), hIL-6 (R&D) at 50ng/ml (**B**) hIL-6 (R&D) at 100ng/ml (**C**) hIL-6 (R&D) at 150ng/ml or (**D**) hIL-6 (R&D) at 200ng/ml, for 2 weeks. The medium was changed every 3 days and the rings were imaged using phase contrast microscopy.

Figure 3.4 shows an aortic ring experiment with recombinant hIL-6 at varying concentrations i.e. 50ng/ml (**A**), 100ng/ml (**B**), 150ng/ml (**C**) and 200ng/ml (**D**). Sprout formation is visible in Figure 4.3 (**A**), (**B**) and (**C**), indicating 50-150ng/ml of hIL-6 is pro-angiogenic and can stimulate microvessel growth. Concentrations higher than 150ng/ml as shown in Figure 3.4(**D**) have attenuating effect on vessel growth, indicating similar to VEGF, too high concentration of hIL-6 can be toxic to vessel formation.

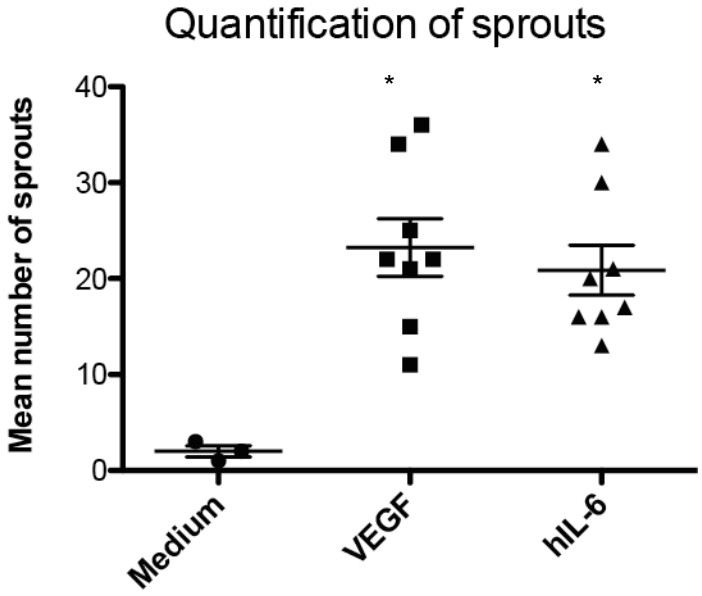

Figure 3.5 Mean number of sprouts in aortic rings treated with Medium, VEGF and hIL-6.

Aortas removed following cervical dislocation of 8-12 week old mice were treated with optimem medium containing 1% FCS with 30ng/ml VEGF (R&D) or 50ng/ml hIL-6 (R&D) for 2 weeks. The medium was changed every 3 days. The rings were imaged using phase contrast microscopy and microvessel outgrowth was counted and quantified. Combined results from 3 independent experiments. * Represents statistical significance. Medium vs VEGF (p value < 0.002), medium vs hIL-6 (p value < 0.002).

Figure 3.5 shows that the mean number of sprouts in aortic rings treated with medium, VEGF 30ng/ml and hIL-6 50ng/ml. There was a significant difference between the number of sprouts induced by medium compared to VEGF and hIL-6, however there was no significant difference in vessel sprouting observed between VEGF and hIL-6 treated aortic rings at these doses. The molecular weight of VEGF and IL-6 are very similar hence the molar concentrations were 1.4μM for 30ng/ml VEGF and 2.0μM for 50ng/ml of hIL-6. Higher concentrations of hIL-6 might be

required compared to VEGF because of the specificity of the mouse VEGF to mouse aortic ring compared to hIL-6 on mouse aortic ring. There were some anomalous rings which either produced too high or too low number of sprouts. Hence, the highest and lowest outliers from both groups were eliminated from the mean. Collectively, results from Figure 3.4 and 3.5 indicate that hIL-6 itself can induce microvessel growth and is as potent as VEGF in the aortic ring assay.

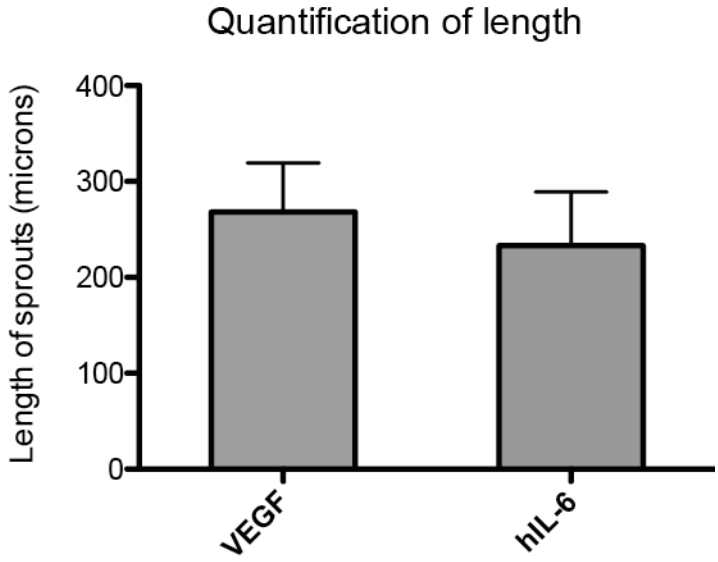

Figure 3.6 Mean length of sprouts in aortic rings treated with VEGF or hIL-6.
Aortas removed from 8-12 week old mice were treated with optimem medium containing 1% FCS with 30ng/ml VEGF (R&D) or 50ng/ml hIL-6 (R&D) for 2 weeks. The medium was changed every 3 days. The rings were imaged using phase contrast microscopy and the length of sprouts was measured using ImageJ analysis. Results from 3 independent experiments, average of three rings each per experiment.

Another angiogenic parameter that can be measured with the aortic ring assay is the length of the sprouting vessels. This also gives an indication of the proliferation capacity of the stalk cells in the presence of the angiogenic stimulator or inhibitor. This is usually carried out using the ImageJ software by drawing radial lines from the base of the aortic ring to the lengths of the sprouting microvessel and saving these data to calculate average values per treatment. Figure 3.6 shows that there was no significant difference in the lengths of sprouts between the VEGF and hIL-6 treated groups.

3.4 To study the effects of mouse IL-6 in the mouse aortic ring assay

Once the effects of hIL-6 on mouse aortic ring assay were established, it was important to confirm this effect using recombinant mouse IL-6 (mIL-6). This would give further validation of the binding of the recombinant protein to its receptor and also verify the effects observed with hIL-6. In order to investigate the effects of mIL-6, first an optimisation experiment was carried out with differing concentrations of mIL-6.

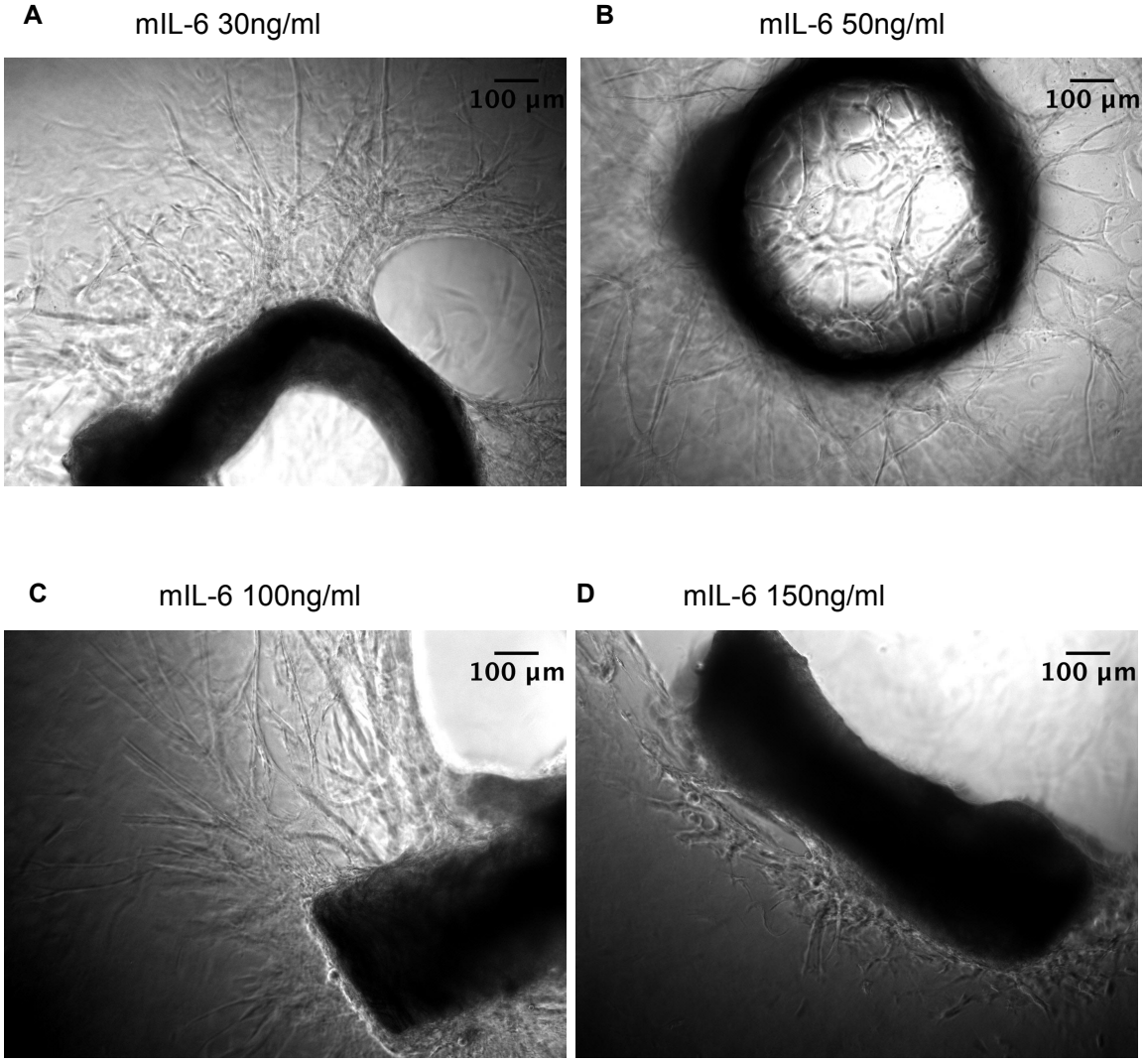

Figure 3.7 Phase-contrast images of aortic rings embedded in type I collagen showing microvessel outgrowth.
Aortas removed following cervical dislocation of 8-12 week old mice were treated with optimem medium containing 1% FCS (**A**), mIL-6 (R&D) at 30ng/ml (**B**) mIL-6 (R&D) at 50ng/ml (**C**) mIL-6 (R&D) at 100ng/ml and (**D**) and mIL-6 (R&D) at 200ng/ml, for 2 weeks. The medium was changed every 3 days and the rings were imaged using phase contrast microscopy.

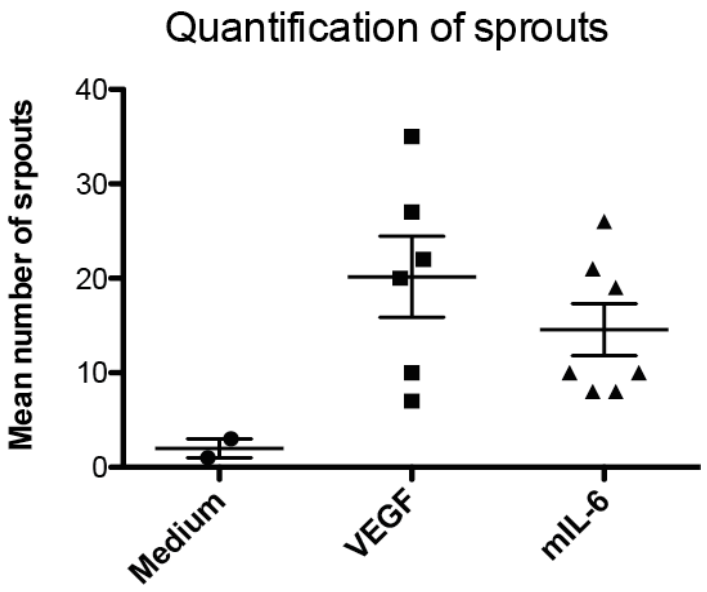

Figure 3.8 Mean number of sprouts in aortic rings treated with Medium, VEGF or mIL-6.

Aortas removed following cervical dislocation of 8-12 week old mice were treated with optimem medium containing 1% FCS, 30ng/ml VEGF (R&D) or 30ng/ml mIL-6 (R&D) for 2 weeks. The medium was changed every 3 days. The rings were imaged using phase contrast microscopy and microvessel outgrowth was counted and quantified. Results from 2 independent experiments are shown above. Medium vs VEGF (p value < 0.06), medium vs mIL-6 (p value < 0.06)

Figure 3.7 shows the phase contrast images for the dose response experiment carried out with mIL-6 at 30, 50, 100 and 200ng/ml. The results indicated that concentrations as low as 30ng/ml of mIL-6 can induce microvessel sprouting. Similar to hIL-6, high concentrations of mIL-6 i.e. 200ng/ml had an inhibitory effect on vessel sprouting. This experiment verified the previous angiogenic effects observed with hIL-6 on mouse aortic rings.

After the completion of the initial mIL-6 dose response experiment, aortic ring experiments were set up to quantify the difference in 30ng/ml VEGF and 30ng/ml mIL-6 induced sprouting. Figure 3.8 shows the mean number of sprouts between VEGF and mIL-6 treated aortic rings. The quantification of number of sprouts between medium and VEGF and mIL-6 just failed to reach significance. This could have been because the sprouting witnessed in the above mIL-6 experiment (Figure 3.8) was relatively low compared to the initial dose response experiment (Figure 3.7). It was clear there were some inconsistencies in the mouse aortic ring experiments.

This could have happened because the mice used sometimes were older than 12 weeks resulting in more accumulation of fat around the aortas, which makes it difficult to remove the fat and ultimately leads to tissue damage.

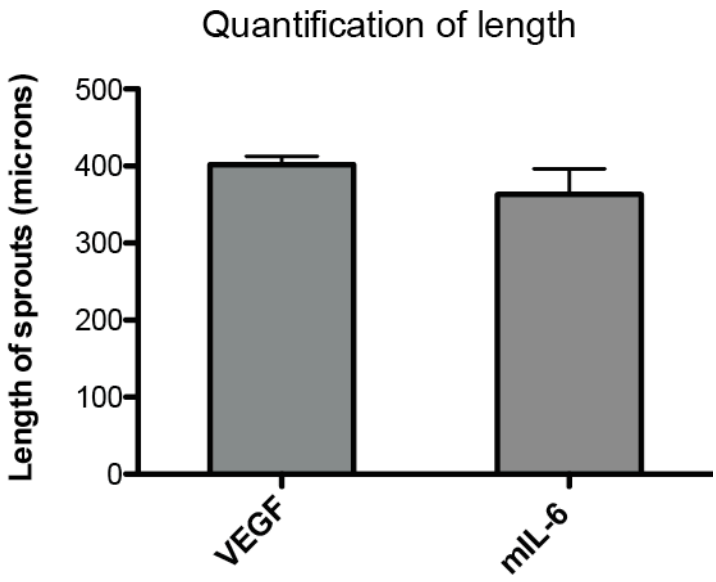

Figure 3.9 Mean length of sprouts in aortic rings treated with VEGF or mIL-6.
Aortas removed following cervical dislocation of 8-12 week old mice were treated with optimem medium containing 1% FCS with either 30ng/ml VEGF (R&D) or 30ng/ml mIL-6 (R&D) over a course of 2 weeks. The medium was changed every 3 days. The rings were imaged using phase contrast microscopy and the length of sprouts was measured using ImageJ analysis. Results from 2 independent experiments, n= 5 for VEGF and 7 for mIL-6.

Figure 3.9 shows the quantification of length of sprouts between VEGF and mIL-6 treated aortic rings. The results were quantified as mentioned earlier by using the ImageJ software by drawing radial lines from the base of the aortic ring to the lengths of the sprouting microvessel and saving these data to calculate average values per treatment. The above results were similar to the results obtained with the hIL-6 and showed no significant difference in the lengths of sprouts between the VEGF and mIL-6 treated groups.

3.5 To study the effects of rat IL-6 in the rat aortic ring assay

Due to the difficulty in obtaining enough rings to gather consistent data from the mouse aortic ring experiments, I decided to experiment with rat aortic rings, which had been tested and shown to be more sensitive to VEGF by other labs in my Institute. Rat aortas are considerably bigger in size than mouse aortas, hence, around 25-30 rings can be cut from each rat aorta compared to 15-20 rings from the mouse aortas. This increases the success rates of each experiment by allowing the use of more rings per condition and also helps in the handling of the aortas since they are not so easily damaged as mouse aortas. Also, unlike the mouse aortic ring experiments, which usually take two weeks to obtain results, the rat assay only requires about a week in culture with just two medium changes. Rat aortic rings had already been tested by one of our collaborators who had also established the optimal dose of VEGF (10ng/ml) to be used in the rat aortic ring assay. Therefore, for the dose response experiment of rIL-6, I used 10ng/ml as the initial starting concentration.

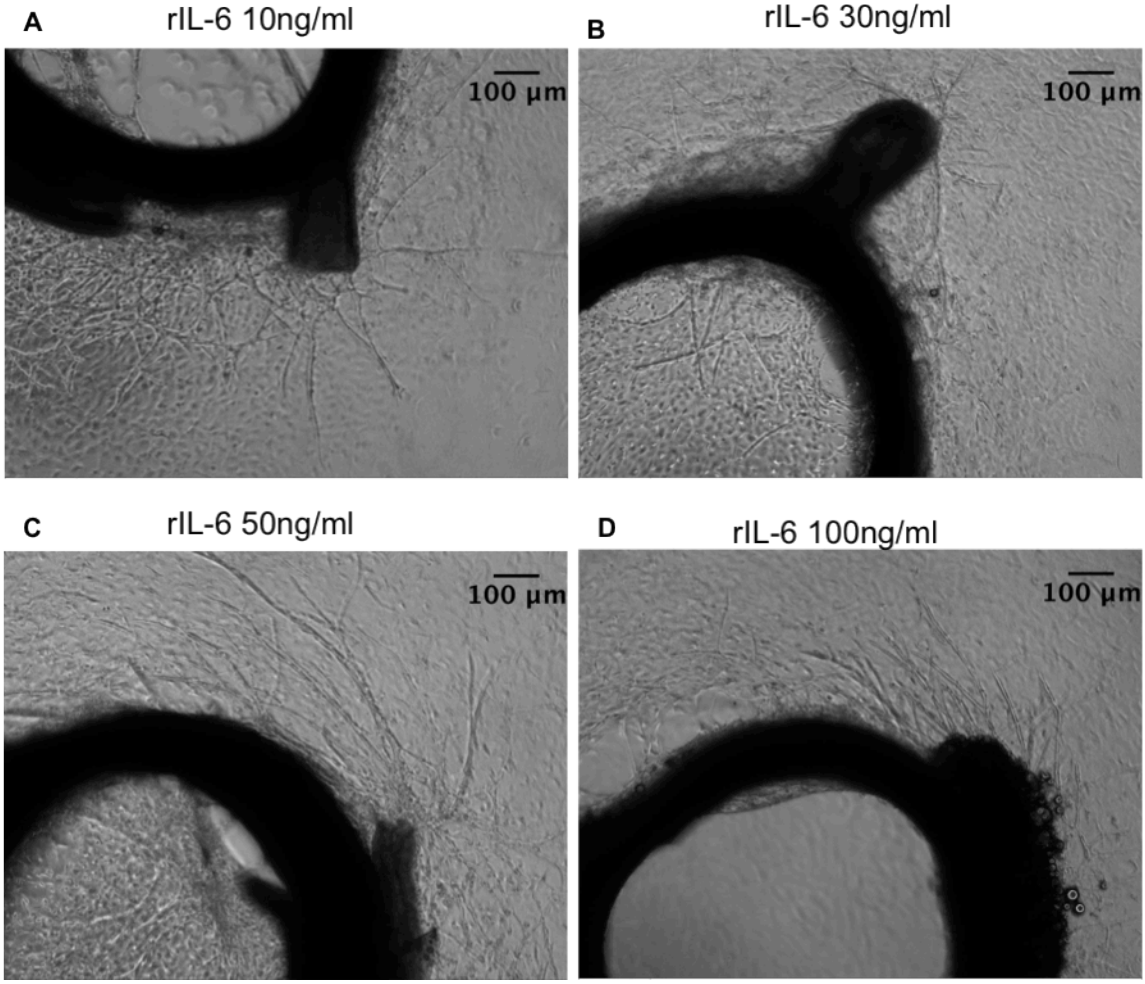

Figure 3.10 Phase-contrast images of aortic rings embedded in type I collagen showing microvessel outgrowth.

Aortas removed following cervical dislocation of 180-200g wistar male rats were treated with optimem medium containing 1% FCS (**A**), rIL-6 (R&D) at 10ng/ml (**B**) rIL-6 (R&D) at 30ng/ml (**C**) rIL-6 (R&D) at 50ng/ml and (**D**) rIL-6 (R&D) at 100ng/ml, for one week. The medium was changed every 3 days and the rings were imaged using phase contrast microscopy.

As shown in Figure 3.9, concentrations starting from 10-100ng/ml of rIL-6 were capable of inducing sprouting in the rat aortic ring assay. The results were similar to hIL-6 and mIL-6 dose response experiments, high concentrations of rIL-6 resulted in less microvessel outgrowths. Since the rat aortic rings are considerably bigger in size than mouse aortic rings it was not possible to take phase contrast image of the entire rings.

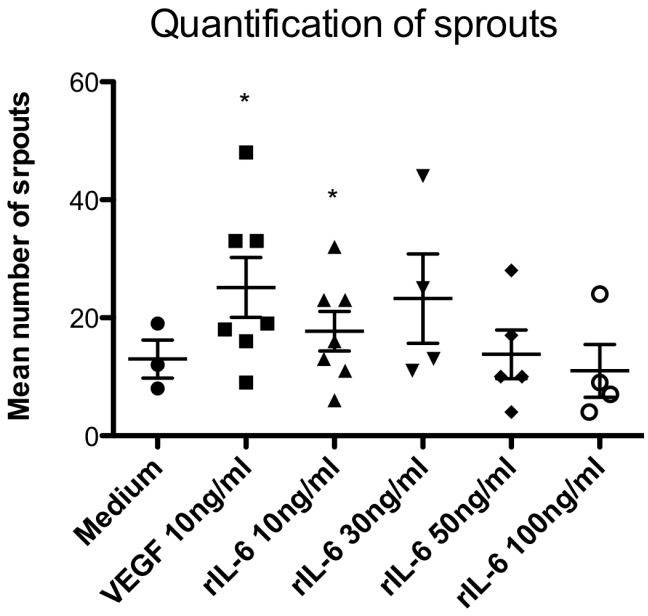

Figure 3.11 Mean number of sprouts in rat aortic rings treated with medium, VEGF or rIL-6.

Aortas removed following cervical dislocation of 180-200g rats were treated with optimem medium containing 1% FCS with either 10ng/ml VEGF (R&D) or 10, 30, 50 or 100ng/ml rIL-6 (R&D) for one week. The medium was changed every 3 days. The rings were imaged using phase contrast microscopy and microvessel outgrowth was counted and quantified.*Represents statistical significance. Medium vs VEGF (p value < 0.01), medium vs rIL-6 10ng/ml (p value < 0.03)

Figure 3.10 shows the results of the rIL-6 dose response experiment with 10, 30, 50 and 100ng of rIL-6. Among the varying concentrations of rIL-6 used, concentrations from 10-100ng/ml of rIL-6 led to formation of microvessel growth. There were 8 aortas used per condition and out of those 10ng/ml of VEGF and rIL-6 led to blood vessel formation in 90% of the aortas. Concentrations from 30-100ng/ml of rIL-6 resulted in 50% sprouting, however the mean number of sprouts per ring was considerably lower in these groups compared to 10ng/ml of rIL-6. This experiment showed 10ng/ml of rIL-6 to be the ideal concentration to use in the rat aortic ring assay.

After deciding on the concentration of rIL-6, I went on to carry out a repeat for the rat aortic ring experiment with 10ng/ml of VEGF and rIL-6.

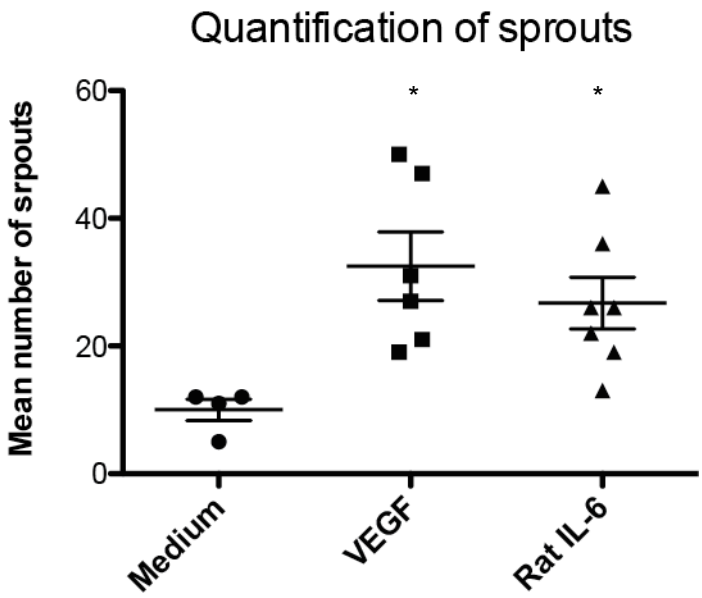

Figure 3.12 Mean number of sprouts in aortic rings treated with Medium, VEGF or rIL-6.
Aortas removed following cervical dislocation of a 180-200g rats were treated with optimem medium containing 1% FCS with 10ng/ml VEGF (R&D) or 10ng/ml rIL-6 (R&D) over a course of 2 weeks. The medium was changed every 3 days. The rings were imaged using phase contrast microscopy and microvessel outgrowth was counted and quantified. * Represents statistical significance. Medium vs VEGF (p value < 0.01), medium vs rIL-6 (p value < 0.02).

The second rat aortic ring repeat experiment (Figure 3.11) agreed with the initial dose response experiment and showed no significant difference in the number of sprouts between VEGF and rIL-6 treated aortic rings. There was a significant difference in the number of sprouts in media vs 10ng/ml VEGF and media vs 10ng/ml rIL-6 treated aortic rings.

Collectively these aortic ring experiments show that human, mouse and rat IL-6 can induce sprouting in mouse and rat aortic ring assays and that there is no significant difference in the number of sprouts between VEGF and IL-6 treated rings. Concentrations of 50ng/ml of hIL-6 and 30ng/ml of mIL-6 in mouse aortic ring and 10ng/ml of rIL-6 in rat aortic ring were effective in inducing microvessel growth. However, higher concentrations such as 150ng/ml of hIL-6 and 200ng/ml of mIL-6 were shown to have inhibitory effect on sprout formation in the mouse aortic ring assay. There was also no significant difference in the length of sprouts between hIL-6 and mIL-6 treated rings with VEGF treated rings in the mouse aortic ring assay. This chapter shows IL-6 is as effective as VEGF in inducing angiogenesis in the aortic ring assay. In the next set of experiments I wanted to study the direct effects of IL-6 on endothelial cells.

4 The interaction of IL-6 with mouse endothelial cells

Once it was established that IL-6 could drive angiogenesis in the aortic ring assay, it was important to study the interaction of IL-6 with endothelial cells. In order to investigate this I used a primary mouse lung endothelial cell line (MLEC), which was kindly given to me by members of Prof Kairbaan Hodivala Dilke's group. The generation of the cell line is briefly described in the methods section 2.2.

I wanted to use this endothelial cell line as a tool to understand the effects and mechanisms of IL-6 on inducing different stages of angiogenesis. The experiments I planned to do with MLEC were:

- Investigate if IL-6 can drive MLEC proliferation and migration.
- Study the existence and functionality of the IL-6Rα in MLEC
- Study downstream target of IL-6 i.e. pSTAT3 after treatment with VEGF, to determine if VEGF can induce IL-6 signalling in endothelial cells.
- Study downstream target of VEGF i.e. pERK after stimulation with IL-6, to determine if IL-6 can induce VEGF signalling in endothelial cells.

4.1 The effects of IL-6 on MLEC proliferation

First, I wanted to investigate if human and mouse IL-6 can drive mouse endothelial cell proliferation and if there is a difference between VEGF and IL-6 induced MLEC proliferation.

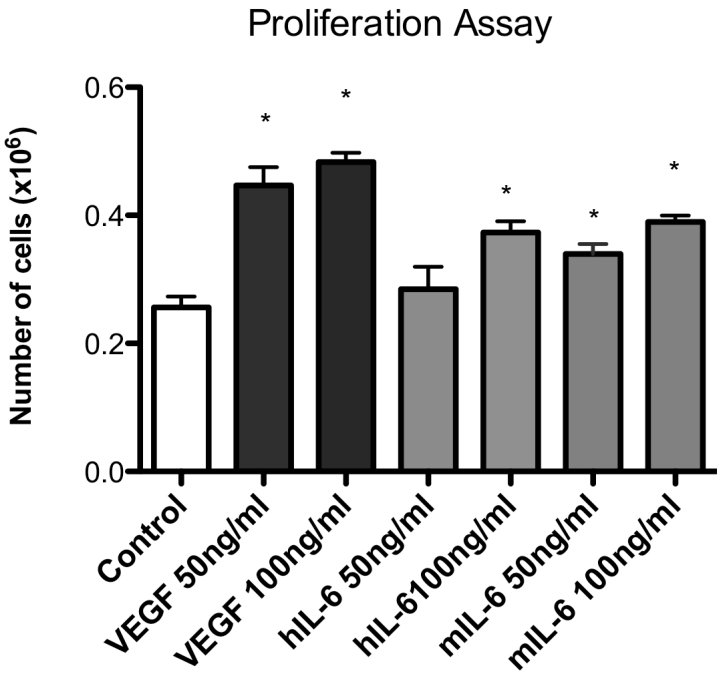

Figure 4.1Graph showing the effects of VEGF, hIL-6 or mIL-6 on cell proliferation in MLEC.
70,000 MLEC were plated and treated with either PBS (Control), VEGF (50 or 100ng/ml), hIL-6 (50 or 100ng/ml) or mIL-6 (50 or 100ng/ml) for 72 hours. The cells were then trypsinised and counted using a cell counter and the mean of the triplicates were calculated. *Represents statistical significance. Control vs VEGF 50 (p value < 0.0008), control vs VEGF 100 (p value < 0.0001), control vs hIL-6 100 (p value < 0.004), control vs mIL-6 50 (p value < 0.02), control vs mIL-6 100 (p value < 0.001). Results typical of 3 independent experiments.

Figure 4.1 shows the effect of VEGF, hIL-6 and mIL-6 on MLEC proliferation. The concentration of VEGF was decided based on observation from previous studies, where doses ranging from 50-100ng were used in *in vitro* cell based assays with VEGF [180]. The molar doses used for VEGF was very similar to that used for hIL-6 and mIL-6 and this helped to compare the effects on endothelial cell proliferation over a period of 72 hours. As shown in Figure 4.1, 50 and 100ng/ml of VEGF had a significant effect on endothelial cell proliferation. In the case of hIL-6 there was no significant increase in proliferation at 50ng/ml, however there was a significant

increase in the MLEC proliferation with 100ng/ml of hIL-6 compared to control. In the case of mIL-6, there was a significant increase in MLEC proliferation at 50 and 100ng/ml.

4.2 The effects of IL-6 on MLEC migration in the scratch assay

Since endothelial cell migration plays a major role in tumour angiogenesis, I then wanted to study the effects of IL-6 on endothelial cell migration using the MLEC line. In order to do this, I decided to set up a scratch assay using a time lapse microscopy. The scratch assay is commonly used to study *in vitro* cell migration. This assay is carried out by creating a scratch on a cell monolayer, which causes the cells at the edge to move inwards to close the scratch. Using a time lapse microscopy, 'wound' closure can be measured by comparing images captured at the onset with the ones taken at endpoint or with the ones taken at intervals. I used VEGF as a positive control [181].

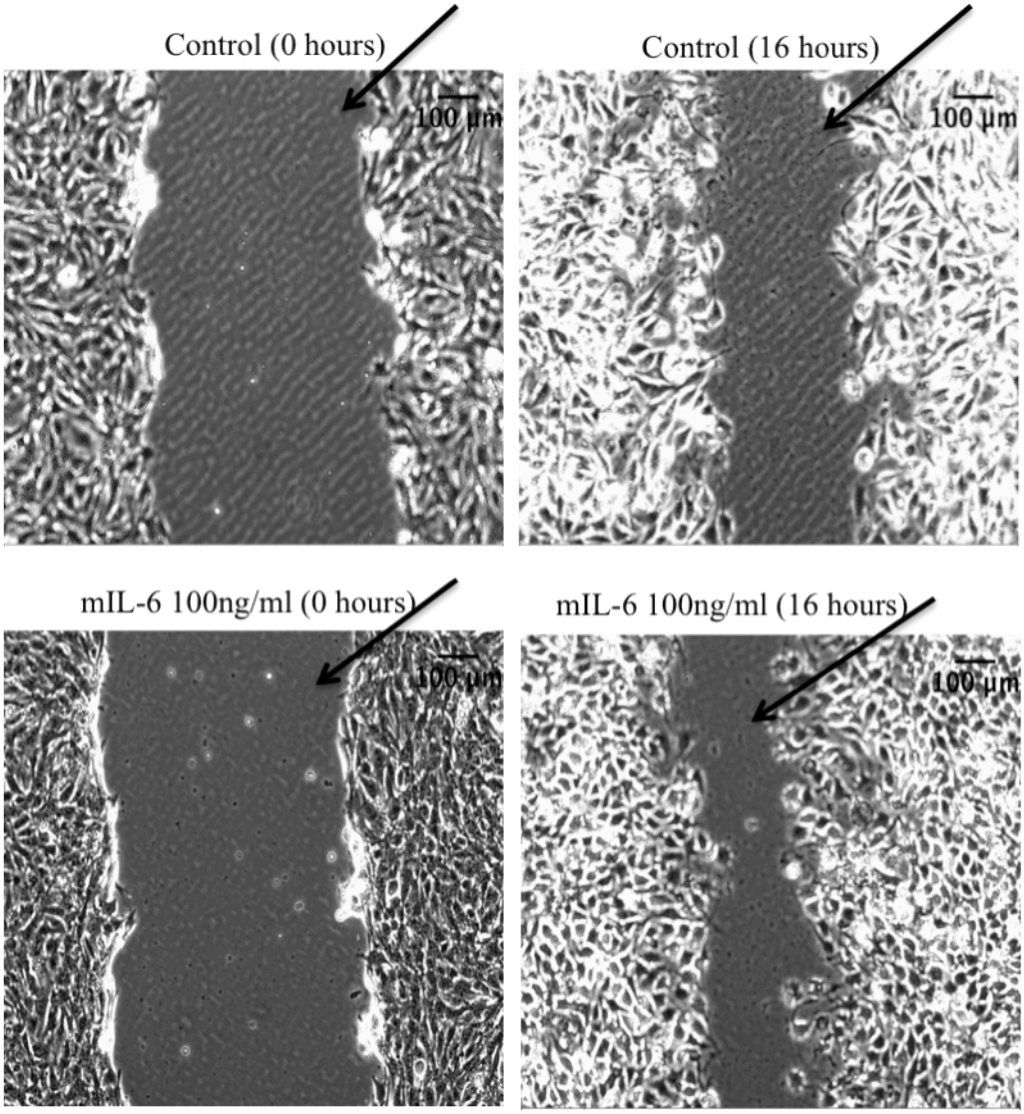

Figure 4.2 Graph showing the effects of control and mIL-6 on cell migration in MLEC.

70,000 MLEC were plated on a 12 well plate and once the cells were confluent, scratch was made using a p20 tip in the centre of the well to make the 'wound'. The medium was then changed and the cells were treated with either PBS (control) or mIL-6 (100ng/ml) for 16hours. Images were taken of the wound closure every hour using a time-lapse microscopy. ⟶ Indicates the 'wound'

Figure 4.2 shows examples of phase contrast images of scratch assay taken using a time-lapse microscope at 0 and 16 hours. A dose response experiment with concentrations of 25-100ng/ml of VEGF and IL-6 was conducted. Since there is always some variation in the size of the scratch made using a p20 tip, it was important to take this into consideration when comparing the migration between different conditions. A formula is generally used to calculate the difference in the area of the 'wound' at zero hours and at the end of the assay (see methods for more detail).

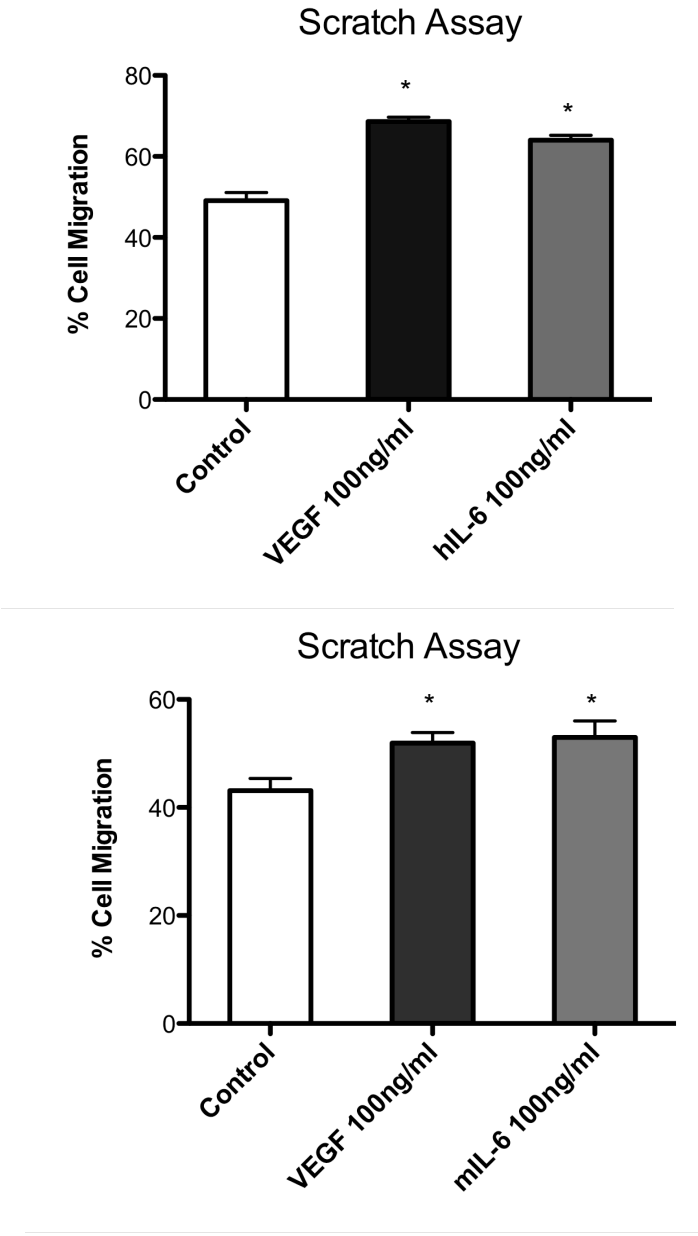

Figure 4.3 Graph showing the effects of VEGF, hIL-6 or mIL-6 on cell migration of MLEC.

70,000 MLEC were plated on a 12 well plate and once the cells were confluent, scratch was made using a p20 tip in the centre of the well. The medium was then changed and the cells were treated with PBS (Control), VEGF (100ng/ml), hIL-6 (100ng/ml) or mIL-6 (100ng/ml) for 16hours. Images were taken of the wound closure every hour using a time-lapse microscopy. * Represents statistical significance. Results typical of 3 independent experiments. Control vs VEGF 100ng (p value < 0.02), control vs hIL-6 100ng (p value < 0.05), control vs VEGF (p value < 0.03) control vs mIL-6 (p value < 0.04).

Figure 4.3 shows the results of the scratch assay after treatment of MLEC with VEGF, hIL-6 or mIL6. There was a significant difference in the percentage cell migration in the VEGF or hIL-6 treated wells as compared to the control group in Figure 4.3. There was also a significant difference in the percentage cell migration of MLEC in the VEGF and mIL-6 treated groups. 100ng/ml of human and mouse IL-6

is almost as potent as VEGF in inducing MLEC cell migration in scratch assays. Concentrations below 100ng/ml of VEGF, hIL-6 and mIL-6 did not show a significant effect on MLEC migration.

4.3 IL-6Rα (gp80) on endothelial cells

There has been conflicting evidence on the existence of IL-6Rα on endothelial cells. A study conducted by Nillson *et a*l, showed that tumor associated microvascular endothelial cells residing in the peritoneum expressed IL-6Rα [47]. The endothelial cell IL-6Rα was functional and when stimulated with IL-6 led to activation of STAT3. However, a study later conducted by Lo *et al*, investigating the effects of IL-6 trans signalling in malignant ovarian cancer ascities suggested that endothelial cells lack IL-6Rα expression [161]. Therefore, it was important to investigate and confirm the existence of IL-6Rα on MLEC and I decided to test this using immunofluorescence and western blotting analysis.

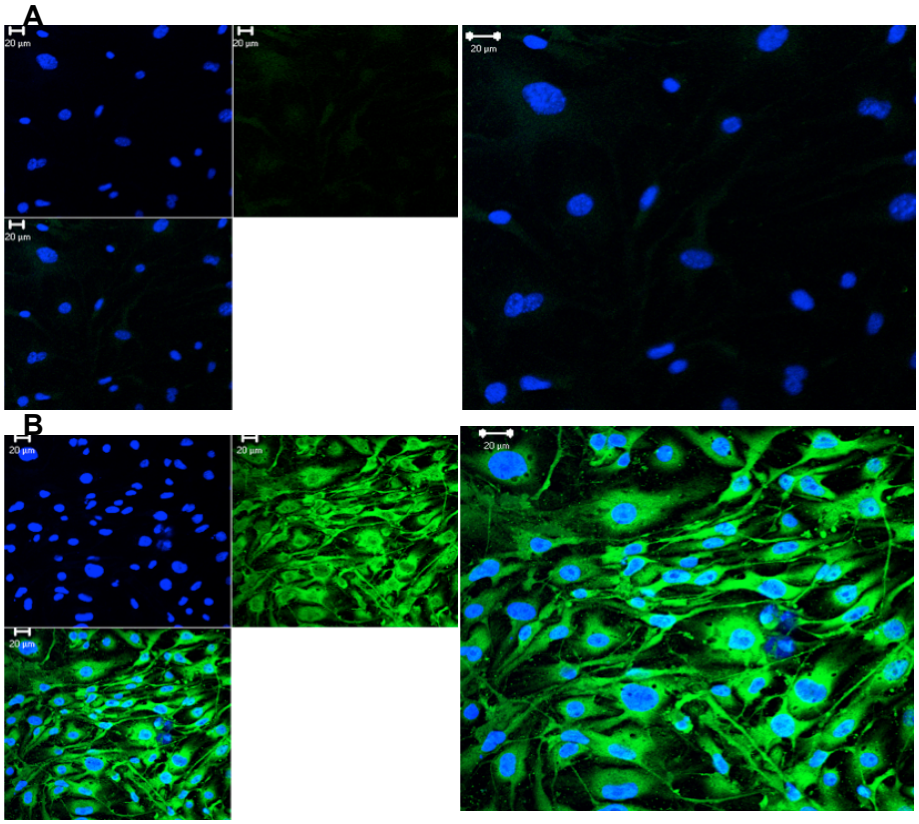

Figure 4.4 Confocal images of the IL-6Rα staining in MLEC.
$2x10^5$ MLEC were plated on cover slips in a 12 well plate. The cover slips were stained with (**A**) Rabbit IgG (R&D) or (**B**) anti-IL-6Rα antibody (Santa cruz) overnight at 4°C and secondary anti-rabbit Alexa 488 for 2 hours at room temperature. The coverslips were then mounted on slides with Prolong Gold DAPI (blue) containing medium. The image displays DAPI nuclear staining (blue) and IL-6Rα membrane staining (green) Scale bar = 20 microns.

Figure 4.4 shows the immunofluorescent confocal microscopy staining of IL6Rα on MLEC. The negative control (Figure 4.4A) is of MLEC treated with the secondary antibody mounted with DAPI (blue), showed staining of nucleus without any background. Figure 4.4 (B) shows a positive IL-6Rα (green) membrane staining in MLEC. This result correlates with the earlier published findings of Nilsson *et al* [47].

4.4 To determine if the IL-6Rα present in MLEC is functional

I next wanted to show that the IL-6Rα on MLEC is functional and that it can signal via downstream IL-6 targets. In order to determine this, I decided to look at pSTAT3 levels, which is the direct downstream read out of IL-6 signalling. I investigated the pSTAT3 levels using immunofluorescence and western blotting analysis. Since I observed sprouting after treatment with human and mouse IL-6, I decided to look at pSTAT3 after treatment of MLEC with either human and mouse IL-6.

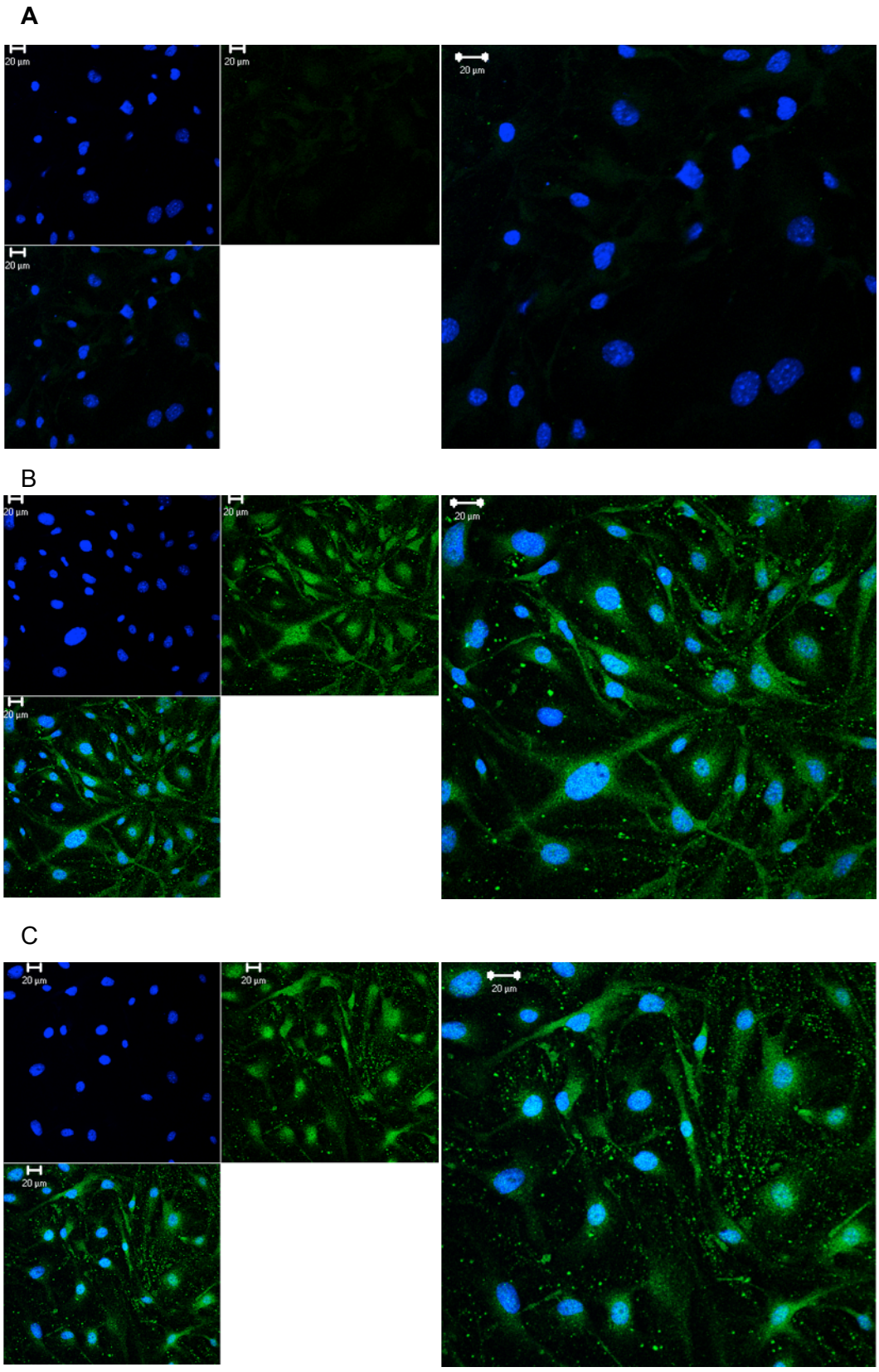

Figure 4.5 Confocal images of the pSTAT3 staining in MLEC.
$2x10^5$ MLEC cells were plated on cover slips in a 12 well plate and treated with either PBS (Control), 30ng/ml hIL-6 (B) or mIL-6 (C). Following 24 hours (A) was stained with rabbit IgG (B) and (C) were stained for pSTAT3 (green) overnight at 4°C. The next day the cells were stained with secondary anti-rabbit Alexa 488 for 2 hours at room temperature. The coverslips were then mounted on slides with Prolong Gold DAPI (blue) containing medium. Scale bar = 20 microns.

Figure 4.5 shows the confocal staining of pSTAT3 (green) on MLEC. The negative controls used were either untreated MLEC stained for the secondary antibody (Alexa 488) or human/mouse IL-6 treated MLEC stained for secondary antibody. Figure 4.5 (A) shows DAPI (blue) staining in the negative control without background. Figure 4.5 (B) and (C) show positive pSTAT3 staining in the nucleus for human and mouse IL-6 treated MLEC. This showed that IL-6Rα in MLEC is functional and it can bind recombinant human and mouse IL-6 to induce downstream pSTAT3 signalling. I also wanted to verify the functionality of the receptor using western blotting analysis.

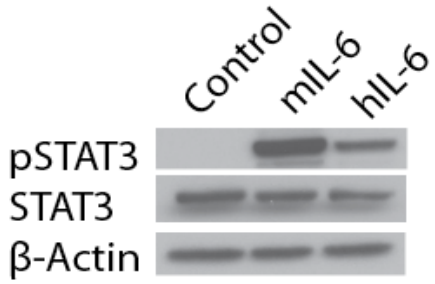

Figure 4.6 Western blot showing the expression of pSTAT3 in MLEC after treatment with hIL-6 or mIL-6.
$2X10^5$ cells of MLEC were plated and treated with either PBS (Control), hIL-6 (30ng/ml) or mIL-6 (30ng/ml) for 24 hours. The cells were then lysed and 20ng of protein was loaded for western blot analysis. pSTAT3 and STAT3 levels were analysed and loading control was measured using β-actin.

Figure 4.6 shows the levels of pSTAT3 in MLEC after treatment with human or mIL-6. There was an induction of pSTAT3 after treatment with both human and mIL-6 treated groups as compared to the control without any changes in the total protein levels. Total protein levels were measured to determine the changes in phosphorylated protein fraction with treatment relative to the total fraction. The loading control measured with β-actin was consistent between the different groups. This was an additional confirmation for the existence and function of the IL-6Rα in MLEC.

4.5 IL-6Rα (gp80) in the aortic ring assay

In order to confirm the angiogenic effects seen in the aortic ring assay after treatment with IL-6, it was then important to study the expression of IL-6Rα in the aortic ring assay.

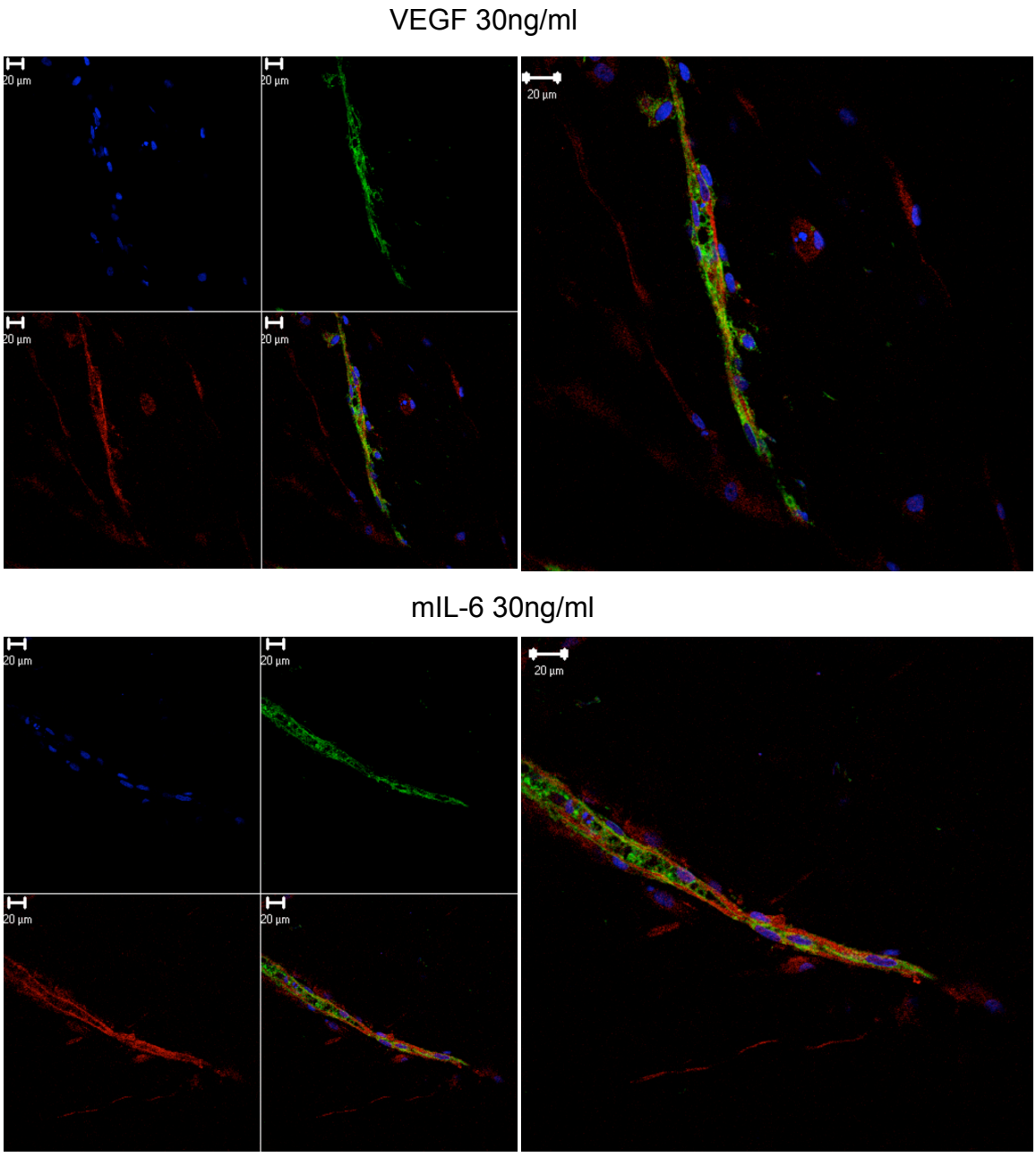

Figure 4.7 Confocal images of IL-6Rα on vessels in mouse aortic ring treated with VEGF (30ng/ml) or mIL-6 (30ng/ml).
Aortic ring assay treated with VEGF or mIL-6 were stained for endothelial vessels using BS1 lectin (green), IL-6Rα (red) and DAPI (blue). Scale bar = 20 microns.

Figure 4.7 shows the staining for IL-6Rα in the aortic ring vessels after treatment with VEGF or mIL-6. As witnessed with MLEC, in the aortic ring vessels (green), there was positive staining for the IL-6Rα (red). This confirms that the IL-6Rα is not only present in the mouse endothelial cell line but also on endothelial cells in the aortic ring assay. I then tried to stain the aortic ring vessels for pSTAT3, however I was unable to do this successfully.

4.6 Downstream signalling pathways after IL-6 and VEGF stimulation of MLEC cells

After establishing the existence and functionality of IL-6Rα in endothelial cells, I wanted to explore the differences in IL-6 and VEGF induced signalling in MLEC and investigate if the two pathways are dependent on each other for their angiogenic effects. I first asked if VEGF can induce downstream IL-6 signalling i.e. pSTAT3 in MLEC. In order to do this, I decided to carry out a time point experiment to determine the optimal time for IL-6 induced pSTAT3 induction and to study if VEGF can induce pSTAT3 at any of those time points.

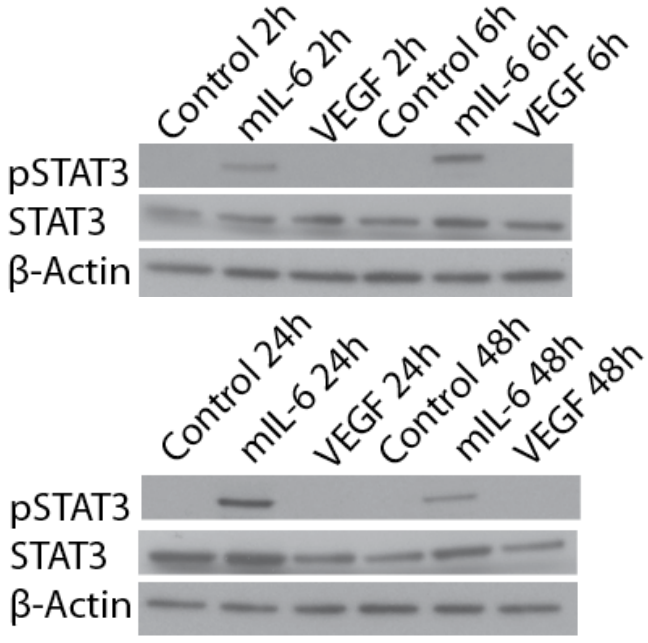

Figure 4.8 Western blot showing the expression of pSTAT3 in MLEC after treatment with mIL-6 at 2h, 6h, 24h and 48h.
$2X10^5$ cells of MLEC were plated and treated with either PBS (Control), mIL-6 (30ng/ml) or VEGF (30ng/ml) for 2h, 6h, 24h or 48hours. The cells were then lysed and 20ng of protein was loaded for western blot analysis. pSTAT3 and STAT3 levels were analysed and loading control was measured using β-actin.

Figure 4.8 shows the induction of pSTAT3 over a course of 2 hours to 48 hours. There was a gradual increase of pSTAT3 from 2 hours to 24hours with the highest induction at 24 hours after treatment with mIL-6. At 48 hours the levels of pSTAT3 levels started to decrease showing a cycling induction of pSTAT3 with mIL-6 treatment. Therefore, the optimum time point for investigating stimulation of pSTAT3 by mIL-6 seems to be the 24 hour time point.

The other observation that can be made from Figure 4.8 is that VEGF did not seem to induce pSTAT3 in MLEC at any of those time points. Hence, according to this finding VEGF signalling is not dependent on IL-6 signalling in MLEC and suggests that VEGF does not induce IL-6.

4.7 Does IL-6 induce VEGF in MLEC?

Once I established that the IL-6Rα is functional on MLEC, I wanted to investigate if IL-6 can induce VEGF signalling. In order to study this, I decided to look at the downstream target of VEGF, i.e. pERK, 24 hours after treatment with mIL-6 or VEGF in MLEC.

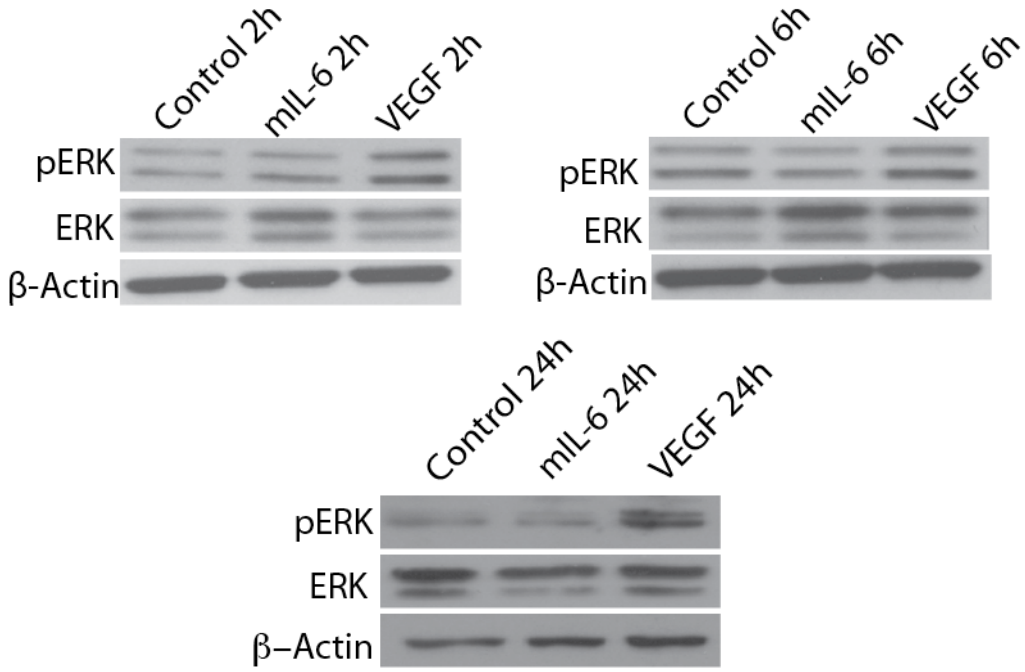

Figure 4.9 Western blot showing the expression of pERK in MLEC after treatment with mIL-6 or VEGF.

$2X10^5$ cells of MLEC were plated and treated with either PBS (Control), mIL-6 (30ng/ml) or VEGF (30ng/ml) for 2 hours, 6 hours and 24 hours. The cells were then lysed and 20ng of protein was loaded for western blot analysis. pERK and ERK levels were analysed and loading control was measured using β-actin.

Figure 4.9 shows that, as expected, there is pERK induction after treatment of MLEC with VEGF at 2 hours, 6 hours and 24 hours. However, there did not seem to be an induction in pERK levels after treatment with mIL-6. I did not see any difference in the level of pERK in the mIL-6 and VEGF treated MLEC in the 48hour time point. The levels of the total protein (ERK) and the loading control (β-actin) remain consistent between the different groups. This shows that IL-6 might not signal via VEGF i.e. pERK in MLEC. This gives an indication that IL-6 and VEGF might have different mechanism of action on endothelial cells. The induction of pSTAT3 and pERK with IL-6 and VEGF were also repeated at early time points (30 min and 2 hours) and similar results were observed (data not shown).

In conclusion, I was able to confirm that IL-6 was active on endothelial cells using *in vitro* proliferation and migration assays. I then confirmed the existence and functionality of the IL-6Rα in MLEC by looking at its downstream target pSTAT3. I was also able to show that hIL-6 can also induce pSTAT3 in MLEC, which correlates with the sprouting observed with hIL-6 in the mouse aortic ring assay. In order to obtain an insight into the mechanism of action of IL-6 on endothelial cells, I also looked at the interaction of IL-6 with VEGF signalling. According to the data obtained from the western blot analysis of pSTAT3 and pERK after treatment with IL-6 and VEGF, it seems as if the two pathways are independent of each other, at least in MLEC. The data suggest that IL-6 might have a different mechanism of action in inducing angiogenesis as compared to VEGF. This will require further investigation in other assays such as the aortic ring assay.

Although technically challenging, I would aim to extract protein from the aortic rings treated with IL-6 or VEGF and do the same experiments.

5 The interaction of IL-6 with pericytes

As previously discussed, pericytes are important regulators of vascular development, stabilisation, maturation and remodelling. Pericytes promote vessel stability and control vessel permeability by inducing endothelial cell-cell adhesions and tight junctions [138]. Loss of pericytes has been linked to different pathological conditions such as oedema, diabetic retinopathy and even embryonic lethality [135]. Studies have shown that loss of pericytes play a major role in the development of tumour metastasis [182, 183].

Pericytes play a major role in the type of angiogenesis stimulated in physiological and pathological conditions. In the presence of pericytes, the newly formed vasculature rapidly matures, becomes stable and stops proliferating. However, in some pathological conditions, blood vessels deficient of pericytes can undergo excessive sprouting which can ultimately lead to aberrant angiogenesis [135] .

IL-6 has been previously shown to stimulate destabilised angiogenesis in models of rheumatoid arthritis [184]. However, the underlying mechanism involved in the induction of the aberrant angiogenesis by IL-6 has not been studied in detail and it is not known if this effect is only found in inflammatory disease. Therefore, in this chapter I was interested in investigating the morphology and maturation status of the vessels after treatment with IL-6 as compared to VEGF in the aortic ring assay, by determining the pericyte coverage around the vessels.

5.1 Lectin and α-SMA staining of mouse aortic ring vessels after treatment with VEGF and hIL-6

Once I established that IL-6 can induce sprouting in the aortic ring assay and that IL-6 probably does not act via VEGF induction and signalling in the MLEC, I wanted to investigate how the differences in IL-6 and VEGF induced signalling could affect the morphology of vessels in the aortic ring assay. Therefore, I decided to stain the vessels for the endothelial cell marker BS1 lectin and pericyte marker α-SMA.

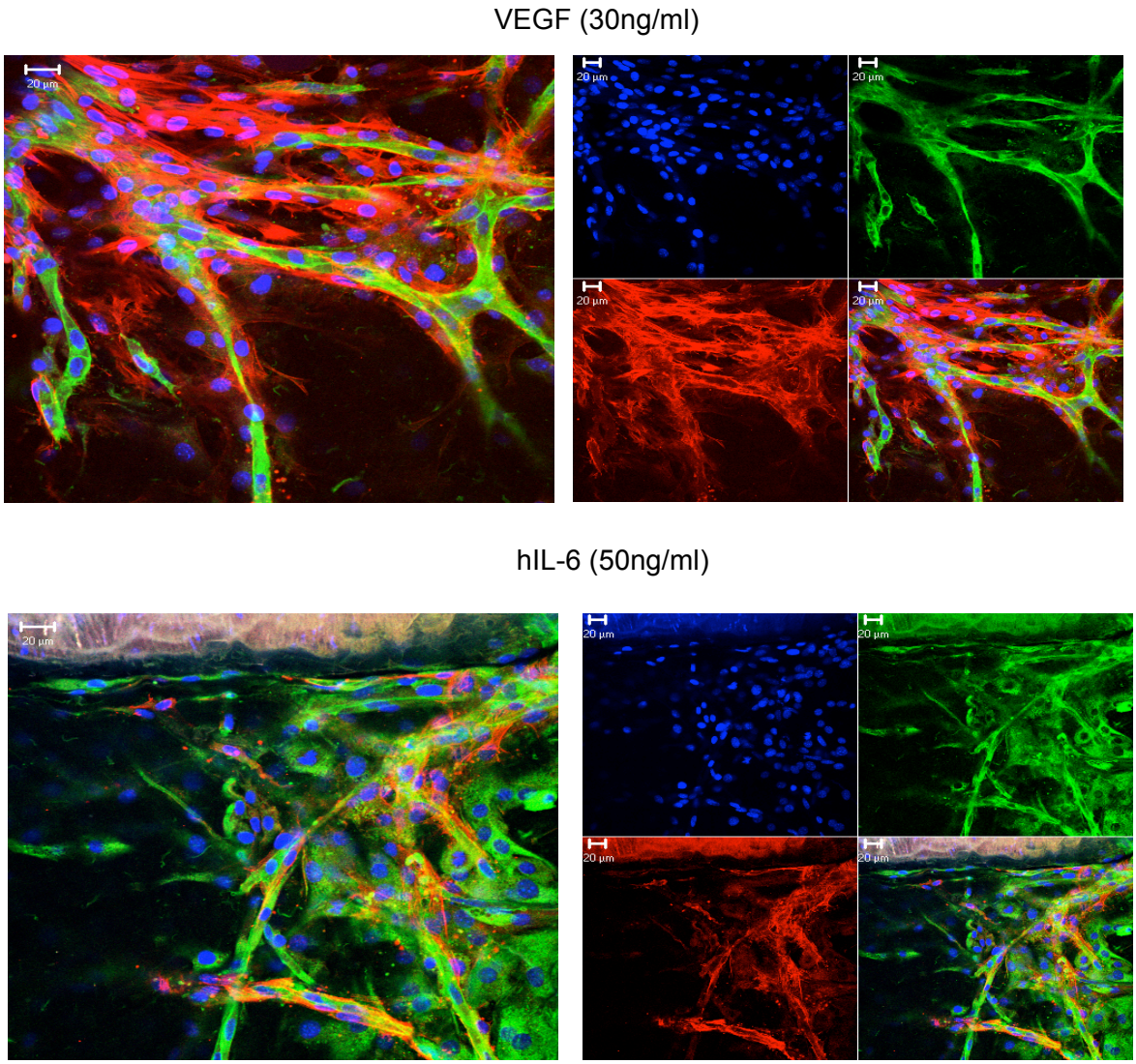

Figure 5.1 Immunofluorescence staining of mouse aortic aortic rings after treatment with VEGF (30ng/mL) or hIL-6 (50ng/ml) over a course of 2 weeks.
BS1 lectin-FITC (green) stains endothelial sprouts, anti-α-SMA-Cy3 (red) stains the pericytes/activated fibroblast and DAPI (blue) is for staining the nucleus. The images display the pericyte coverage (red) around the matured endothelial sprouts (green). Scale bar = 20µm

Figure 5.1 shows the confocal images of the mouse aortic ring blood vessels treated with VEGF or hIL-6 stained for BS1 lectin for endothelial cells (green) and α-SMA for pericytes (red). The observations I made from these confocal images was that in the VEGF treated sprouts, the vessels seemed to be more organised compared to the IL-6 treated vessels which appeared to be more disorganised and chaotic. There also seemed to be more α-SMA staining around the vessels treated with VEGF compared to the vessels treated with hIL-6. This suggested that there was more maturation of vessels in the aortas treated with VEGF compared to hIL-6. This was an interesting observation because it fitted in with the study carried out in rheumatoid arthritis showing IL-6 could lead to formation of destabilised vasculature [184].

I next decided to quantify this pericyte coverage by concentrating on the tip of the vessels in the aortic rings treated with VEGF or hIL-6. This was done to eliminate any false positive α-SMA staining, which could have resulted due to staining of activated fibroblasts (myofibroblasts), which are normally found near the stalk of the vessels.

VEGF (30ng/ml)

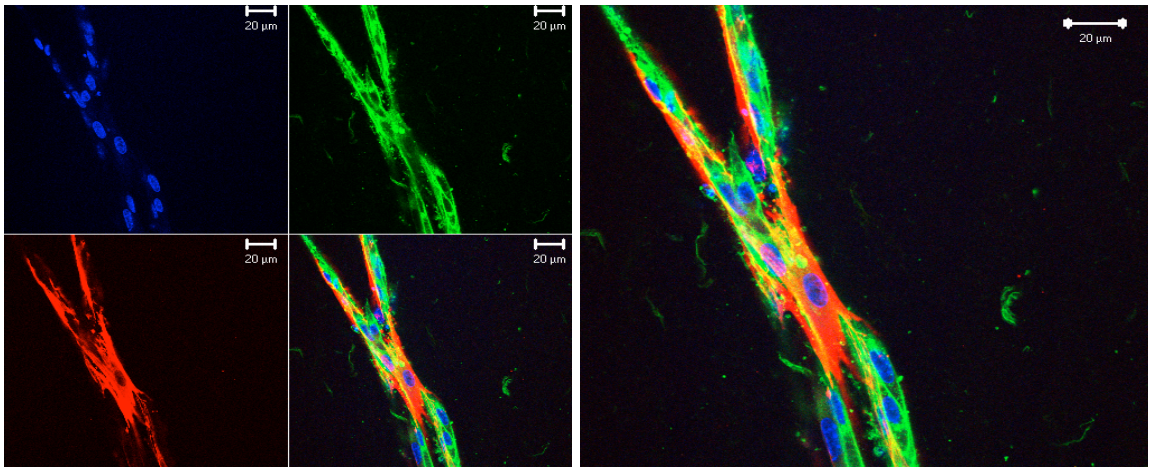

hIL-6 (50ng/ml)

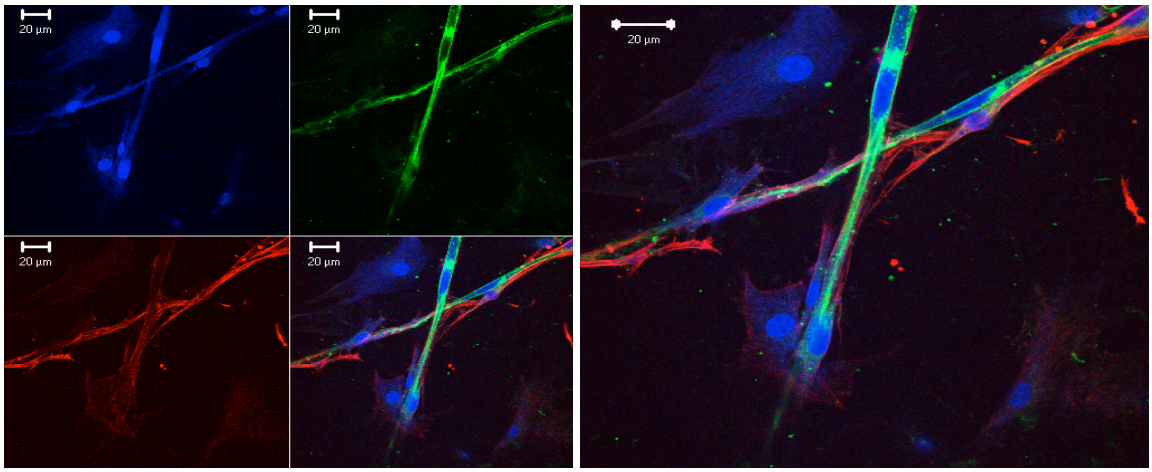

Figure 5.2 Immunofluorescence staining of mouse aortic rings after 2 weeks treatment with VEGF (30ng/mL) or hIL-6 (50ng/ml).
BS1 lectin-FITC (green) stains endothelial sprouts, anti-α-SMA-Cy3 (red) stains the pericytes and DAPI (blue) is for the nucleus. The images display the pericyte coverage (red) around the matured endothelial sprouts (green). Scale bar = 20µm

Figure 5.2 shows confocal images of the tips of vessels treated with VEGF or hIL-6 stained for BS1 lectin and α-SMA. As observed in Figure 5.1, there was good pericyte coverage in the vessels treated with VEGF and this was noticed in majority of the vessels. However, in case of the hIL-6 treated vessels, there were reduced pericyte coverage in majority of the vessels. There were also some cases in the hIL-6 treated group where the pericytes seemed to be detaching from the vessels as shown in Figure 5.2.

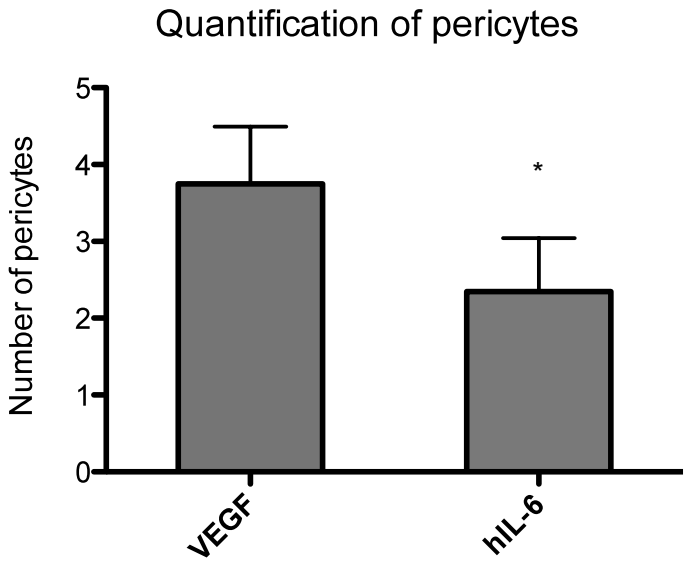

Figure 5.3 Quantification of number of pericyte in the VEGF or hIL-6 treated mouse aortic ring vessels.
Confocal images were taken of the tip of the vessels treated with VEGF (30ng/ml) or hIL-6 (50ng/ml) stained for BS1 lectin and α-SMA. The number of pericytes were counted 250microns from the tip of the vessels. * Represents statistical significance (p value < 0.004). Combined results from 3 independent experiments (9 rings per condition).

Figure 5.3 shows the quantification of the pericytes in the vessels treated with VEGF or hIL-6. The α-SMA staining was significantly lower in the hIL-6 treated aortic rings compared to the VEGF group. This showed less maturation of vessels treated with hIL-6 suggesting that these vessels could have weak tight junctions that could be leaky and permeable.

5.2 Lectin and α-SMA staining of mouse aortic ring vessels after treatment with VEGF or mIL-6

Once I established that there was less pericyte coverage after treatment with hIL-6 compared with VEGF, I wanted to make sure that the effect I saw on pericytes with hIL-6 was not because I used hIL-6 in the mouse aortic ring assay. Therefore, in order to verify this effect of depletion of pericyte with IL-6 treatment, it was important to investigate the pericyte coverage after treatment of mouse aortic rings with mIL-6.

VEGF (30ng/ml)

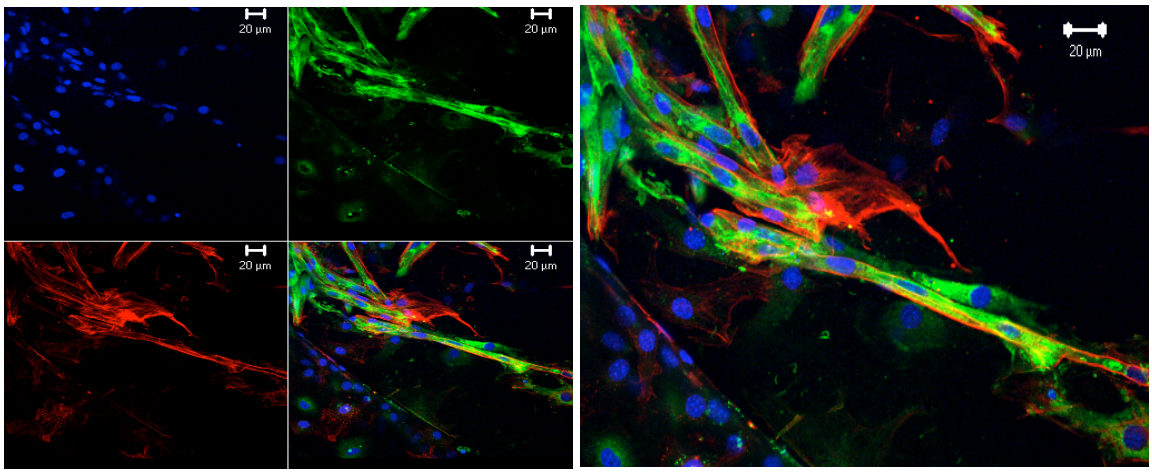

mIL-6 (30ng/ml)

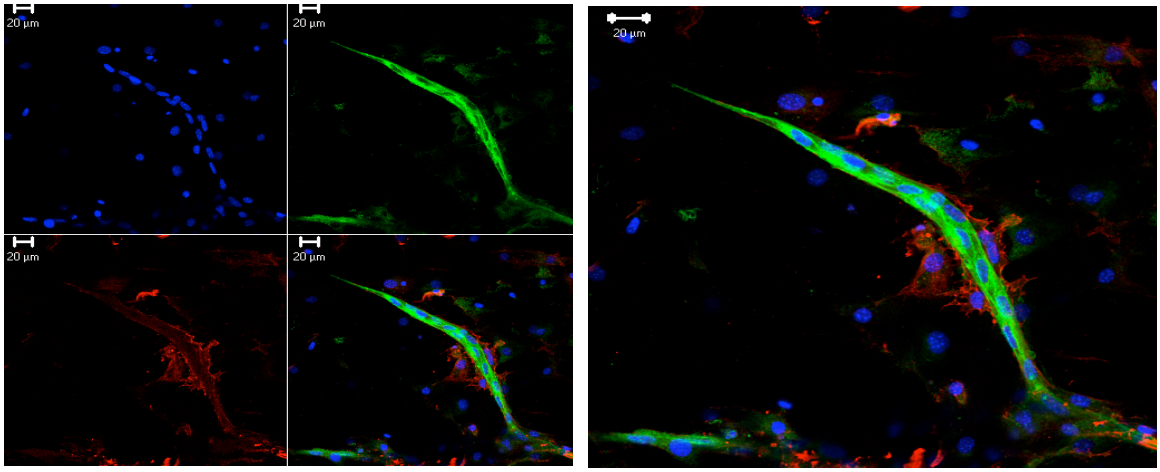

Figure 5.4 Immunofluorescence staining of mouse aortic rings after 2 weeks treatment with VEGF (30ng/mL) or mIL-6 (30ng/ml).
BS1 lectin-FITC (green) stains endothelial sprouts, anti-α-SMA-Cy3 (red) stains the pericytes and DAPI (blue) is for the nucleus. The images display the pericyte coverage (red) around the matured endothelial sprouts (green). Scale bar = 20µm

Figure 5.4 shows the confocal images of the tip of the vessels from mouse aortic rings treated with either VEGF or mIL-6 stained for BS1 lectin and α-SMA. As observed in Figure 5.2, there was good pericyte coverage in the vessels treated with VEGF. However, in case of the mIL-6 treated vessels, the staining was similar to the hIL-6 treated vessels with diminished pericyte coverage around the vessels. As shown in Figure 5.4 there were also some cases in the mIL-6 treated group where the pericytes

were not closely associated with the vessels and they seemed to be detaching from the vessels.

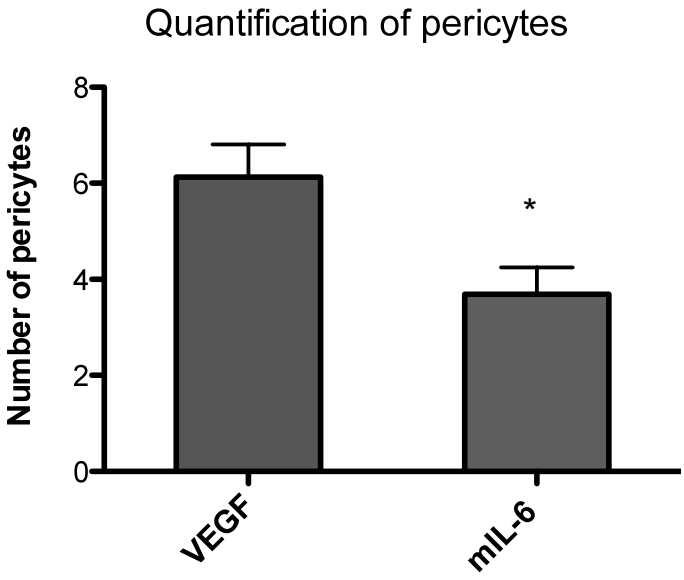

Figure 5.5 Quantification of number of pericyte in the VEGF or mIL-6 treated mouse aortic ring vessels.
Confocal images were taken of the tip of the vessels treated with VEGF (30ng/ml) or hIL-6 (50ng/ml) stained for BS1 lectin and α-SMA. The number of pericytes were counted 250microns from the tip of the vessels. * Represents statistical significance. (p value < 0.002). Combined results from 2 independent experiments (6 rings per condition).

Figure 5.5 show the quantification of the pericytes in the vessels treated with VEGF or mIL-6. The α-SMA staining was significantly lower in the mIL-6 treated aortic rings compared to the VEGF group. This correlates with the findings of the hIL-6 treated vessels indicating decreased maturation of vessels when treated with IL-6 compared with VEGF.

5.3 Lectin and α-SMA staining of rat aortic ring vessels after treatment with VEGF and rIL-6

In order to further confirm the effects of IL-6 on pericyte coverage, I felt it was important to establish this finding in the rat aortic ring assay where I used rIL-6. As

stated in chapter 3, I started using the rat aortic ring assays because the success rate of these assays was higher than the mouse aortic ring assays.

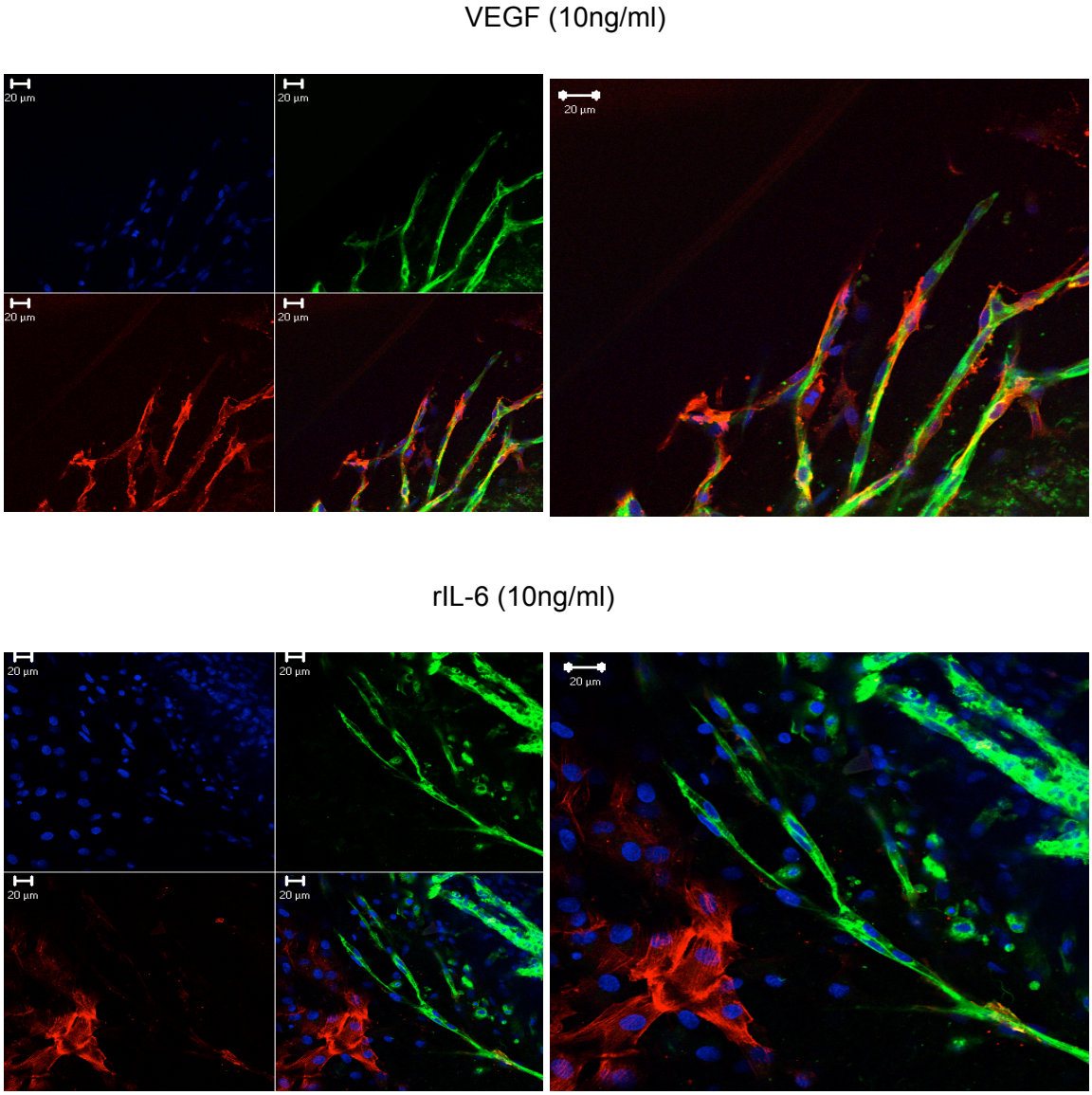

Figure 5.6 Immunofluorescence staining of rat aortic rings after 2 weeks treatment with VEGF (10ng/mL) or rIL-6 (10ng/ml) over a course.
BS1 lectin-FITC (green) stains endothelial sprouts, anti-α-SMA-Cy3 (red) stains for the pericytes and DAPI (blue) is for the nucleus. The images display the pericyte coverage (red) around the matured endothelial sprouts (green). Scale bar = 20µm

Figure 5.6 shows the confocal images of the tip of the rat aortic ring vessels treated with VEGF or rIL-6 stained for BS1 lectin and α-SMA. This again showed the differences in the pericyte coverage in the VEGF and rIL-6 treated aortic rings. The rIL-6 group not only seemed to have very few pericyte coverage but as witnessed

with the human and mouse IL-6 treated vessels the pericytes in the rIL-6 treated aortic rings seemed to be detached from the vessels.

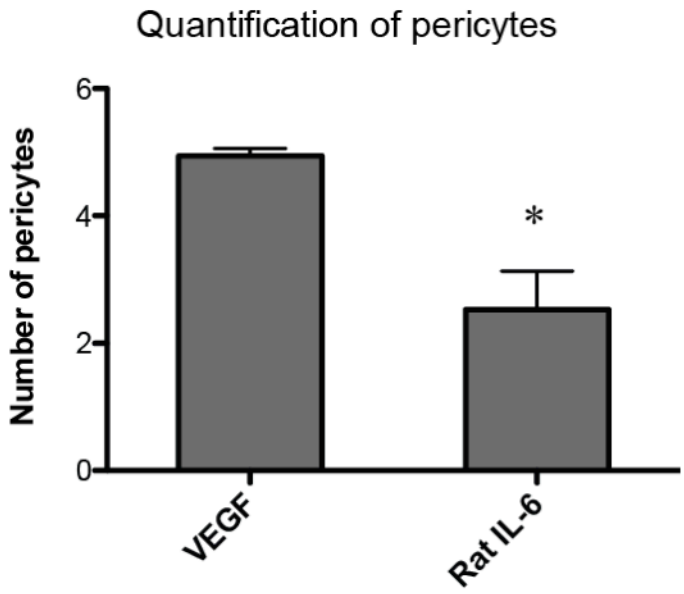

Figure 5.7 Quantification of number of pericyte in the VEGF or rIL-6 treated rat aortic ring vessels.
Confocal images were taken of the tip of the vessels treated with VEGF (10ng/ml) or rIL-6 (10ng/ml) stained for BS1 lectin and α-SMA. The number of pericytes were counted 250microns from the tip of the vessels. * Represents statistical significance. (p value < 0.01). Combined results from 2 independent experiments (5 rings per condition).

Figure 5.7 shows the quantification of pericytes in the VEGF and rIL-6 treated aortic ring vessels. The quantification confirmed significantly lower number of pericyte coverage in the rIL-6 treated vessels compared with the VEGF. This again correlated with the findings of the human and mouse IL-6 aortic ring experiments.

5.4 IL-6Rα expression on pericytes

So far my study had shown that IL-6 can drive angiogenesis or sprouting in the aortic ring assay and that there was decreased vessel-associated pericytes in the IL-6 treated vessels compared to the VEGF treated ones. Therefore, my next aim was to investigate why there is a difference in the pericyte coverage in the IL-6 and VEGF treated vessels. To understand the mechanism involved in the depletion of pericytes in IL-6 treated group, it was important to first see if pericytes expressed IL-6Rα.

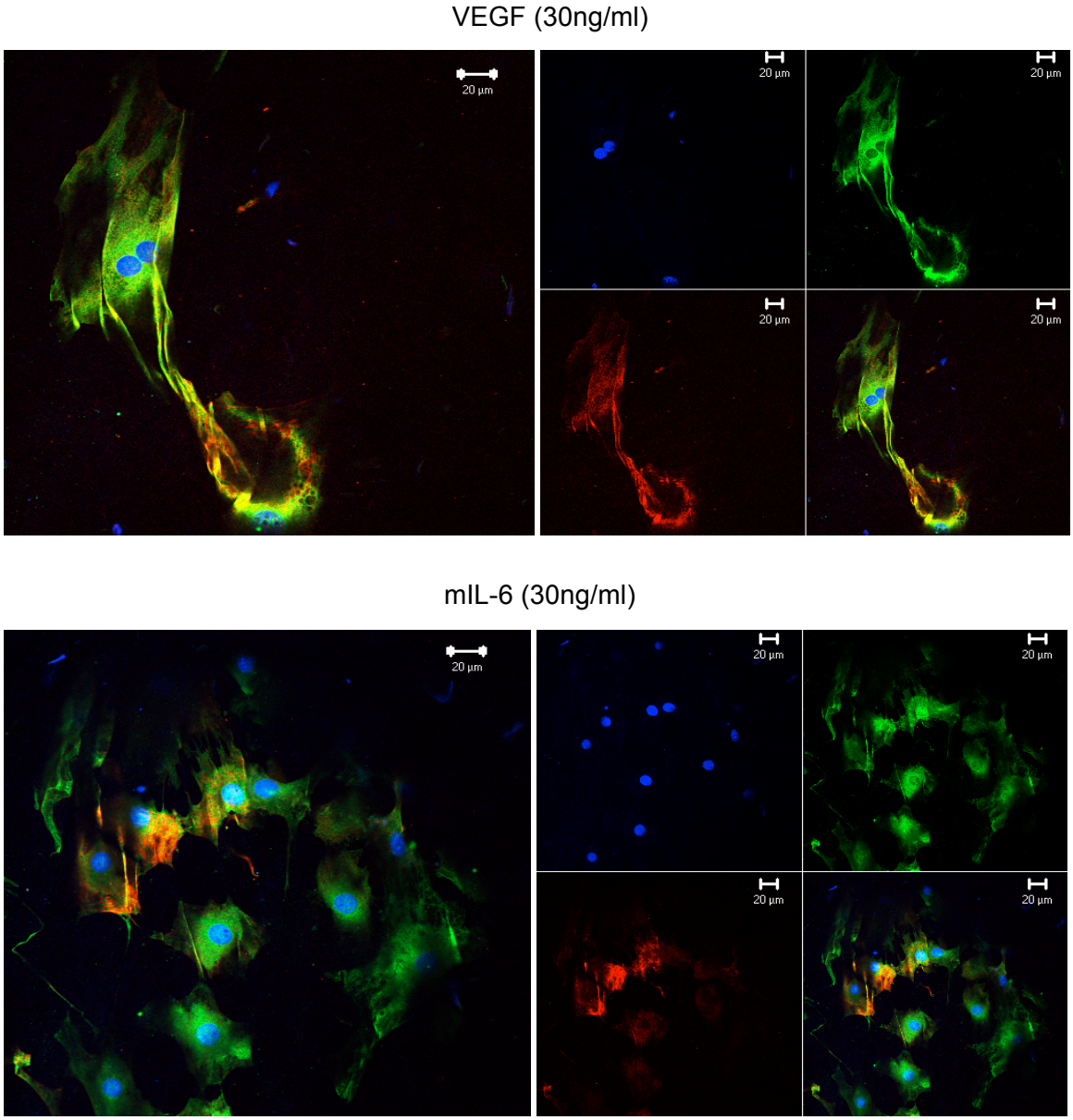

Figure 5.8 Confocal images of IL-6Rα on pericytes in mouse aortic rings treated with VEGF (30ng/mL) or mIL-6 (30ng/ml).
Aortic rings treated with VEGF or mIL-6 were stained for IL-6Rα (green), α-SMA (red) and DAPI (blue). Yellow shows the area of co-localisation of the IL-6Rα with the pericytes. Scale bar = 20µm

Figure 5.8 shows staining of IL-6Rα on pericytes in the mouse aortic ring assay. The pericyte in both the VEGF and mIL-6 treated groups seemed positive for IL-6Rα, shown in yellow as a result of the green (IL-6Rα) and red (pericytes) co-localisation. There was more co-localisation in the VEGF treated group compared to the mIL-6 treated groups and this could be due the presence of more pericytes in VEGF treated vessels. This result therefore confirms the existence of the IL-6Rα on pericytes.

In summary, this chapter showed that unlike VEGF, IL-6 could lead to aberrant angiogenesis with defective pericyte coverage in the aortic ring assay. This was established in human, mouse and rat aortic ring assays. Staining for IL-6Rα on pericytes and on endothelial sprouts (Chapter 4) showed positive expression of the receptor on both the cell types. Hence, the next step is to understand the mechanism by which IL-6 leads to defective pericyte coverage compared to VEGF.

6 The mechanism of differential effect of IL-6 and VEGF on pericyte coverage of blood vessels

In chapter 4, I found that VEGF did not signal via pSTAT3 and that IL-6 did not signal via pERK in MLEC. The aortic ring assay showed clear differences in the IL-6 and VEGF-induced sprouting especially in terms of the morphology and maturation status of the vessels. This gave a further indication that IL-6 and VEGF might signal using different pathways and supports my hypothesis that 'IL-6 drives aberrant angiogenesis independent of VEGF signalling'.

Therefore, using MLEC as a model, I wanted to investigate alternative angiogenic signalling pathways that could be regulated by IL-6. I initially decided to use MLEC to explore the Notch signalling pathway because of the previously known link of IL-6 with the Notch ligand Jagged1 in ovarian cancer [185]. As mentioned earlier, a study conducted by Ralph Adams showed the opposing regulation of the Notch ligands Jagged1 and DLL4 on the endothelial cells [109]. The results showed that DLL4, which is present in the tip cells, can activate the Notch receptors in the stalk cell leading to maturation of the vessels. However, Jagged1 present in the stalk cell can antagonise the effects of DLL4 by blocking its binding to the Notch receptor and this leads to more of a tip phenotype characterised by excessive sprouting. VEGF has previously been shown to regulate this Notch-DLL4 signalling and thereby lead to activation of the downstream repressor gene Hey [109].

Various studies have also shown that high levels of DLL4 on endothelial cells correlate with high levels of pericytes on vessels [142, 186]. Therefore, I decided to study the regulation of the Notch ligands Jagged1 and DLL4 in MLEC after treatment with VEGF or mIL-6.

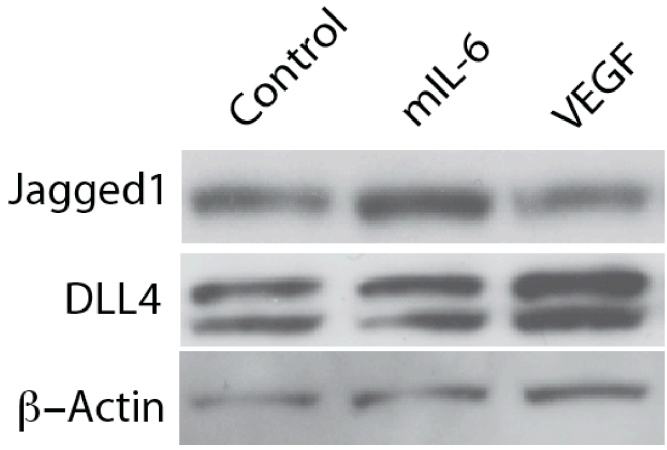

Figure 6.1 Western blot analysis of the expression of Jagged1 and DLL4 in VEGF and mIL-6 treated MLEC.
$2x10^5$ MLEC cells were plated and treated with control (PBS), VEGF or mIL-6 for 24 hours. The cells were then lysed and 20ng/ml of protein was used to detect the levels of Jagged1 and DLL4 using western blotting analysis. β-actin was used as loading control. This is typical of two independent experiments. This experiment was also repeated at 2 hours and 6 hours.

Figure 6.1 shows the expression of the Notch ligands DLL4 and Jagged1 after treatment with VEGF or mIL-6. Mouse IL-6 induced more Jagged1 than VEGF and VEGF induced more DLL4 than mIL-6 in MLEC. Collectively these data confirm the findings of the opposing regulation of the Notch ligands Jagged1 and DLL4 in endothelial cells. Since the angiogenic ligand DLL4 is also reported to play a role in vessel maturation, these data give a possible insight into why there could be less pericyte coverage in the IL-6 treated vessels compared to the VEGF treated ones.

As mentioned previously, induction of DLL4 via VEGF leads to activation of the downstream transcription factor Hey. Therefore, I tested the expression of Hey in the VEGF or mIL-6 treated MLEC.

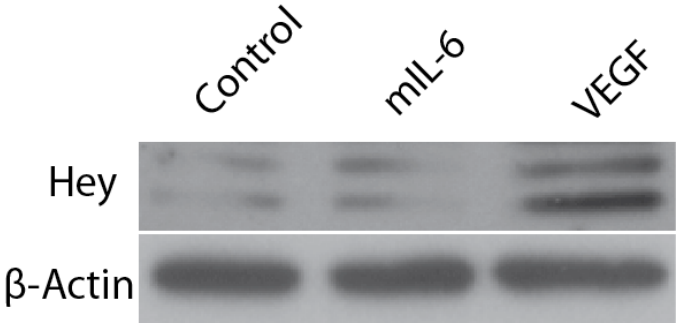

Figure 6.2 Western blot analysis of the expression of Hey in VEGF or mIL-6 treated MLEC.
$2x10^5$ MLEC cells were plated and treated with control (PBS), VEGF or mIL-6 for 24 hours. The cells were then lysed and 20ng/ml of protein was used to detect the levels of Hey using western blotting analysis. β-actin was used as loading control. This is typical of two independent experiments. This experiment was also repeated at 2 hours and 6 hours.

Figure 6.2 showed an increase in expression of Hey in the VEGF treated group but not in the mIL-6 or control treated groups. This further gives proof of the activation of the DLL4-Notch signalling in the MLEC after stimulation with VEGF but not with IL-6.

Once I established the differential regulation of the angiogenic ligand Jagged1 and DLL4 being a possible explanation for the decreased level of pericyte in the IL-6 treated group, I was then interested to look further into the mechanism and understand the reasons for the loose association of pericytes in the IL-6 treated vessels. It was at this point that I came across a study carried by Kayakabe *et al*, that showed a regulation of Angiopoeitin2 (Ang2) by IL-6 [184]. Angiopoeitin1 (Ang1) plays a key role in the attachment of the pericytes to the endothelium and Ang2 is known to be an antagonist of Ang1. Ang2 blocks the interaction between the Ang1 on the pericytes and the Tie receptor on the endothelial cells [187]. I therefore wanted to study the regulation of Ang2 in MLEC after treatment with VEGF or mIL-6

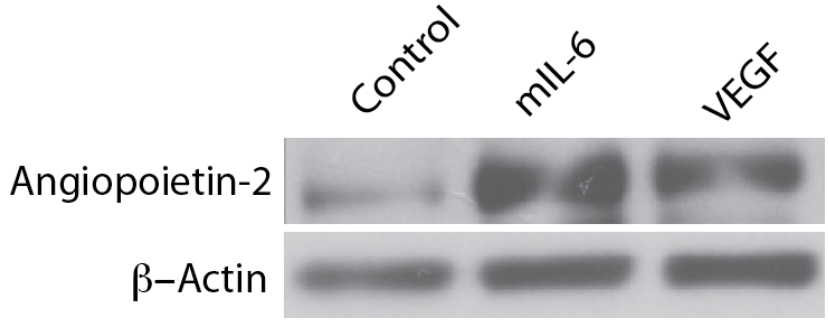

Figure 6.3 Western blot analysis of the expression of Angiopoietin-2 in VEGF and mIL-6 treated MLEC.
$2x10^5$ MLEC cells were plated and treated with control (PBS), VEGF or mIL-6 for 24 hours. The cells were then lysed and 20ng/ml of protein was used to detect the levels of Angiopoietin-2 using western blotting analysis. β-actin was used as loading control. This is typical of two independent experiments. This experiment was also repeated at 2 hours and 6 hours.

Figure 6.3 shows the expression of Ang-2 in MLEC treated with VEGF or mIL-6 after 24 hours. There is an increase in level of Ang-2 in the VEGF and mIL-6 treated MLEC, with mIL-6 inducing higher expression of Ang-2 compared to VEGF. This difference in expression of Ang-2 could be a possible reason for the altered maturation status observed in the aortic ring assay after treatment with VEGF or mIL-6.

Next, I decided to look into N-cadherin which is another protein that is involved in endothelial-pericyte interaction [188]. As already mentioned, N-cadherins are glycoproteins that mediate calcium dependent cell-cell adhesion. A study also suggested that, N-cadherin deficiency leads to impaired pericyte recruitment [140]. This study showed that N-cadherin is not essential for endothelial migration or sprouting but it is required for the subsequent maturation of the endothelial sprouts. So, I wanted to investigate the effects of mIL-6 and VEGF on the expression of N-cadherin in MLEC.

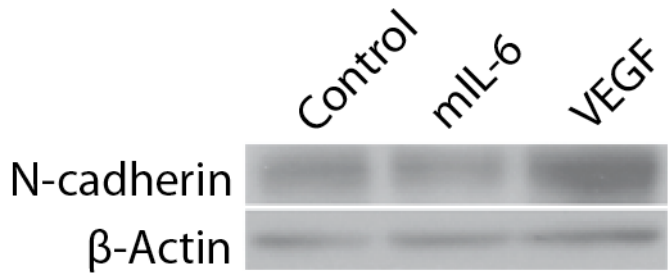

Figure 6.4 Western blot analysis of the expression of N-cadherin in VEGF and mIL-6 treated MLEC.
$2x10^5$ MLEC cells were plated and treated with control (PBS), VEGF or mIL-6 for 24 hours. The cells were then lysed and 20ng/ml of protein was used to detect the levels of N-cadherin using western blotting analysis. β-actin was used as loading control. This experiment was also repeated at 2 hours and 6 hours.

Figure 6.4 shows the expression of N-cadherin in MLEC after treatment with mIL-6 and VEGF. There was a slight decrease in the level of N-cadherin in the mIL-6 treated MLEC compared to the control. However, in the VEGF treated group there was an increase in expression of N-cadherin compared to the mIL-6 and the control group. This result correlated with the findings of the previous study and adds a possible explanation for the impaired interaction between the endothelial cells and pericytes in the presence of IL-6 [140]. This is however a preliminary result and it needs to be repeated for further confirmation.

Unravelling the mechanisms of action of VEGF and IL-6 on MLEC showed differential regulation of the Notch ligands Jagged1 and DLL4 by IL-6 and VEGF in MLEC. This correlated with the known role of DLL4 in vessel maturation and Jagged1 in excessive sprouting. The VEGF induced activation of the downstream repressor gene Hey also correlated with the known regulation of DLL4-Notch signalling by VEGF. Investigating more into mechanism of pericyte detachment showed a positive regulation of Ang-2 and a negative regulation of N-cadherin by IL-6 in MLEC. This also gave a possible explanation for the detachment of pericytes on the IL-6 treated vessels.

Although technically challenging, I would aim to extract protein from the aortic rings treated with IL-6 or VEGF and do the same experiments.

7 Study the effects of VEGFR inhibitor on aortic ring assay and on MLEC

In the previous chapter, experiments on mechanism of action of VEGF and IL-6 in MLEC showed differential regulation of the Notch ligands and Ang2 by IL-6 and VEGF. These findings along with the differences in pericyte coverage observed after treatment with VEGF or IL-6 in the aortic ring assay (chapter 5), further suggest that these pathways don't depend on each other for their angiogenic effects. Therefore, I wanted to investigate the angiogenic effects of IL-6 in the presence of a VEGFR inhibitor.

In this chapter I will present some preliminary data from studies with a VEGFR inhibitor in the aortic ring assay and in MLEC. The VEGFR inhibitor used for my study was cediranib, which is a VEGFR2 inhibitor that is currently used in clinical trial in various cancers. Cediranib was recently used in a Phase III clinical trial in ovarian cancer patients and it prolonged progression free survival by 3 months compared to standard chemotherapy alone [189].

7.1 To study the angiogenic effects of IL-6 using a VEGFR inhibitor in the aortic ring assay

The first set of experiments that I carried out using the VEGFR inhibitor, which further confirmed IL-6 could drive angiogenesis independent of VEGF signalling, were in the aortic ring assay. First I carried out a dose response experiment with cediranib to identify the optimal dose needed to inhibit sprouting in the VEGF treated group. Using the aortic ring assay, I wanted to investigate if IL-6 can still induce sprouting in the aortic ring assay in the presence of a VEGFR inhibitor, cediranib.

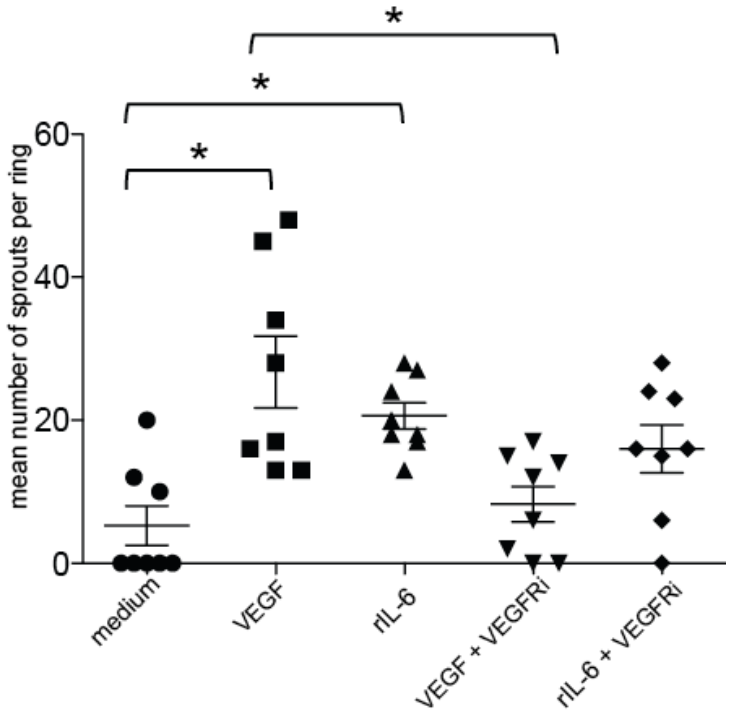

Figure 7.1 Mean number of sprouts in aortic rings treated with medium, VEGF, rIL-6, VEGF + cediranib (VEGFRi) and rIL-6 + VEGFRi.
Aortas removed following cervical dislocation of a 180-200g rats were treated with optimem medium containing 1% FCS with 10ng/ml VEGF (R&D) or 10ng/ml rIL-6 (R&D), 10nM VEGFRi + VEGF/rIL-6 over a course of 2 weeks. The medium was changed every 3 days. The rings were imaged using phase contrast microscopy and microvessel outgrowth was counted and quantified (p value < 0.002 between medium and VEGF), (p value < 0.0004 between medium and rIL-6), (p value < 0.0054 between VEGF and VEGF +VEGFRi), (p value < 0.24 between rIL-6 and rIL-6 + VEGFRi). *Represents statistical significance. This result represents typical of two independent experiments.

Figure 7.1 shows the result of the aortic ring assay treated with VEGF and rIL-6 in combination with the VEGFRi. As expected, there were a significantly higher

number of sprouts in the VEGF and rIL-6 treated group as compared to the medium. In the terms of the VEGF + VEGFRi treated group, the VEGFRi inhibited sprouting in some of the aortas and even the aortas that managed to overcome the inhibition had significantly lower number of sprouts as compared to the VEGF alone treated group. However, in case of the rIL-6 + VEGFRi group, most of the aortas were able to overcome the inhibition of the VEGFRi. Even in terms of number of sprouts, there were not any significant difference between the rIL-6 and rIL-6 + VEGFRi group. This further supports the findings from the MLEC suggesting IL-6 and VEGF signalling might not be dependent on each other for its angiogenic effects.

7.2 The effects VEGFRi on pSTAT3 induction in the MLEC

I then decided to investigate the effects of the VEGFRi on MLEC after treatment with recombinant VEGF or mIL-6. I was interested in exploring this because elevated levels of IL-6 in patient plasma has shown to correlate with anti- angiogenic therapy resistance in various cancers [159, 160]. However, the effects of VEGFRi on IL-6 signalling on endothelial cells are still unknown.

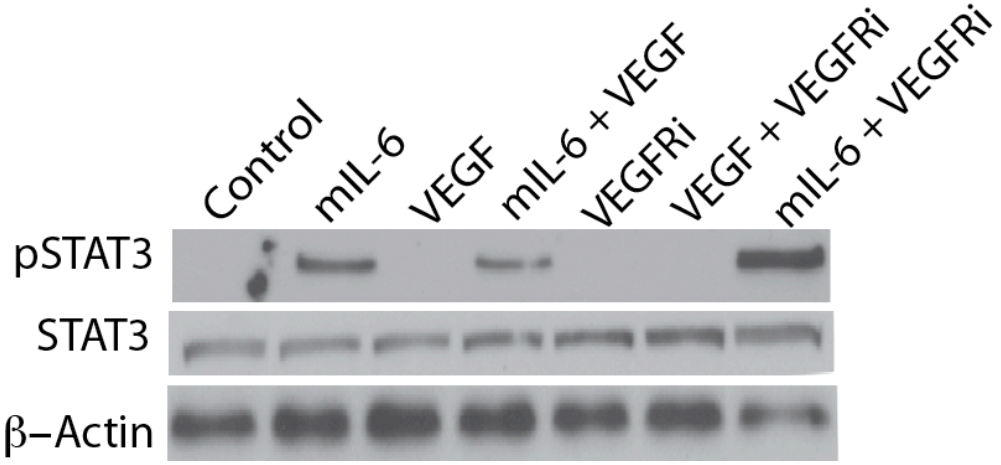

Figure 7.2 Western blot analysis of the expression of pSAT3 in VEGF, mIL-6, cediranib (VEGFRi) treated MLEC.
$2x10^5$ MLEC cells were plated and treated with control (PBS), VEGF (30ng/ml), mIL-6 (30ng/ml), VEGFRi (100nM), VEGF + VEGFRi and mIL-6 + VEGFRi for 24 hours. The cells were then lysed and 20ng/ml of protein was used to detect the levels of pSTAT3 and STAT3 using western blotting analysis. β-actin was used as loading control.

The western blot shown in Figure 7.2 shows the expression of pSTAT3 after treatment with recombinant mIL-6, VEGF, VEGFRi +/- VEGF or rIL-6. As expected, mIL-6 treatment resulted in upregulation of pSTAT3 in MLEC, however treatment with mIL-6 and VEGF led to a slight decrease in pSTAT3 levels. This might suggest VEGF has an inhibitory effect on IL-6 downstream signalling in endothelial cells. However, the interesting finding from this western blot analysis was the increased expression of pSTAT3 observed in the mIL-6 + VEGFRi group as compared to the mIL-6 group. This upregulation of pSTAT3 in the presence of IL-6 on MLEC was also observed with other VEGFR inhibitors i.e. Brivanib and Apatanib (data not shown). This suggests endothelial cell inhibition of VEGFR in tumours expressing IL-6 can lead to upregulation of pSTAT3. With reference to Chapter 5, this finding implies a vasculature with very defective pericyte coverage and increased chances of metastasis after treatment with VEGFRi. This result therefore suggested a potential for combination of VEGFR and IL-6 inhibitor for targeting tumours with high levels of IL-6.

7.3 The effects VEGFRi + rIL-6 on pericyte coverage in aortic ring assay

I was then interested in studying the effects of VEFFRi on pericyte coverage in aortic ring vessels treated with rIL-6. I wanted to investigate this because of the previous finding, which suggested VEGFRi inhibition on endothelial cells treated with recombinant IL-6 leads to increased expression of pSTAT3 compared to recombinant IL-6 alone.

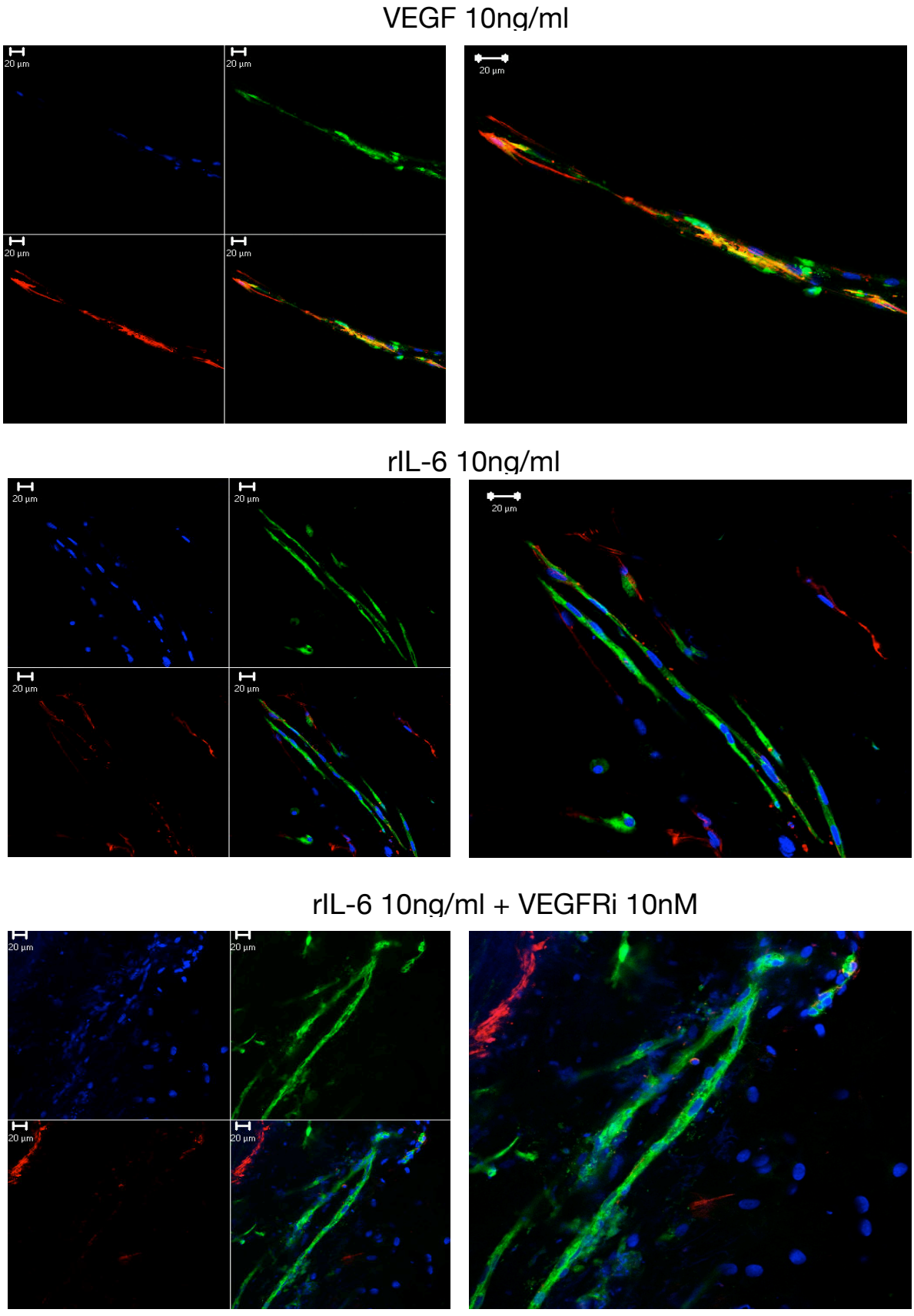

Figure 7.3 Immunofluorescence staining of aortic rings after treatment with VEGF 10ng/ml, rIL-6 or rIL-6 10ng/ml + VEGFRi 10nM over a course of 2 weeks.

BS1 lectin-FITC (green) stains endothelial sprouts, α-SMA-Cy3 (red) stains the pericytes and DAPI (blue) is for staining the nucleus. The images display the pericyte coverage (red) around the matured endothelial sprouts (green). Scale bar = 20µm

Figure 7.3 show the pericyte (red) coverage on the aortic ring vessels (green) after treatment with VEGF, rIL-6 and rIL-6 + VEGFRi. These preliminary results show good pericyte coverage on the VEGF treated vessels as expected and poor or detached pericyte coverage on the rIL-6 treated vessels. However in case of VEGFRi + rIL-6 treated vessels there are hardly any pericytes associated with the vessels compared to the other two groups. This further supported the pSTAT3 upregulation observed in the MLEC after treatment with the VEGFR inhibitor.

A summary of the proposed mechanism of action of VEGFRi on endothelial cells in the presence of IL-6 is shown in Figure 7.4. This summary is based on studies, which have reported that sustained Src inhibition as a result of VEGFR inhibition could lead to increase in pSTAT3 expression [190]. My preliminary data on MLEC also correlated with this study and showed a compensatory effect on pSTAT3 as a result of Src inhibition using the VEGFR inhibitor (data not shown). This increased pSTAT3 expression as a result of Src inhibition leads to even weaker perciyte coverage as on vessels as shown in Figure 7.3.

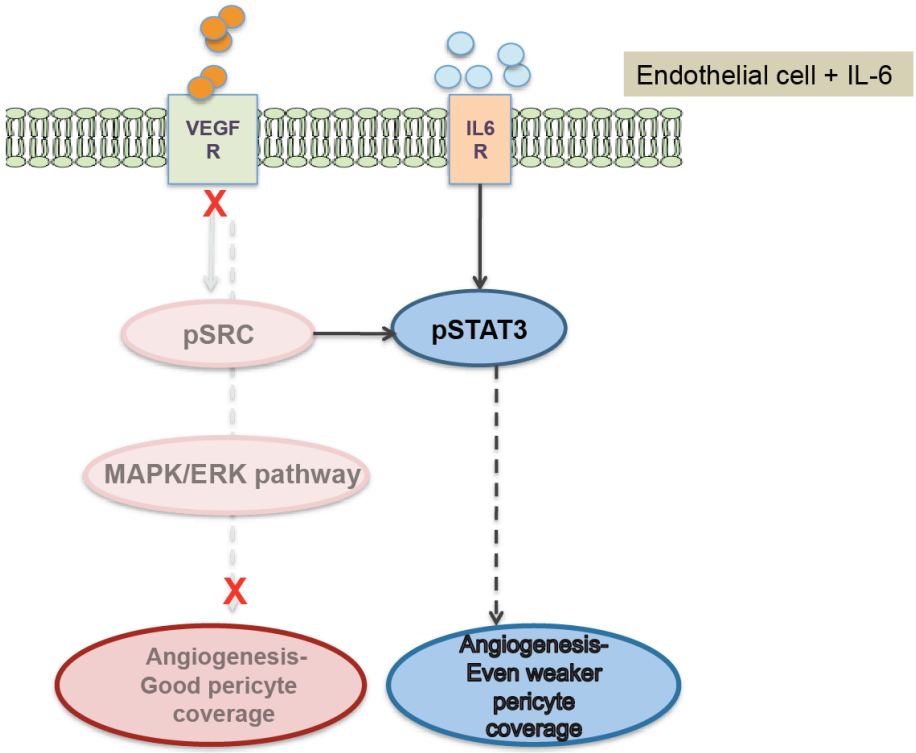

Figure 7.4 Showing the proposed mechanism of action of VEGFi on endothelial cells in the presence of IL-6.
VEGFRi leads to inhibition of pSrc, which results in increased expression of pSTAT3 and even weaker pericyte coverage.

All the above shown results in this section are preliminary data and therefore they need to be repeated and carried out at different time points with different doses of inhibitors to fully validate these findings. However, they do give further evidence that IL-6 and VEGF have different mechanism of action on endothelial cells. The VEGFRi induced upregulation of pSTAT3 in the presence of IL-6 also suggest a compensatory effect on IL-6 signalling upon VEGFR inhibition in the endothelial cells. This therefore suggests a potential for combining VEGFR inhibitors with anti-IL-6 agents in IL-6 driven tumours.

8 Study the effects of the anti-IL-6 antibody on pericyte coverage in IGROV-1 xenografts

In parallel to the *ex vivo* and *in vitro* work that was carried to understand the effects and mechanism of IL-6 and VEGF induced angiogenesis, I was also interested in studying the effects of an anti-IL-6 antibody in ovarian cancer xenografts. This is because tumour cells use blood vessels as a route to spread during metastasis and also the growth of the primary tumour depends on the formation of the tumour vasculature. There are often abnormalities within the primary tumour that lead to increased perfusion and escape of the tumour cells into the circulation. The abnormal vasculature is often characterised by leaky vessels displaying gaps in the endothelium [191, 192]. This not only leads to increased metastasis but also increased drug resistance due to poor drug delivery to the organs.

As previously described, IL-6 is linked to poor prognosis in ovarian cancer patients [35]. A recent study in prostate cancer showed endothelial cells enhance prostate cancer metastasis via IL-6 [193]. Treatment of ovarian cancer xenografts with an anti-IL-6 antibody not only led to reduction in vasculature but also resulted in normalisation of the blood vessels [35]. This suggests that IL-6 production in the tumour microenvironment could contribute to the destabilised and chaotic vasculature.

Therefore, in this chapter I was interested in investigating the pericyte coverage in IL-6 producing IGROV-1 ovarian cancer xenografts after treatment with the anti-IL-6 antibody. I also wanted to investigate some of mechanisms previously studied in the MLEC in the vivo tumour samples after treatment with the anti-IL-6 antibody.

8.1 Staining for Lectin, α-SMA and DAPI in anti-IL-6 treated IGROV-1 xenografts

Mice injected intraperitoneally with IGROV-1 cells (IL-6 producing cells) were treated with either 20mg/kg of IgG control antibody or anti-IL-6 antibody. To visualise the vasculature the terminal animals were anaesthetised with isoflourane and injected with FITC conjugated lectin via tail vein 3 min before animals were perfused with 4% paraformaldehyde. In these lectin stained frozen tumour sections, I decided to stain for pericytes with a widely used marker for pericytes i.e. α-SMA. This was carried out to compare the differences in the pericyte coverage of the tumour vessels in the IGROV-1 control and anti-IL-6 treated tumours.

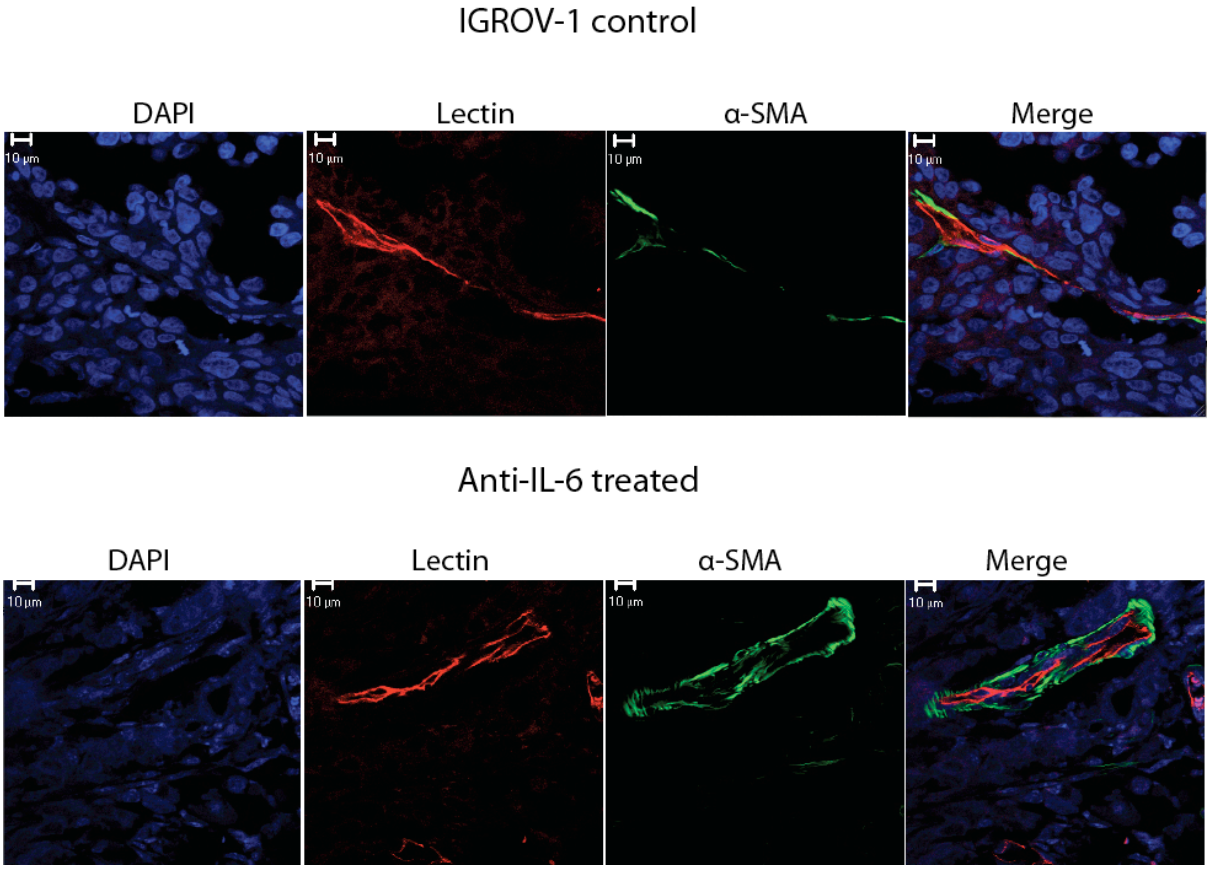

Figure 8.1 Confocal images of IGROV-1 control antibody and anti-IL-6 treated IGROV-1 tumours stained for lectin (red), α-SMA (green) and DAPI (blue).
The control antibody (20mg/kg) and anti-IL-6 (20mg/kg) treated mice were injected with lectin via tail vein 3 min before fixing. This was followed by snap freezing, sectioning of the tumour and staining for α-SMA (green). Images of the stained sections were taken using confocal microscopy (Scale bar = 10microns)

Figure 8.1 shows the IGROV-1 xenograft tumours treated with an anti-IL-6 antibody stained for blood vessels and pericytes using lectin and α-SMA.

In the IGROV-1 control group there were very few pericytes around the vessels and this was noted in majority of the cases. Also, the vessels in the control group seemed to be more disorganised and discontinuous, which might suggest a leaky vasculature. However, in the anti-IL-6 treated group there seemed to be good pericyte around the tumour vessels indicating mature vasculature. These results correlate with the findings from the aortic ring assay where the recombinant IL-6 led to decreased vessel maturation.

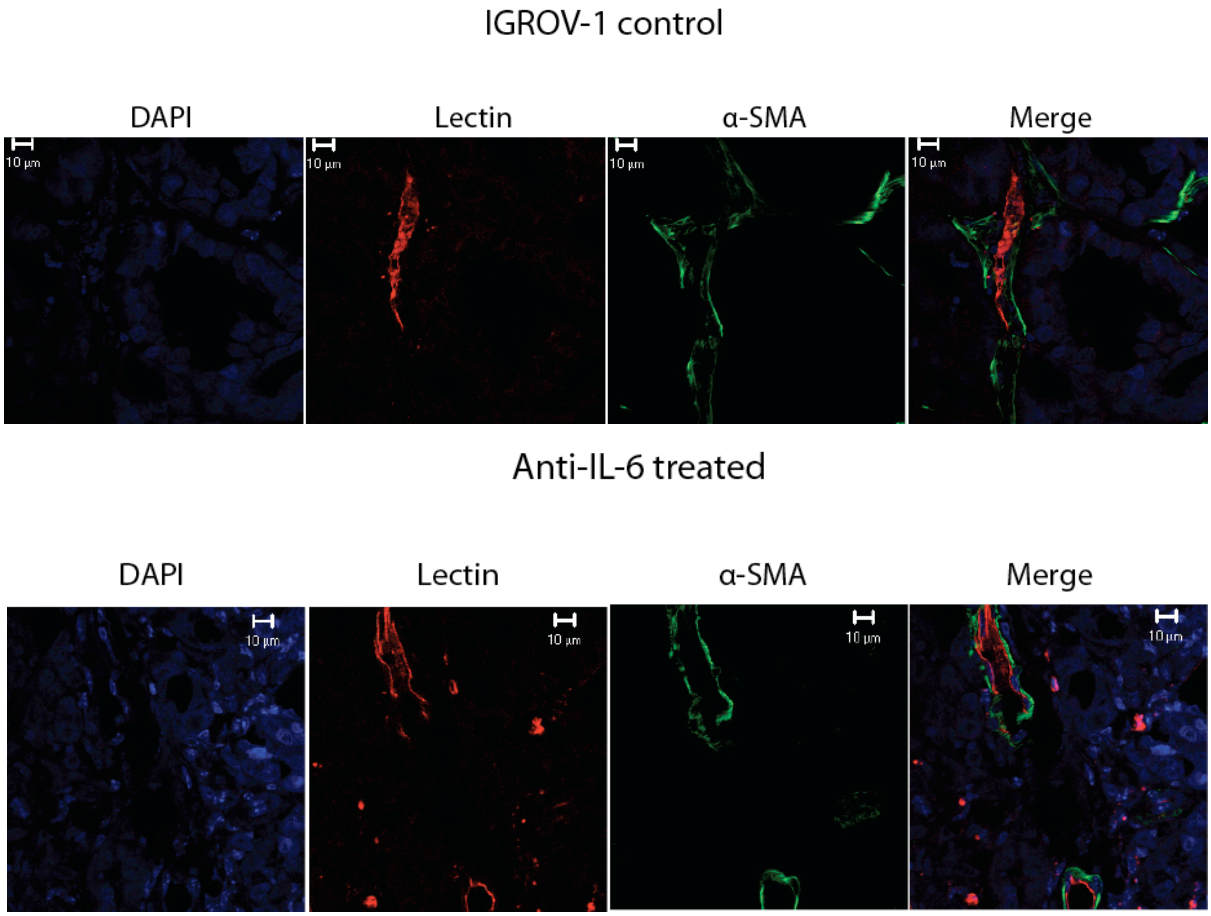

Figure 8.2 Showing the staining for Lectin (red), α-SMA (green) and DAPI (blue) on IGROV-1 control antibody and anti-IL-6 treated tumours.
The control and anti-IL-6 treated mice were injected with lectin via tail vein 3 min before fixing. This was followed by snap freezing, sectioning of the tumour and staining for α-SMA (green). Images of the stained sections were taken using confocal microscopy (Scale bar = 10microns)

Figure 8.2 shows the IGROV-1 control antibody and anti-IL-6 treated tumours stained for blood vessels and pericytes using lectin and α-SMA. This figure is shown to highlight the fact that in some cases especially with the IGROV-1 control tumour sections, the pericytes seemed to be loosely attached or detaching from the vessels, however this was hardly noticed with the anti-IL-6 treated tumours. This again links

with the finding from the aortic ring assay where treatment with recombinant IL-6 led to detachment of pericytes from the vessels.

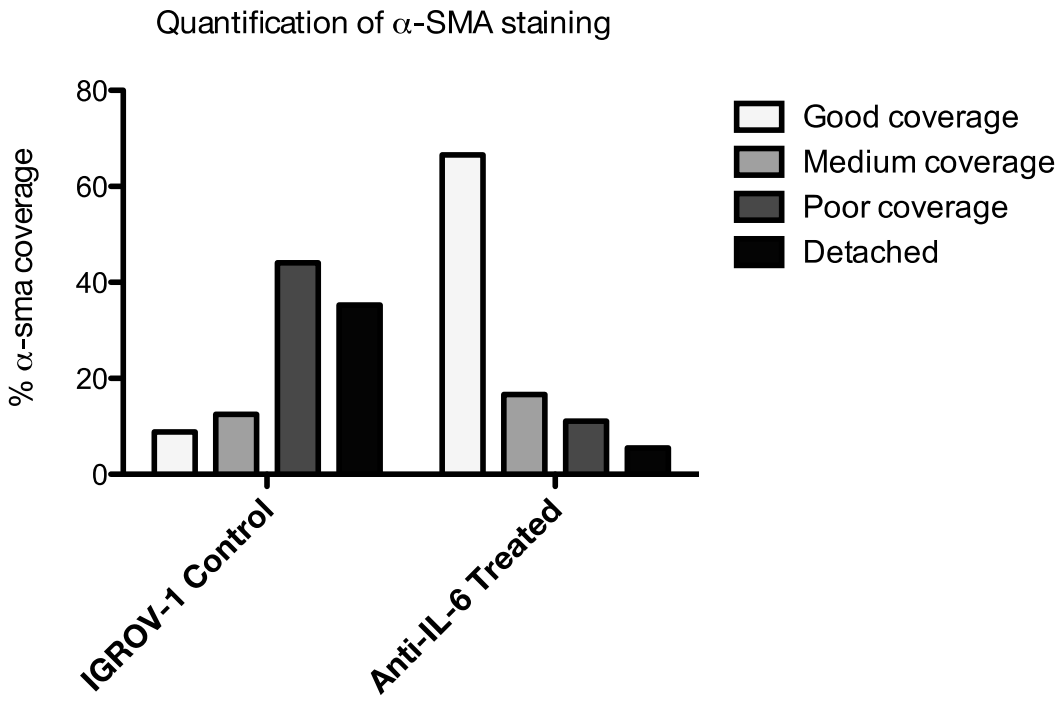

Figure 8.3 Quantification of α-SMA on tumour vessels treated with either IGROV-1 control antibody or anti-IL-6 antibody.
The control and anti-IL-6 treated mice were injected with lectin via tail vein 3 min before fixing. This was followed by snap freezing, sectioning of the tumour and staining for α-SMA. The blinded images from two independent experiments (n=6 per group) were quantified according to the 4 different criteria i.e. good coverage, medium coverage, poor coverage and detached by two independent reviewers. (IGROV-1 control vs anti-IL-6 treated, chi square test p value <0.001)

Figure 8.3 shows the quantification of the α-SMA staining in the IGROV-1 control antibody and anti-IL-6 antibody treated tumours. In the IGROV-1 control antibody treated tumours 44% of the vessels showed poor staining of α-SMA and 35% of the vessels had detached pericytes. The remaining 21% of vessels had either good or medium α-SMA staining. However, in case of the anti-IL-6 antibody treated tumours, 66% of the vessels showed good pericyte coverage and 17% of the vessels had medium pericyte coverage according to the α-SMA staining observed. Only the remaining 16% of vessels showed either poor or detached pericyte coverage. This observation again correlates with the findings from the aortic ring assay, where IL-6 led to poor or detached pericyte coverage.

Since α-SMA can also stain for activated fibroblasts in the tumour vasculature it was important to use another marker to confirm the differences in the pericyte staining observed with the control and the anti-iL-6 treated IGROV-1 tumours.

8.2 Staining for Lectin, NG2 and DAPI in anti-IL-6 treated IGROV-1 xenografts

There is no known single entirely specific marker for pericytes, therefore generally two or more pericyte markers are used alongside endothelial cell staining. Neural glial antigen 2 (NG2) is a proteoglycan that is expressed on pericytes in the tumour vasculature [194]. Therefore, I decided to stain the IGROV-1 tumour sections with NG2.

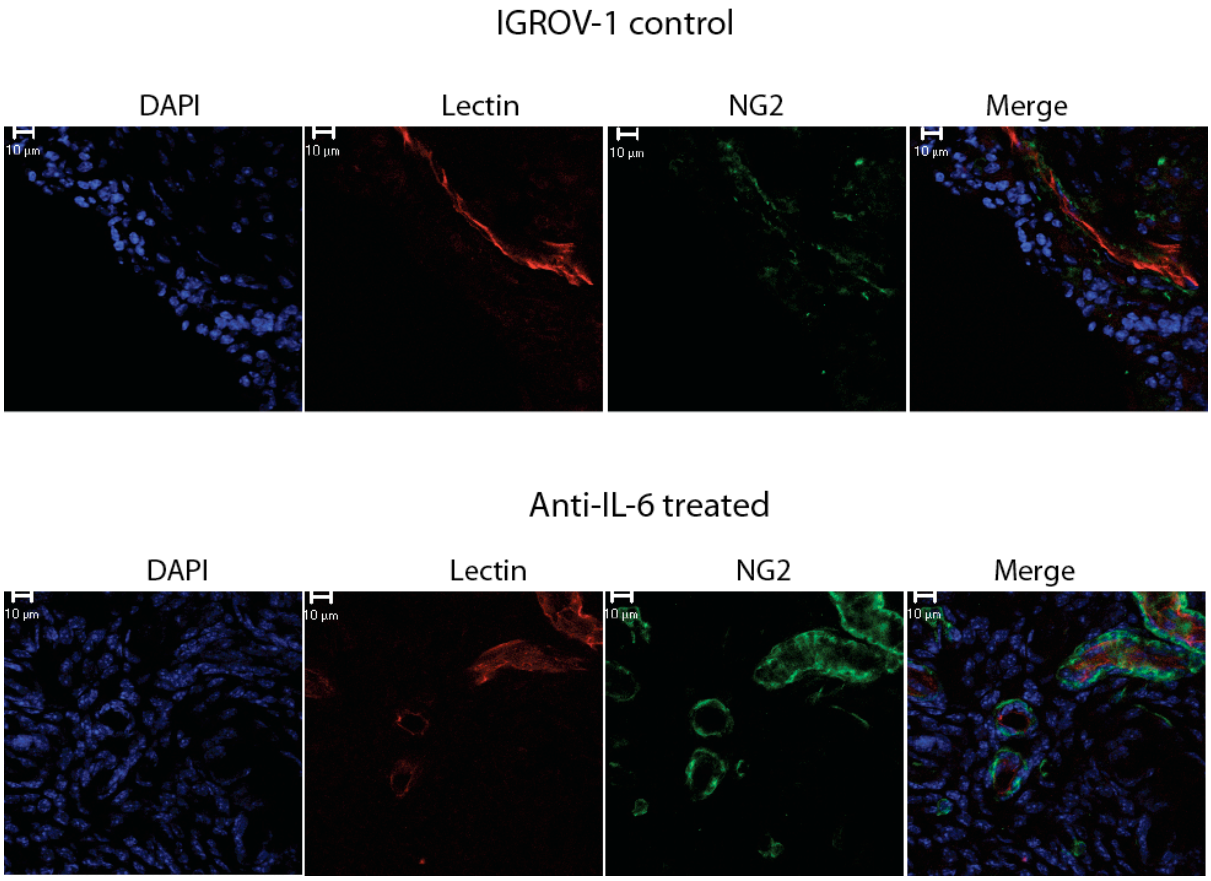

Figure 8.4 Confocal images of IGROV-1 control antibody and anti-IL-6 treated IGROV-1 tumours stained for lectin (red), NG2 (green) and DAPI (blue).
The control and anti-IL-6 treated mice were injected with lectin via tail vein 3 min before fixing. This was followed by snap freezing, sectioning of the tumour and staining for NG2 (green). Images of the stained sections were taken using confocal microscopy (Scale bar = 10microns)

Figure 8.4 shows the IGROV-1 control tumours stained for blood vessels and pericytes using lectin and anti-NG2. The NG2 staining in the tumour endothelium in the IGROV-1 control and anti-IL-6 treated IGROV-1 tumours are similar to the α-SMA staining observed in Figure 7.1. The IGROV-1 control tumours seems to have poor pericyte coverage as compared to the anti-IL-6 treated tumours.

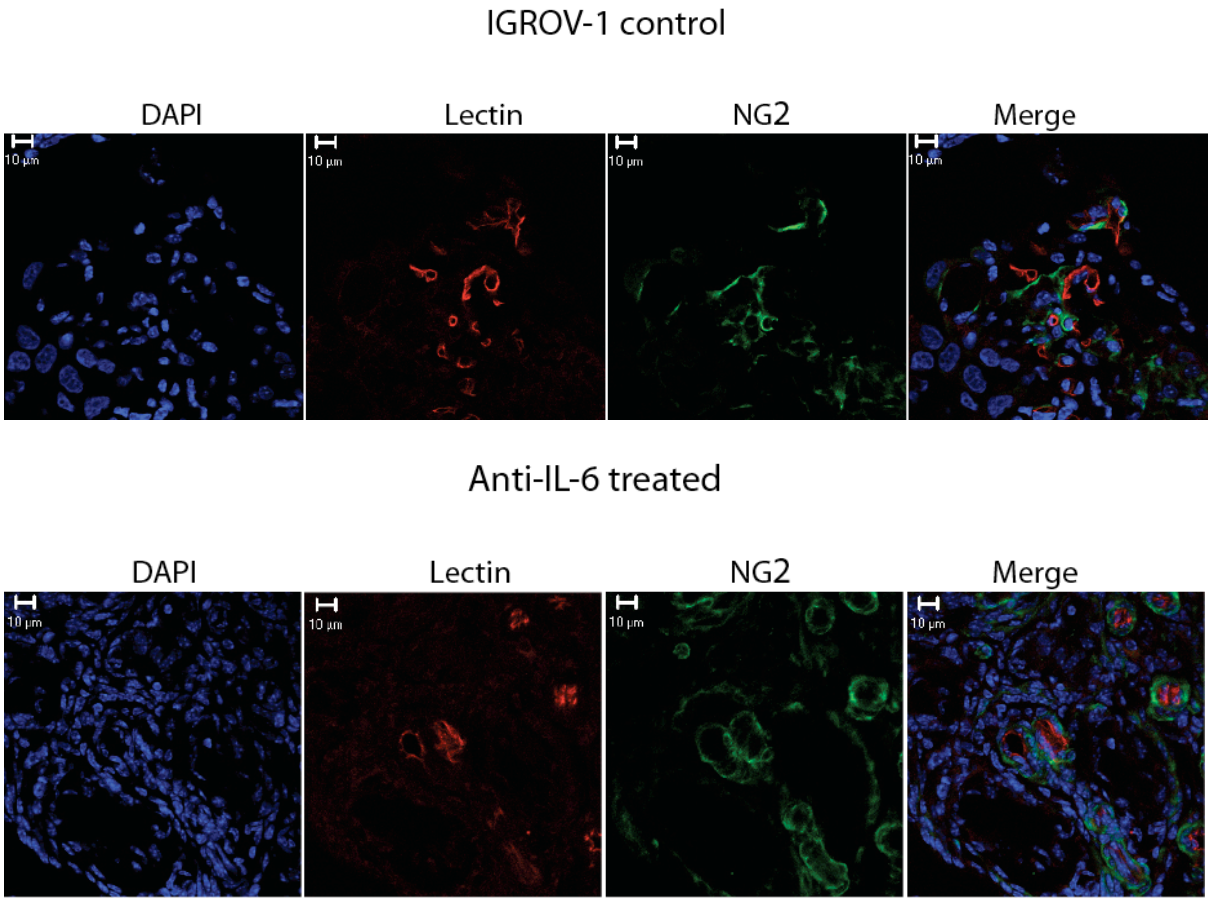

Figure 8.5 Showing the staining for Lectin (red), NG2 (green) and DAPI (blue) on anti-IL-6 treated IGROV-1 tumours.

The control and anti-IL-6 treated mice were injected with lectin via tail vein 3 min before fixing. This was followed by snap freezing, sectioning of the tumour and staining for α-SMA (green). Images of the stained sections were taken using confocal microscopy (Scale bar = 10microns)

Figure 8.5 shows the IGROV-1 control tumours stained for blood vessels and pericytes using lectin and anti-NG2. As witnessed with the α-SMA staining in Figure 7.2, NG2 staining also showed loose attachment of pericytes with the blood vessels in the some of the IGROV-1 control tumours. This implicated the possible involvement of some angiogenic genes that is regulated by IL-6 in the detachment of pericyte from the endothelium.

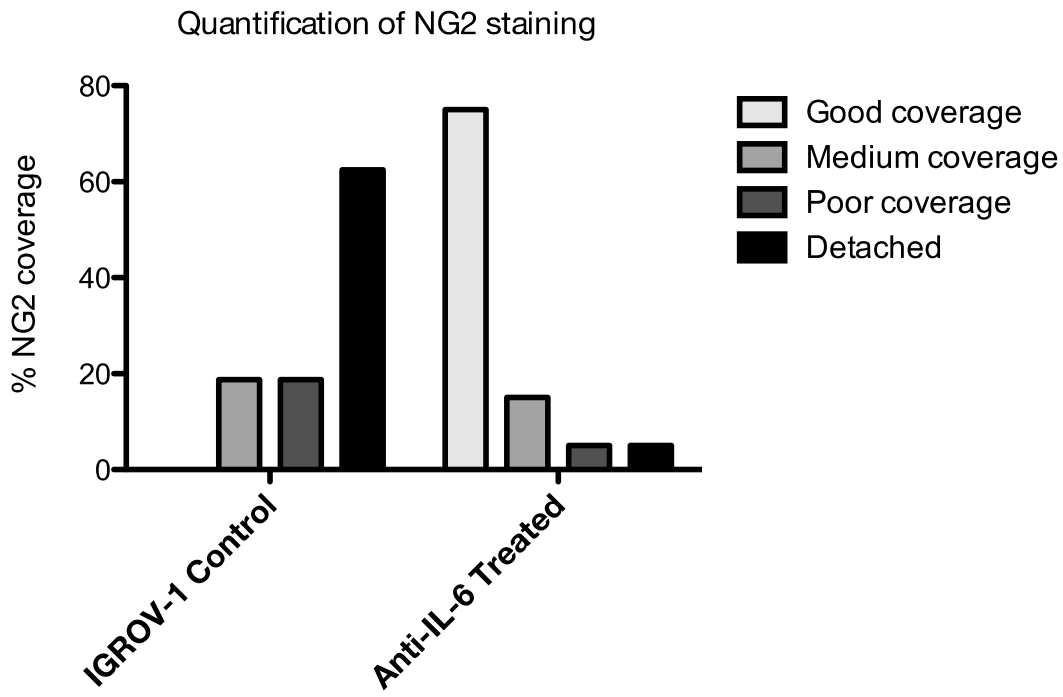

Figure 8.6 Quantification of NG2 on tumour vessels treated with either IGROV-1 control antibody or anti-IL-6 antibody.
The control and anti-IL-6 treated mice (n=3) were injected with lectin via tail vein 3 min before fixing. This was followed by snap freezing, sectioning of the tumour and staining for NG2. The blinded images from two independent experiments (n=6 per group) were quantified according to the 4 different criteria i.e. good coverage, medium coverage, poor coverage and detached by two independent individuals. (IGROV-1 control vs Anti-IL-6 treated, chi square test p value <0.001)

Figure 8.6 shows the quantification of the NG2 staining in the IGROV-1 control antibody and anti-IL-6 antibody treated tumours. According to the NG2 staining in the IGROV-1 control antibody group, 62.5% of the vessels had detached pericyte coverage and 18% of the vessels had poor pericyte coverage. The results were similar to the α-SMA staining with majority of the vessels showing poor or detached pericyte coverage, however there were almost twice the number of detached pericytes in the NG2 stained vessels than in the α-SMA stained vessels. This might therefore suggest that α-SMA staining might have picked up some activated fibroblast bound to the tumour vasculature thereby reducing the number of detached pericytes. However in case of the anti-IL-6 treated vessels, the NG2 staining were similar to the α-SMA staining with 75% of the vessels showing good pericyte coverage and 15% with medium pericyte coverage. Only 10% of the vessels had poor or detached pericyte coverage.

8.3 Immunohistochemistry staining of Jagged1, DLL4 and Ang2 in IGROV- 1 xenografts

It was important to investigate the mechanism previously explored in the MLEC cells (Chapter 6) regarding the regulation of the angiogenic factors by IL-6. This included looking at the expression of Jagged1, DLL4 and Ang2 in the IGROV-1 control and the anti-IL-6 treated tumours.

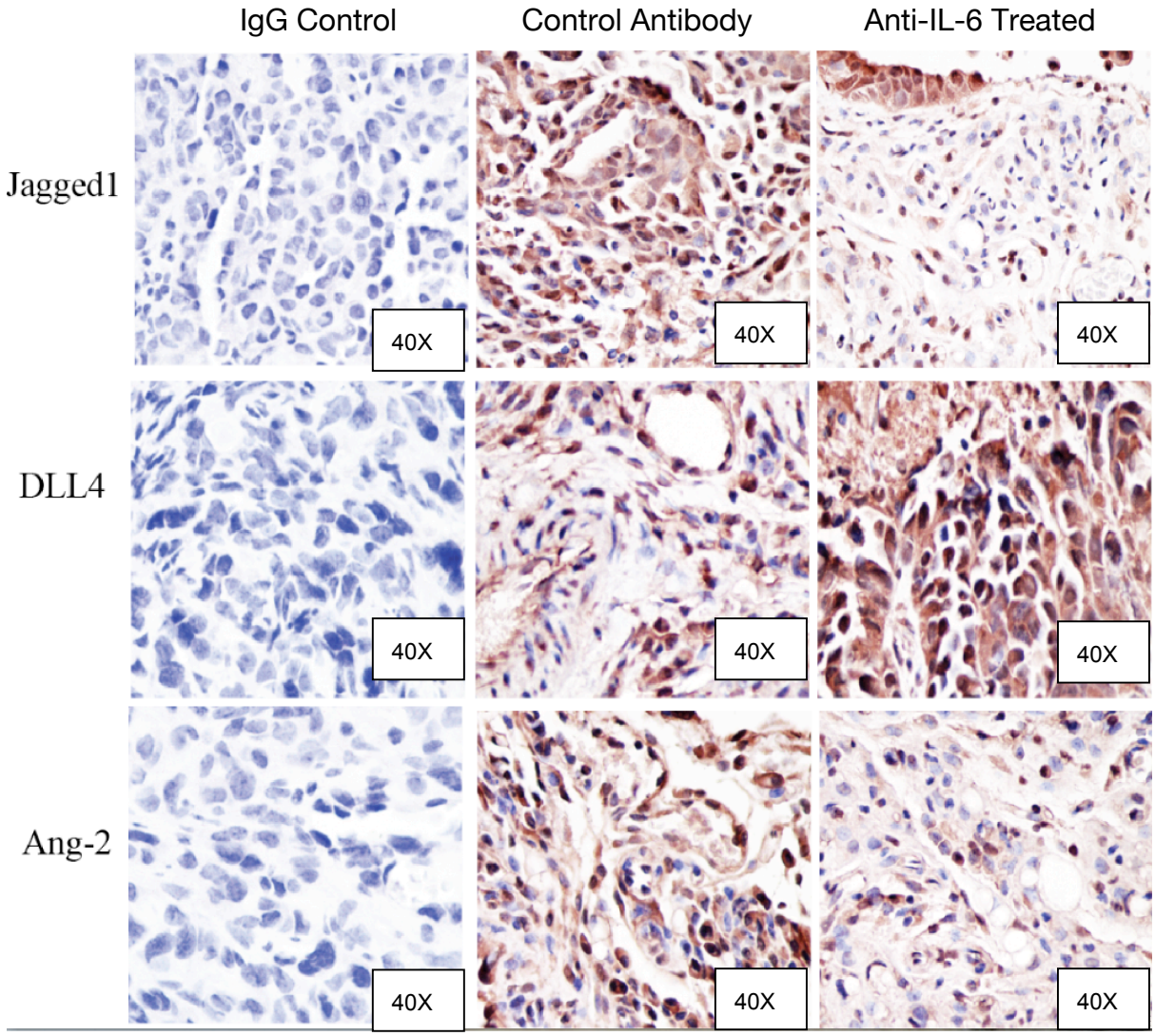

Figure 8.7 Jagged1, DLL4 and Ang-2 staining on IGROV-1 control antibody and anti-IL-6 treated mouse tumours.

The tumour sections collected from mice treated with either 20mg/kg of control antibody or anti-IL-6 antibody were paraffin fixed and cut into sections. The slides were then deparaffinised and stained with rabbit IgG control, Jagged1, DLL4 and Ang2 antibodies overnight at 4°C. The slides were then left for 2 hours with biotinylated anti-rabbit secondary antibody. Images were taken from two independent experiments using X40 magnification.

Figure 8.7 shows the staining for Jagged1, DLL4 and Ang-2 in the IGROV-1 control and anti-IL-6 treated tumour sections. As previously reported, Jagged1 staining is weaker in the anti-IL-6 treated group as compared to the control [35]. In terms of DLL4 the opposite was observed, there were more intense DLL4 staining in the malignant and stromal components in the anti-IL-6 treated group as compared with the control. Ang-2 was similar to the Jagged1 staining with weaker expression in the anti-IL-6 treated tumours as compared to the control. These findings further confirm the regulation of Jagged1 and Ang-2 by IL-6 and also suggest a possible explanation for the decreased pericyte coverage observed in the IGROV-1 control tumours.

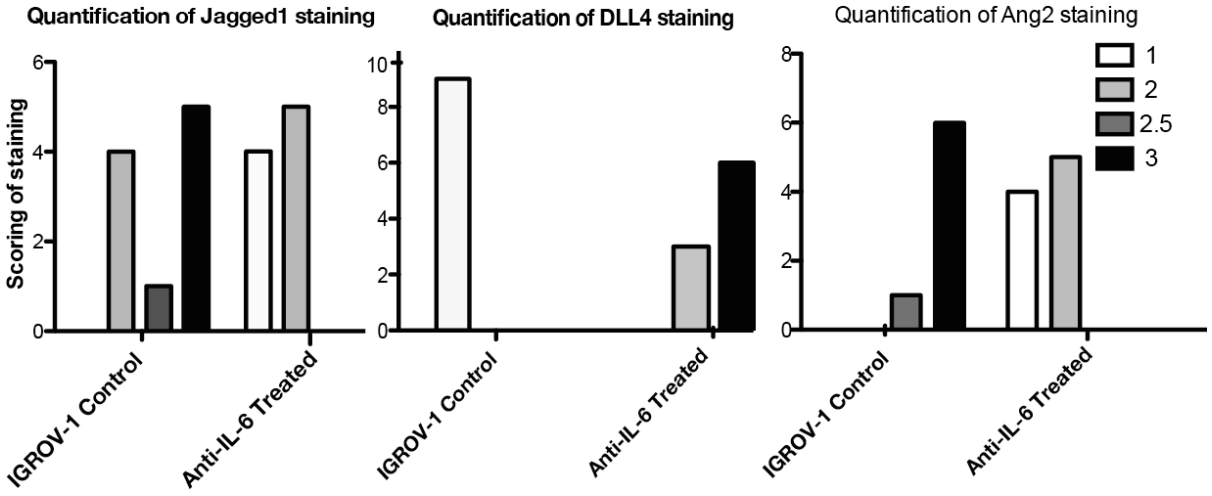

Figure 8.8 Quantification of Jagged1, DLL4 and Ang2 on mouse tumours treated with either IGROV-1 control antibody or anti-IL-6 antibody.
The tumours sections collected from mice treated with either 20mg/kg of control antibody or anti-IL-6 antibody were paraffin fixed and cut into sections. The slides were then stained for Jagged1, DLL4 or Ang2. Images were taken from 3 mouse sections per group using X40 magnification. The blinded images from two independent experiments were quantified according to the following scoring system (1 = little staining, 2 = faint partial staining, 2.5 = moderate staining, 3 = strong staining) by two independent reviewers.

Figure 8.8 shows the quantification of Jagged1, DLL4 and Ang2 staining using the above mentioned scoring criteria i.e. 1, 2, 2.5 and 3 with 1 being the faintest and 3 being the strongest. In the IGROV-1 control antibody group majority of the Jagged1 staining scored either 2 or 3, however in case of the anti-IL-6 treated group most of the Jagged1 staining only scored 1 or 2. The staining was opposite for DLL4 with

the entire control antibody treated group scoring the faintest 1 and the anti-IL-6 treated scoring 2 or 3. The Ang2 scoring was similar to the Jagged1 staining with majority of the control antibody tumours scoring 3 and the anti-IL-6 treated sections only scoring 1 or 2.

8.4 Analysis of the gene expression data set from the HGSC patient biopsies

I was then interested in looking into the gene expression dataset from HGSC patient biopsies to find any correlations with my *in vitro* and *in vivo* analysis. Therefore, gene expression data from 285 ovarian cancer biopsies from the AOCS (Australian Ovarian Cancer Study) dataset along with 245 samples obtained by merging two other publicly available datasets were ranked for expression of IL-6 pathway genes. Then 50 samples with the highest (high IL-6) and 50 samples with the lowest (low IL-6) levels of expression were selected and from that a list was generated of the differentially expressed genes between the high and low IL-6 samples [35]. These differentially expressed genes were then associated with various pathways and processes as shown below.

A

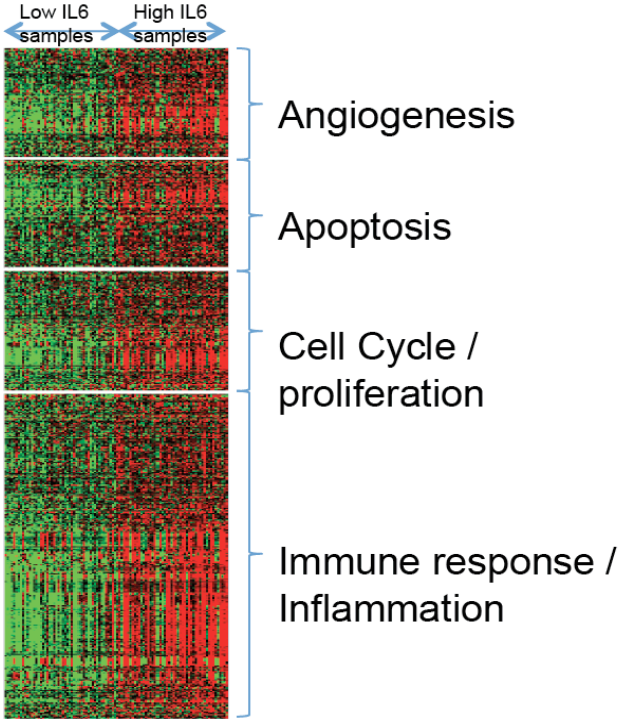

B

Gene symbol	Gene description	P value
ANGPT2	Angiopoietin2	0.015
JAG1	Jagged1	0.001

Figure 8.9 Heat map generated from the bioinformatics analysis of IL-6 pathway carried out in ovarian cancer patients.
A shows the differentially expressed genes from the high and low IL-6 samples were associated with various pathways and processes i.e. Angiogenesis, Apoptosis, Cell Cycle/proliferation and Immune response/ Inflammation. **B** indicates two of the angiogenic genes positively correlated with high IL-6 pathway expression.

Figure 8.9A shows the differentially expressed genes between the high and low IL-6 samples linked with the following pathways and processes i.e. Angiogenesis, Apoptosis, Cell Cycle/proliferation and Immune response/ Inflammation. Significant associations were found between the high IL-6 pathway gene expression and with various processes including angiogenesis. 8.9B shows that the high IL-6 pathway expression also correlated positively with genes that were reduced by the anti-IL-6 antibody treatment in the *in vivo* IGROV-1 xenografts i.e. Jagged1 and Ang2.

Finally, my studies so far on the differential regulation of IL-6 and VEGF on endothelial cells and the mechanism of action of VEGFR inhibitor on downstream IL-6 signalling have indicated a potential for the combination of anti-IL-6 antibody with the VEGFR inhibitor. Therefore, to sum up my study, I was interested in investigating the effects of combining an anti-IL-6 antibody with the VEGFR inhibitor in an IL-6 producing ovarian cancer cell line.

8.5 Study the effect of VEGFRi +/- anti-IL-6 antibody on pSTAT3 expression in IGROV-1

I wanted to investigate the effect of VEGFRi +/- anti-IL-6 antibody on pSTAT3 expression in IGROV-1 cells. This was carried out to find out if VEGFR inhibition leads to further upregulation of pSTAT3 in malignant cells expressing high levels of IL-6.

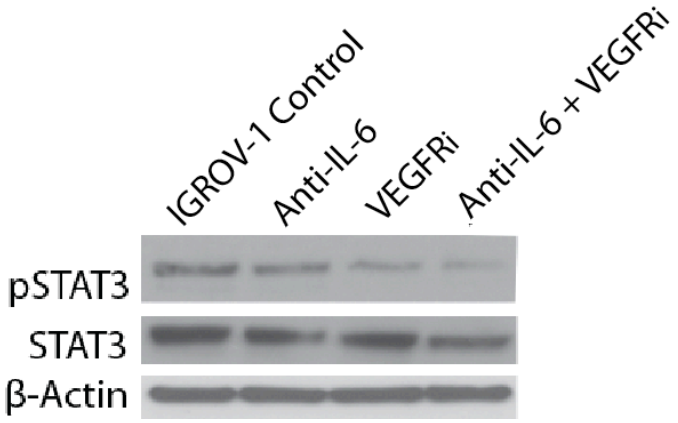

Figure 8.10 Western blot analysis of the expression of pSAT3 in IGROV-1 treated with Anti-IL-6 and VEGFRi.
$2x10^5$ IGROV-1 cells were plated and treated with 10ug/ml Anti-IL-6, 100nM VEGFRi and Anti-IL-6 + VEGFRi for 24 hours. The cells were then lysed and 20ng/ml of protein was used to detect the levels of pSTAT3 and STAT3 using western blotting analysis. β-actin was used as loading control.

Figure 8.10 shows the western blot analysis of pSTAT3 in IGROV-1 cells after treatment with anti-IL-6 and VEGFRi. These preliminary results show a slight decrease in pSTAT3 expression after treatment with an anti-IL-6 antibody as compared to control. However, treatment with VEGFRi inhibitor led to further decrease in expression of pSTAT3 and VEGFRi + anti-IL-6 antibody led to almost abolishment of pSTAT3 levels. This was very interesting because this showed that the VEGFR inhibitor had different effect on malignant and endothelial cells in the presence of IL-6.

In overall, using this *in vivo* chapter, I was able to confirm the observations I made in the previous *ex vivo* and *in vitro* chapters regarding the type of angiogenesis stimulated by IL-6 and its possible mechanisms of actions. The IGROV-1 xenograft study also showed it was possible to restore the pericyte coverage in the vasculature by treatment with an anti-IL-6 antibody. The HGSC patient gene expression dataset gave a further confirmation for the mechanistic findings regarding the regulation of Jagged1 and Ang2 by IL-6. This along with the findings from the previous chapter on VEGFR inhibitor further suggests the potential for combining VEGFR inhibitor with an anti-IL-6 agent. The combination therapy will be beneficial if VEGFR inhibition leads to upregulation of pSTAT3 in IL-6 expressing tumours thereby further leading to aberrant angiogenesis with poor pericyte coverage. Hence, combination with anti-IL-6 agents will help restore the pericyte coverage and help in tissue perfusion, limit metastasis and increase drug delivery.

9 Discussion & Plans for Future Work

9.1 Effects of IL-6 on normal and tumour angiogenesis

The pleiotropic cytokine IL-6 has been implicated in angiogenesis in diseases such as stroke, rheumatoid arthritis and various cancers [50, 184, 195]. Despite this evidence, to our knowledge there has been no in depth investigation undertaken to study the direct effects of IL-6 on endothelial cells. This thesis has presented the findings from an *ex vivo* model of angiogenesis along with a number of functional and mechanistic *in vitro* studies in the MLEC cells. These experiments were conducted in parallel with an IGROV-1 xenograft study and analysis of the HGSC patient gene expression datasets to find correlations with the *ex vivo* and *in vitro* findings. The experiments were undertaken to answer the following questions..

1) Does IL-6 have direct angiogenic effects on endothelial cells?
2) What are the differences in IL-6 and VEGF induced angiogenesis in the aortic ring assay?
3) What are the mechanisms of action of IL-6 on endothelial cells?
4) What is the effect on the ovarian cancer vasculature after treatment with an anti-IL-6 antibody?
5) Does this study suggest any possible combination therapy to target with an anti-IL-6 antibody?

In this chapter, I aim to discuss the extent to which this research has answered these questions addressed above and outline future studies that will be conducted as a result of this thesis.

9.1.1 Does IL-6 have direct angiogenic effects on endothelial cells?

The primary objective of the *ex vivo* study was to investigate if recombinant IL-6 can be angiogenic and lead to endothelial sprouting. Using the aortic ring assay, I was able to show that IL-6 alone can induce sprouting of vessels at concentrations similar

to VEGF. I used the number and length of sprouts as the two parameters to examine the angiogenic potency of IL-6 compared to VEGF. The results of my study showed no significant difference in the two parameters suggesting IL-6 is almost as potent as VEGF in inducing sprouting in the aortic ring assay. This finding was further confirmed with recombinant human, mouse and rat IL-6 in mouse and rat aortic ring assays.

Alongside this, *in vitro* studies were conducted in MLEC cells to study the functional and mechanistic effects of IL-6 as an angiogenic agent. My findings confirmed previous studies indicating IL-6 can drive endothelial proliferation and migration [163, 164]. In addition to this, the MLEC line was used to study the downstream mechanism via which IL-6 drives angiogenesis. This was mainly carried out to understand if the angiogenic effects observed with IL-6 were due to a response via VEGF and if the two pathways are dependent on each other for signalling in MLEC. Investigating the direct downstream targets of IL-6 and VEGF i.e. pSTAT3 and pERK suggested that the two pathways are independent of each other for signalling in the MLEC.

9.1.2 What are the differences in IL-6 and VEGF induced angiogenesis in the aortic ring assay?

Further exploration of the results from the *ex vivo* studies led to the most interesting observation of the study. This finding came from the confocal images of aortic ring vessels stained for lectin and α-SMA, which showed a striking difference in the pericyte coverage of the vessels treated with recombinant VEGF and IL-6. Quantification of this staining later showed a significantly reduced number of pericytes in the IL-6 treated vessels as compared to the VEGF treated ones. Another interesting observation made from the confocal images was of the detachment of pericytes in some of the IL-6 treated vessels. The observations relating to pericytes and IL-6 have clinical implications in malignant and other diseases especially as studies in various cancers suggest that pericyte depletion leads to increased metastasis in tumours [138, 182, 183].

The role of pericytes in the tumour vasculature is controversial [183]. Whilst a normalised, functional and perfused vasculature could enhance tumour growth by providing oxygen and nutrients to the primary tumour, destabilised, non-functional and permeable vasculature can enhance metastasis and chemoresistance. This may be why approaches of treating cancers with an anti-VEGF agent that targets the immature vasculature and then combining it with an agent such as a PDGFRβ inhibitor that affects the mature vasculature, have not shown much promise [151]. This is also shown in various studies such as the one carried out in invasive breast cancer, where low pericyte coverage correlated with decreased patient survival. The study showed that depletion in pericytes inhibited tumour growth but lead to formation of defective tumour vasculature and increased metastasis [183].

Therefore, the sustained tumour vascular normalisation concept proposes the idea of restoring the functionality of the vessels in the tumour rather than disrupting them. This approach will improve perfusion and oxygenation and counteract the genes controlling hypoxia driven epithelial-mesenchymal transition and dissemination that would trigger the metastatic switch [196, 197].

9.1.3 What are the mechanisms of action of IL-6 on endothelial cells?

It was important to understand the mechanism involved in inducing this immature vasculature phenotype in the IL-6 treated vessels. MLEC were used to understand the downstream mechanisms involved in inducing IL-6 mediated angiogenesis. My previous studies in chapter 4 on direct downstream VEGF and IL-6 targets suggested a possible differential mechanism of action of IL-6 compared to VEGF. Hence, I was interested in investigating other signalling pathways that were known to be associated with IL-6 signalling. Exploring the regulation of the Notch ligands, Jagged1 and DLL4, indicated a positive regulation of Jagged1 by IL-6 and DLL4 by VEGF in the MLEC. For further confirmation, I investigated the downstream activation of Hey in the presence of VEGF or IL-6 and the positive Notch-DLL4 interaction was confirmed in the VEGF treated MLEC. In terms of future experiments, exploring the regulation of fringe family members which are involved in the glycosylation and activation of Notch-DLL4 signalling would give further validation for mechanism of action of IL-6 and VEGF in MLEC [108, 109].

There has been a lot of debate about the role of these Notch ligands in pericyte differentiation and formation. An earlier study suggested Notch-3 and Jagged1 to be important for differentiation of pericytes [198]. Apart from this finding, the majority of studies have shown endothelial DLL4 to play a critical role in pericyte formation during normal and tumour angiogenesis [142, 186, 199]. Inhibition of DLL4 signalling *in vivo* induced proliferation of immature vessels and resulted in poor tissue perfusion [143]. Even the recent study with the DLL4 inhibitor MEDI0639 in human endothelial cell angiogenesis assay promoted vessel formation with reduced smooth muscle actin positive pericytes [130]. The results obtained from exploring Notch signalling in MLEC after treatment with VEGF or IL-6 fit with the majority of the published data. My results also show a correlation between endothelial DLL4 expression and pericyte coverage in the VEGF treated vessels.

Further exploring the mechanism of action of IL-6 in MLEC led to the investigation of Ang/Tie signalling. Ang2, as previously mentioned, is involved in detaching pericytes from the endothelial cells. Ang2 was also regulated by IL-6 and promoted destabilised vasculature in models of rheumatoid arthritis [184]. My findings showed increased Ang2 expression in the IL-6 treated MLEC as compared to the VEGF treated group. This gave an insight for the possible mechanism of detachment of pericytes from some of the IL-6 treated vessels in the aortic ring assay. This was again an interesting finding in the study because Ang2 expression was shown to correlate with metastasis in various cancers [150].

9.1.4 What is the effect on the ovarian cancer vasculature after treatment with an anti-IL-6 antibody?

The *in vivo* experiments were conducted to study the effects of an anti-IL-6 antibody on pericyte coverage in IGROV-1 xenografts (IGROV-1 cells constitutively produce IL-6). There were very few pericyte-associated vessels in tumours in the IGROV-1 control group. However, treatment with an anti-IL-6 antibody led to a significant increase in pericyte associated vessels suggesting blocking IL-6 in tumours can lead to restoration of normalised vasculature. Immunohistochemistry analysis of Jagged1, DLL4 and Ang-2 in the IGROV-1 control and anti-IL-6 treated tumours showed a regulation of Jagged1 and Ang2 by IL-6. This again correlated with the data from

the previous findings of my lab and also with the results obtained from the MLEC study [35].

However, recent studies by Domcke *et al*, questioned the use of IGROV-1 for further research in HGSCs [200]. This study compared copy number changes, mutations and mRNA expression profiles of 47 ovarian cancer cell lines with the TCGA data. Twelve of these cell lines were defined as 'likely high-grade serous' but some of the commonly used cell lines such as SKOV3, A2780 and IGROV-1 had little profile similarities to high grade serous cancer. IGROV-1 was hypermutated and it clustered more with endometrioid and clear cell ovarian tumours. Therefore, this experiment needs to be repeated with a cell line which is more representative of HGSC [200].

9.1.5 Does this study suggest any possible combination therapy to target with an anti-IL-6 antibody?

The observed differences in the IL-6 and VEGF signalling on endothelial cells further prompted me to study the dependency of IL-6 on VEGF in the aortic ring assay by using a VEGFR inhibitor. The results further confirmed previous finding suggesting IL-6 could induce sprouting in the aortic ring assay in the presence of a VEGFR inhibitor. Further studies into understanding the effects of VEGFR inhibition on endothelial cells showed upregulation of pSTAT3 in the VEGFRi + IL-6 group as compared to the IL-6 treatment alone. This finding was further supported by α-SMA staining of the aortic ring vessels which showed further reduced pericyte coverage in the VEGFRi + IL-6 treated vessels as compared to vessels treated with IL-6 or VEGF alone. This was an interesting finding which indicated the potential for combining an anti-IL-6 agent with a VEGF inhibitor.

Earlier studies looking at biomarker of response and resistance to anti-angiogenic therapies have identified elevated plasma levels of IL-6 after sunitinib treatment to be associated with poor outcome in patients with advanced HCC and renal cell carcinoma [160, 201]. Bevacizumab treatment along with chemoradiotherapy also increased plasma levels of IL-6 in the rectal cancer patients [169]. Alongside this there have been several studies showing the involvement of IL-6 pathway i.e. pSTAT3 in bevacizumab treatment failure in glioblastoma patients [159]. In the

bevacizumab resistant glioblastoma tumours there was a 40% increase in pSTAT3 expression compared to pretreatment samples from the same patients [97]. Moreover, none of these studies have specifically looked at the effects of VEGFR inhibition on IL-6 production by endothelial cells. Hence, findings from these studies along with my preliminary data indicate a potential for combining a VEGFR inhibitor with an anti-IL-6 antibody to target the tumour vasculature.

Therefore, using the IGROV-1 cells I studied the effects of VEGFR inhibition +/- anti-IL-6 antibody on pSTAT3 levels in malignant cells. Surprisingly, VEGFR inhibition decreased the expression of pSTAT3 in the IL-6 producing cell line IGROV-1 and the combination therapy with VEGFRi and anti-IL-6 antibody further reduced pSTAT3 levels. This indicated that VEGFR inhibition has different effects on malignant and endothelial cells in the presence of IL-6.

In summary the *ex vivo*, *in vitro* and *in vivo* studies have shown IL-6 to be a potent angiogenic agent in normal and tumour angiogenesis. However the type of angiogenesis stimulated by IL-6 is aberrant with very few pericytes associated vessels compared to the VEGF induced angiogenesis. Also, IL-6 seems to have differential mechanism of inducing angiogenesis in MLEC as compared to VEGF. The positive regulation of Jagged1 and Ang2 by IL-6 and DLL4 by VEGF could explain the differences in pericyte coverage observed in the IL-6 and VEGF treated vessels. Studies with VEGFR inhibitor on endothelial cells have also suggested the potential for combining anti-VEGF therapies with anti-IL-6 antibodies. However more detailed experiments should be executed to substantiate these findings further and this will be addressed in the future studies section.

A summary of the proposed mechanism of action of IL-6, VEGF and VEGFR inhibitor on endothelial cells is shown in Figure 9.1.

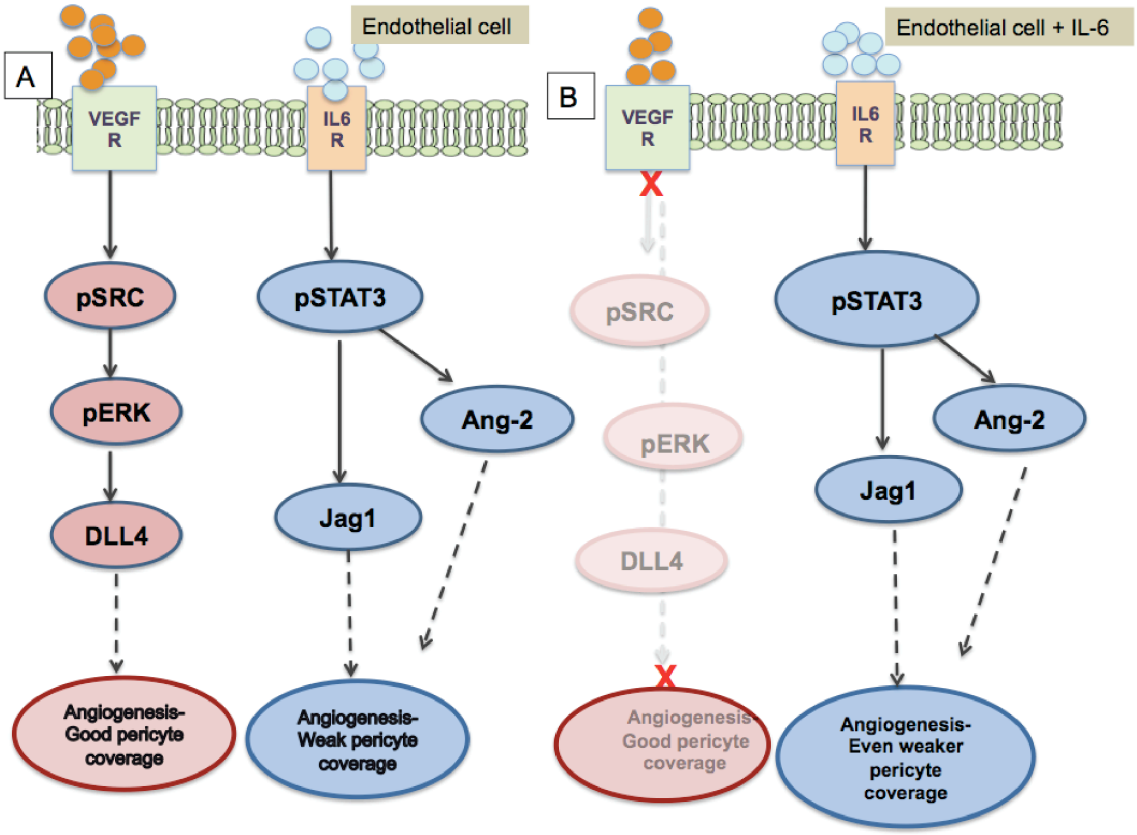

Figure 9.1 Showing the proposed mechanism of action of IL-6, VEGF and VEGFR inhibitor on endothelial cells.

A) VEGFA binding to VEGF receptor leads to upregulation of DLL4 resulting in angiogenesis and maturation of vessels. However, IL-6 forms a complex with IL-6 receptors to activate Jagged1 and Ang2 resulting in angiogenesis with weak or defective pericyte coverage. **B)** VEGF inhibition in the presence of IL-6 leads to further upregulation of pSTAT3 resulting in angiogenesis with even weaker pericyte coverage. - - - -> Outcome

9.2 Future work

There are two main areas of research that I now would like to pursue. First, relates to the angiogenic actions of IL-6 and second on combining IL-6 antagonist with other angiogenic inhibitors in treatment of ovarian cancer.

9.2.1 Effects of IL-6 on angiogenesis

This work will be carried out using the aortic ring assay and *in vitro* MLEC cells.

Aortic ring assay

- VEGF in combination with IL-6

  VEGF treatment led to formation of vessels with good pericyte coverage and IL-6 treatment led to vessels with poor pericyte coverage (refer to chapter 5). Therefore, it would be interesting to study the effects of combining IL-6 and VEGF in the aortic ring assay to investigate if VEGF treatment can restore the pericyte coverage in the presence of IL-6.

- Extract protein from aortas treated with VEGF or IL-6

  Investigations into the mechanism of action of IL-6 and VEGF induced angiogenesis were carried out in MLEC cells, *in vivo* xenografts and in the HGSC dataset (refer to chapter 4,6 and 8). Although it would be technically challenging, analysis of the ligands Jagged1, DLL4 and Ang2 from protein extracted from the aortas would give further validation of the mechanism of action of IL-6 and VEGF.

- Knock down of Jagged1 in the aortic ring assay

Studies into mechanism of action of IL-6 have so far suggested a potential role of Jagged1 mediated angiogenic response. Transient gene silencing with siRNA constructs can be delivered to the aortic ring tissue using oligofectamine transfection [176]. In order to quantify the gene knockdown efficiency, RNA or protein can be extracted from the aortic tissue and the endogenous level of Jagged1 RNA/protein levels could be measured in the different treatment groups. Therefore knockdown of Jagged1 in the aortic ring will provide a means of testing the dependency of IL-6 on Jagged1 in sprouting angiogenesis.

In vitro studies

- IL-6 effects on a pericyte cell line

Vascular membrane matrices are important for endothelial tube stabilisation. Laminin, collagen IV and fibronectin are structural components that facilitate assembly of vascular basement membranes. *In vitro* and *in vivo* studies have shown that pericyte recruitment to endothelial tubes is essential to stimulate vascular basement membrane matrix assembly [202]. Endothelial or pericyte only culture studies have shown little or no deposition of these structural proteins indicating the importance of requirement of both the cell types for the proper assembly of the basement membrane [203]. Therefore, using an *in vitro* 3D endothelial/pericyte co-culture systems I would like to study the effects of IL-6 or VEGF on vascular basement membrane assembly [204].

- IL-6 effects on MLEC

Following on from the previous point, pericyte recruitment to the developing tube and subsequent stabilisation of vascular basement membrane requires effective PDGF-BB and HB-EGF signalling [205]. Therefore, I would like to study the changes in receptor expression in MLEC after treatment with IL-6

or VEGF using the mouse phospho receptor tyrosine kinase array. This is a screening tool designed to detect the relative phosphorylation of 39 different RTKs including the PDGFR, TIE, VEGF, EGFR and so on.

9.2.2 Combination of IL-6 targeting agents with angiogenic inhibitors

In view of my data on the effects of VEGFR inhibitor on endothelial cells, I would combine VEGF/VEGFR inhibitors with anti-IL-6 antibodies in models of ovarian cancer, especially HGSC.

In vivo studies with cediranib and anti-IL-6

- IGROV-1 xenografts or even patient derived xenografts with relevant genetic mutations or relevant cell lines that we now have characterised as HGSC

Patient derived tumours tissues at low passages are biologically stable and reflect the patient tumour with regards to histopathology, gene expression, gene mutations and therapeutic response [206]. IGROV-1 human xenografts models or patient derived tumour tissue with relevant genetic mutations such as P53, PTEN and BRCA would be used for efficacy and toxicity studies with anti-IL-6 and VEGFR inhibitors. These models would also be used to study the tumour vasculature in terms of vessel maturation and pericyte coverage in the different treatment groups i.e. anti-VEGF +/- anti-IL-6.

- Syngeneic models

Syngeneic models involve the use of tumours derived from the same genetic background as the host. The use of syngeneic model will be beneficial to study the effects of the treatment on the tumour microenvironment in immunocompetent mice. Therefore, along with studying the effects of anti-IL-6 and VEGFR inhibition on the tumour vasculature, investigation could

also be carried out to investigate the effects of combination treatment on the leukocyte infiltrate.

In these models it would be interesting to study different treatment schedules of the two agents. There is also a potential of translating to clinical trial because both cediranib (VEGFR inhibitor) and anti-IL-6 have been tested in HGSC patients.

Jak inhibitors instead of anti-IL-6

In vitro and *in vivo* Anti-IL-6 studies in HGSC cell lines have shown inhibition of pSTAT3 levels with a compensatory effect observed in pERK and pEGFR signalling. However, *in vitro* studies with the JAK inhibitors in HGSC cell lines resulted in potent inhibition of pSTAT3 along with inhibition of pERK and pEGFR signalling suggesting no compensatory mechanism with the JAK inhibitors as opposed to the anti-IL-6 antibody (data not shown). Therefore, if *in vitro* combination studies with anti-IL-6 antibody and VEGFR inhibitors in HGSC cell lines show increase in EGFR signalling, I would like to carry out *in vitro* and *in vivo* studies testing the efficacy of combining JAK and VEGF inhibitors.

More in vitro experiments with HGSC cell lines and MLEC

As shown in chapter 8, more mechanistic *in vitro* studies with anti-IL-6 antibody and VEGFR inhibitors would be carried out to study the effects of combination therapy on downstream IL-6 and VEGF signalling i.e. pSTAT3, pVEGFR, pERK. These experiments would be carried out at different time points in more relevant HGSC cell lines. Alongside this, further MLEC studies would be carried out to understand the mechanism of increased pSTAT3 expression in the IL-6 and VEGFRi treated groups at various early time points.

Studies in other cancer types

Ovarian clear cell carcinoma and renal cell carcinoma are also high IL-6 producing tumours. CCCs have a strong IL-6/pSTAT3/HIF-1 signature, which is an independent prognostic factor [207]. Previous studies have indicated an anti-angiogenic effect with anti-IL-6 antibody in ovarian clear cell carcinoma [35]. The *in vivo* anti-IL-6 studies in clear cell carcinoma showed reduction in tumour vasculature with normalisation of blood vessels [35]. Also as previously mentioned, IL-6 was associated with anti-VEGF therapy resistance in renal cell carcinoma [201]. Therefore, it would be interesting to carry out *in vitro* and *in vivo* combination studies with anti-IL-6 and anti-VEGF agents in these clear cell carcinomas where IL-6 have been shown to contribute to either angiogeneis or anti-angiogenic therpay resistance.

10 References

1. Karst, A.M. and R. Drapkin, *The new face of ovarian cancer modeling: better prospects for detection and treatment.* F1000 Med Rep, 2011. **3**: p. 22.
2. Vaughan, S., et al., *Rethinking ovarian cancer: recommendations for improving outcomes.* Nat Rev Cancer, 2011. **11**(10): p. 719-25.
3. Shih Ie, M. and R.J. Kurman, *Ovarian tumorigenesis: a proposed model based on morphological and molecular genetic analysis.* Am J Pathol, 2004. **164**(5): p. 1511-18.
4. Lowery, W.J., et al., *Loss of ARID1A-associated protein expression is a frequent event in clear cell and endometrioid ovarian cancers.* Int J Gynecol Cancer, 2012. **22**(1): p. 9-14.
5. Anglesio, M.S., et al., *IL6-STAT3-HIF signaling and therapeutic response to the angiogenesis inhibitor sunitinib in ovarian clear cell cancer.* Clin Cancer Res, 2011. **17**(8): p. 2538-48.
6. Karst, A.M. and R. Drapkin, *Ovarian cancer pathogenesis: a model in evolution.* J Oncol, 2010. **2010**: p. 1-13.
7. Leinster, D.A., et al., *The peritoneal tumour microenvironment of high-grade serous ovarian cancer.* J Pathol, 2012: p. 1-10.
8. Bell, D.B., A. Birrer,M., *Integrated genomic analyses of ovarian carcinoma.* Nature, 2011. **474**(7353): p. 609-15.
9. Banerjee, S. and M. Gore, *The future of targeted therapies in ovarian cancer.* Oncologist, 2009. **14**(7): p. 706-16.
10. Crum, C.P., *Intercepting pelvic cancer in the distal fallopian tube: theories and realities.* Mol Oncol, 2009. **3**(2): p. 165-70.
11. Kim, J., et al., *High-grade serous ovarian cancer arises from fallopian tube in a mouse model.* Proc Natl Acad Sci U S A, 2012. **109**(10): p. 3921-6.
12. Auersperg, N., *The origin of ovarian cancers--hypotheses and controversies.* Front Biosci (Schol Ed), 2013. **5**: p. 709-19.
13. Kurman, R.J. and M. Shih Ie, *Molecular pathogenesis and extraovarian origin of epithelial ovarian cancer--shifting the paradigm.* Hum Pathol, 2011. **42**(7): p. 918-31.
14. Karst, A.M. and R. Drapkin, *Ovarian cancer pathogenesis: a model in evolution.* J Oncol, 2010. **2010**: p. 932371.
15. Tagawa, T., et al., *Ovarian cancer: opportunity for targeted therapy.* J Oncol, 2012. **2012**: p. 1-9.
16. Callahan, M.J., et al., *Primary fallopian tube malignancies in BRCA-positive women undergoing surgery for ovarian cancer risk reduction.* J Clin Oncol, 2007. **25**(25): p. 3985-90.
17. Kindelberger, D.W., et al., *Intraepithelial carcinoma of the fimbria and pelvic serous carcinoma: Evidence for a causal relationship.* Am J Surg Pathol, 2007. **31**(2): p. 161-9.
18. Kurman, R.J. and M. Shih Ie, *The origin and pathogenesis of epithelial ovarian cancer: a proposed unifying theory.* Am J Surg Pathol, 2010. **34**(3): p. 433-43.
19. Perets, R., et al., *Transformation of the fallopian tube secretory epithelium leads to high-grade serous ovarian cancer in Brca;Tp53;Pten models.* Cancer Cell, 2013. **24**(6): p. 751-65.

20. Pignata, S., et al., *Chemotherapy in epithelial ovarian cancer.* Cancer Lett, 2011. **303**(2): p. 73-83.
21. Berns, E.M. and D.D. Bowtell, *The changing view of high-grade serous ovarian cancer.* Cancer Res, 2012. **72**(11): p. 2701-4.
22. Thomson, E., *Integrated genomic analyses of ovarian carcinoma.* Nature, 2011. **474**(7353): p. 609-15.
23. Yang, D., et al., *Association of BRCA1 and BRCA2 mutations with survival, chemotherapy sensitivity, and gene mutator phenotype in patients with ovarian cancer.* JAMA, 2011. **306**(14): p. 1557-65.
24. Patel, A.G., J.N. Sarkaria, and S.H. Kaufmann, *Nonhomologous end joining drives poly(ADP-ribose) polymerase (PARP) inhibitor lethality in homologous recombination-deficient cells.* Proc Natl Acad Sci U S A, 2011. **108**(8): p. 3406-11.
25. O'Malley, D.M., et al., *Addition of bevacizumab to weekly paclitaxel significantly improves progression-free survival in heavily pretreated recurrent epithelial ovarian cancer.* Gynecol Oncol, 2011. **121**(2): p. 269-72.
26. Coussens, L.M. and Z. Werb, *Inflammation and cancer.* Nature, 2002. **420**(6917): p. 860-7.
27. Naylor, M.S., et al., *Tumor necrosis factor and its receptors in human ovarian cancer. Potential role in disease progression.* J Clin Invest, 1993. **91**(5): p. 2194-206.
28. Kulbe, H., et al., *The inflammatory cytokine tumor necrosis factor-alpha generates an autocrine tumor-promoting network in epithelial ovarian cancer cells.* Cancer Res, 2007. **67**(2): p. 585-92.
29. Kulbe, H., et al., *A dynamic inflammatory cytokine network in the human ovarian cancer microenvironment.* Cancer Res, 2011. **72**(1): p. 66-75.
30. Balkwill, F., *Tumour necrosis factor and cancer.* Nat Rev Cancer, 2009. **9**(5): p. 361-71.
31. Hanahan, D. and R.A. Weinberg, *Hallmarks of cancer: the next generation.* Cell, 2011. **144**(5): p. 646-74.
32. Balkwill, F. and A. Mantovani, *Inflammation and cancer: back to Virchow?* Lancet, 2001. **357**(9255): p. 539-45.
33. Courtois, G. and T.D. Gilmore, *Mutations in the NF-kappaB signaling pathway: implications for human disease.* Oncogene, 2006. **25**(51): p. 6831-43.
34. Mantovani, A., et al., *Cancer-related inflammation.* Nature, 2008. **454**(7203): p. 436-44.
35. Coward, J., et al., *Interleukin-6 as a therapeutic target in human ovarian cancer.* Clin Cancer Res, 2011. **17**(18): p. 6083-96.
36. Naugler, W.E., et al., *Gender disparity in liver cancer due to sex differences in MyD88-dependent IL-6 production.* Science, 2007. **317**(5834): p. 121-4.
37. Hong, D.S., L.S. Angelo, and R. Kurzrock, *Interleukin-6 and its receptor in cancer: implications for Translational Therapeutics.* Cancer, 2007. **110**(9): p. 1911-28.
38. Naka, T., N. Nishimoto, and T. Kishimoto, *The paradigm of IL-6: from basic science to medicine.* Arthritis Res, 2002. **4 Suppl 3**: p. S233-42.
39. Drucker, C., et al., *Impact of interleukin-6 classic- and trans-signaling on liver damage and regeneration.* J Autoimmun, 2010. **34**(1): p. 29-37.

40. Trikha, M., et al., *Targeted anti-interleukin-6 monoclonal antibody therapy for cancer: a review of the rationale and clinical evidence.* Clin Cancer Res, 2003. **9**(13): p. 4653-65.
41. Naugler, W.E. and M. Karin, *The wolf in sheep's clothing: the role of interleukin-6 in immunity, inflammation and cancer.* Trends Mol Med, 2008. **14**(3): p. 109-19.
42. Grivennikov, S.I. and M. Karin, *Inflammatory cytokines in cancer: tumour necrosis factor and interleukin 6 take the stage.* Ann Rheum Dis, 2011. **70 Suppl 1**: p. i104-8.
43. Yang, L., et al., *Interleukin-6 differentially regulates androgen receptor transactivation via PI3K-Akt, STAT3, and MAPK, three distinct signal pathways in prostate cancer cells.* Biochem Biophys Res Commun, 2003. **305**(3): p. 462-9.
44. He, G. and M. Karin, *NF-kappaB and STAT3 - key players in liver inflammation and cancer.* Cell Res, 2011. **21**(1): p. 159-68.
45. Grivennikov, S. and M. Karin, *Autocrine IL-6 signaling: a key event in tumorigenesis?* Cancer Cell, 2008. **13**(1): p. 7-9.
46. Hodge, D.R., E.M. Hurt, and W.L. Farrar, *The role of IL-6 and STAT3 in inflammation and cancer.* Eur J Cancer, 2005. **41**(16): p. 2502-12.
47. Nilsson, M.B., R.R. Langley, and I.J. Fidler, *Interleukin-6, secreted by human ovarian carcinoma cells, is a potent proangiogenic cytokine.* Cancer Res, 2005. **65**(23): p. 10794-800.
48. Shain, K.H., et al., *Beta1 integrin adhesion enhances IL-6-mediated STAT3 signaling in myeloma cells: implications for microenvironment influence on tumor survival and proliferation.* Cancer Res, 2009. **69**(3): p. 1009-15.
49. Nishimoto, N., et al., *Humanized anti-interleukin-6 receptor antibody treatment of multicentric Castleman disease.* Blood, 2005. **106**(8): p. 2627-32.
50. Taniguchi, K. and M. Karin, *IL-6 and related cytokines as the critical lynchpins between inflammation and cancer.* Semin Immunol, 2014. **26**(1): p. 54-74.
51. Yi, H., et al., *Blockade of interleukin-6 receptor suppresses the proliferation of H460 lung cancer stem cells.* Int J Oncol, 2012. **41**(1): p. 310-6.
52. Lin, L., et al., *STAT3 is necessary for proliferation and survival in colon cancer-initiating cells.* Cancer Res, 2011. **71**(23): p. 7226-37.
53. Becker, C., et al., *IL-6 signaling promotes tumor growth in colorectal cancer.* Cell Cycle, 2005. **4**(2): p. 217-20.
54. Becker, C., et al., *TGF-beta suppresses tumor progression in colon cancer by inhibition of IL-6 trans-signaling.* Immunity, 2004. **21**(4): p. 491-501.
55. Thiem, S., et al., *mTORC1 inhibition restricts inflammation-associated gastrointestinal tumorigenesis in mice.* J Clin Invest, 2013. **123**(2): p. 767-81.
56. Musteanu, M., et al., *Stat3 is a negative regulator of intestinal tumor progression in Apc(Min) mice.* Gastroenterology, 2010. **138**(3): p. 1003-11 e1-5.
57. He, G., et al., *Hepatocyte IKKbeta/NF-kappaB inhibits tumor promotion and progression by preventing oxidative stress-driven STAT3 activation.* Cancer Cell, 2010. **17**(3): p. 286-97.
58. Ogata, H., et al., *Deletion of the SOCS3 gene in liver parenchymal cells promotes hepatitis-induced hepatocarcinogenesis.* Gastroenterology, 2006. **131**(1): p. 179-93.
59. Corcoran, R.B., et al., *STAT3 plays a critical role in KRAS-induced pancreatic tumorigenesis.* Cancer Res, 2011. **71**(14): p. 5020-9.

60. Leu, C.M., et al., *Interleukin-6 acts as an antiapoptotic factor in human esophageal carcinoma cells through the activation of both STAT3 and mitogen-activated protein kinase pathways.* Oncogene, 2003. **22**(49): p. 7809-18.
61. Dethlefsen, C., G. Hojfeldt, and P. Hojman, *The role of intratumoral and systemic IL-6 in breast cancer.* Breast Cancer Res Treat, 2013. **138**(3): p. 657-64.
62. Sansone, P., et al., *IL-6 triggers malignant features in mammospheres from human ductal breast carcinoma and normal mammary gland.* J Clin Invest, 2007. **117**(12): p. 3988-4002.
63. Wu, C.T., et al., *Significance of IL-6 in the transition of hormone-resistant prostate cancer and the induction of myeloid-derived suppressor cells.* J Mol Med (Berl), 2012. **90**(11): p. 1343-55.
64. Wallner, L., et al., *Inhibition of interleukin-6 with CNTO328, an anti-interleukin-6 monoclonal antibody, inhibits conversion of androgen-dependent prostate cancer to an androgen-independent phenotype in orchiectomized mice.* Cancer Res, 2006. **66**(6): p. 3087-95.
65. Dorff, T.B., et al., *Clinical and correlative results of SWOG S0354: a phase II trial of CNTO328 (siltuximab), a monoclonal antibody against interleukin-6, in chemotherapy-pretreated patients with castration-resistant prostate cancer.* Clin Cancer Res, 2010. **16**(11): p. 3028-34.
66. Stone, R.L., et al., *Paraneoplastic thrombocytosis in ovarian cancer.* N Engl J Med, 2012. **366**(7): p. 610-18.
67. Sato, T., et al., *Acute anterior uveitis after discontinuation of tocilizumab in a patient with rheumatoid arthritis.* Clin Ophthalmol, 2014. **8**: p. 187-90.
68. Carmeliet, P., *Angiogenesis in health and disease.* Nat Med, 2003. **9**(6): p. 653-60.
69. Risau, W., *Mechanisms of angiogenesis.* Nature, 1997. **386**(6626): p. 671-4.
70. Geudens, I. and H. Gerhardt, *Coordinating cell behaviour during blood vessel formation.* Development, 2011. **138**(21): p. 4569-83.
71. Fakhrejahani, E. and M. Toi, *Tumor angiogenesis: pericytes and maturation are not to be ignored.* J Oncol, 2012. **2012**: p. 1-10.
72. Bikfalvi, A. and R. Bicknell, *Recent advances in angiogenesis, anti-angiogenesis and vascular targeting.* Trends Pharmacol Sci, 2002. **23**(12): p. 576-82.
73. Donnem, T., et al., *Vessel co-option in primary human tumors and metastases: an obstacle to effective anti-angiogenic treatment?* Cancer Med, 2013. **2**(4): p. 427-36.
74. Papetti, M. and I.M. Herman, *Mechanisms of normal and tumor-derived angiogenesis.* Am J Physiol Cell Physiol, 2002. **282**(5): p. C947-70.
75. Hahn, W.C. and R.A. Weinberg, *Rules for making human tumor cells.* N Engl J Med, 2002. **347**(20): p. 1593-603.
76. Hanahan, D. and R.A. Weinberg, *The hallmarks of cancer.* Cell, 2000. **100**(1): p. 57-70.
77. Bergers, G. and L.E. Benjamin, *Tumorigenesis and the angiogenic switch.* Nat Rev Cancer, 2003. **3**(6): p. 401-10.
78. Engerman, R.L., D. Pfaffenbach, and M.D. Davis, *Cell turnover of capillaries.* Lab Invest, 1967. **17**(6): p. 738-43.
79. Carmeliet, P. and R.K. Jain, *Angiogenesis in cancer and other diseases.* Nature, 2000. **407**(6801): p. 249-57.

80. Hanahan, D. and J. Folkman, *Patterns and emerging mechanisms of the angiogenic switch during tumorigenesis.* Cell, 1996. **86**(3): p. 353-64.
81. Benjamin, L.E., et al., *Selective ablation of immature blood vessels in established human tumors follows vascular endothelial growth factor withdrawal.* J Clin Invest, 1999. **103**(2): p. 159-65.
82. Morikawa, S., et al., *Abnormalities in pericytes on blood vessels and endothelial sprouts in tumors.* Am J Pathol, 2002. **160**(3): p. 985-1000.
83. Ferrara, N., H.P. Gerber, and J. LeCouter, *The biology of VEGF and its receptors.* Nat Med, 2003. **9**(6): p. 669-76.
84. Olsson, A.K., et al., *VEGF receptor signalling - in control of vascular function.* Nat Rev Mol Cell Biol, 2006. **7**(5): p. 359-71.
85. Neufeld, G., et al., *Vascular endothelial growth factor (VEGF) and its receptors.* FASEB J, 1999. **13**(1): p. 9-22.
86. Dixelius, J., et al., *Ligand-induced vascular endothelial growth factor receptor-3 (VEGFR-3) heterodimerization with VEGFR-2 in primary lymphatic endothelial cells regulates tyrosine phosphorylation sites.* J Biol Chem, 2003. **278**(42): p. 40973-9.
87. Zeng, H., H.F. Dvorak, and D. Mukhopadhyay, *Vascular permeability factor (VPF)/vascular endothelial growth factor (VEGF) peceptor-1 down-modulates VPF/VEGF receptor-2-mediated endothelial cell proliferation, but not migration, through phosphatidylinositol 3-kinase-dependent pathways.* J Biol Chem, 2001. **276**(29): p. 26969-79.
88. Autiero, M., et al., *Role of PlGF in the intra- and intermolecular cross talk between the VEGF receptors Flt1 and Flk1.* Nat Med, 2003. **9**(7): p. 936-43.
89. Ellis, L.M. and D.J. Hicklin, *VEGF-targeted therapy: mechanisms of anti-tumour activity.* Nat Rev Cancer, 2008. **8**(8): p. 579-91.
90. Hurwitz, H., et al., *Bevacizumab plus irinotecan, fluorouracil, and leucovorin for metastatic colorectal cancer.* N Engl J Med, 2004. **350**(23): p. 2335-42.
91. Sandler, A., et al., *Paclitaxel-carboplatin alone or with bevacizumab for non-small-cell lung cancer.* N Engl J Med, 2006. **355**(24): p. 2542-50.
92. Welti, J., et al., *Recent molecular discoveries in angiogenesis and antiangiogenic therapies in cancer.* J Clin Invest, 2013. **123**(8): p. 3190-200.
93. Kopetz, S., et al., *Phase II trial of infusional fluorouracil, irinotecan, and bevacizumab for metastatic colorectal cancer: efficacy and circulating angiogenic biomarkers associated with therapeutic resistance.* J Clin Oncol, 2010. **28**(3): p. 453-9.
94. Kienast, Y., et al., *Real-time imaging reveals the single steps of brain metastasis formation.* Nat Med, 2010. **16**(1): p. 116-22.
95. Li, J.L., et al., *DLL4-Notch signaling mediates tumor resistance to anti-VEGF therapy in vivo.* Cancer Res, 2011. **71**(18): p. 6073-83.
96. Beck, B., et al., *A vascular niche and a VEGF-Nrp1 loop regulate the initiation and stemness of skin tumours.* Nature, 2011. **478**(7369): p. 399-403.
97. Jahangiri, A., et al., *Gene expression profile identifies tyrosine kinase c-Met as a targetable mediator of antiangiogenic therapy resistance.* Clin Cancer Res, 2013. **19**(7): p. 1773-83.
98. You, W.K., et al., *VEGF and c-Met blockade amplify angiogenesis inhibition in pancreatic islet cancer.* Cancer Res, 2011. **71**(14): p. 4758-68.

99. Sennino, B., et al., *Suppression of tumor invasion and metastasis by concurrent inhibition of c-Met and VEGF signaling in pancreatic neuroendocrine tumors.* Cancer Discov, 2012. **2**(3): p. 270-87.
100. Lobry, C., P. Oh, and I. Aifantis, *Oncogenic and tumor suppressor functions of Notch in cancer: it's NOTCH what you think.* J Exp Med, 2011. **208**(10): p. 1931-5.
101. Guruharsha, K.G., M.W. Kankel, and S. Artavanis-Tsakonas, *The Notch signalling system: recent insights into the complexity of a conserved pathway.* Nat Rev Genet, 2012. **13**(9): p. 654-66.
102. Kerbel, R.S., *Tumor angiogenesis.* N Engl J Med, 2008. **358**(19): p. 2039-49.
103. Ranganathan, P., K.L. Weaver, and A.J. Capobianco, *Notch signalling in solid tumours: a little bit of everything but not all the time.* Nat Rev Cancer, 2011. **11**(5): p. 338-51.
104. Andersen, P., et al., *Non-canonical Notch signaling: emerging role and mechanism.* Trends Cell Biol, 2012. **22**(5): p. 257-65.
105. Heitzler, P., *Biodiversity and noncanonical Notch signaling.* Curr Top Dev Biol, 2010. **92**: p. 457-81.
106. D'Souza, B., A. Miyamoto, and G. Weinmaster, *The many facets of Notch ligands.* Oncogene, 2008. **27**(38): p. 5148-67.
107. Kume, T., *Novel insights into the differential functions of Notch ligands in vascular formation.* J Angiogenes Res, 2009. **1**: p. 8.
108. Blanco, R. and H. Gerhardt, *VEGF and Notch in tip and stalk cell selection.* Cold Spring Harb Perspect Med, 2013. **3**(1): p. a006569.
109. Benedito, R., et al., *The notch ligands Dll4 and Jagged1 have opposing effects on angiogenesis.* Cell, 2009. **137**(6): p. 1124-35.
110. Holderfield, M.T. and C.C. Hughes, *Crosstalk between vascular endothelial growth factor, notch, and transforming growth factor-beta in vascular morphogenesis.* Circ Res, 2008. **102**(6): p. 637-52.
111. Demarest, R.M., F. Ratti, and A.J. Capobianco, *It's T-ALL about Notch.* Oncogene, 2008. **27**(38): p. 5082-91.
112. Xu, X., et al., *Activation of Notch signal pathway is associated with a poorer prognosis in acute myeloid leukemia.* Med Oncol, 2011. **28 Suppl 1**: p. S483-9.
113. Jin, S., et al., *Non-canonical Notch signaling activates IL-6/JAK/STAT signaling in breast tumor cells and is controlled by p53 and IKKalpha/IKKbeta.* Oncogene, 2013. **32**(41): p. 4892-902.
114. Konishi, J., et al., *Notch3 cooperates with the EGFR pathway to modulate apoptosis through the induction of bim.* Oncogene, 2010. **29**(4): p. 589-96.
115. Donnem, T., et al., *Prognostic impact of Notch ligands and receptors in nonsmall cell lung cancer: coexpression of Notch-1 and vascular endothelial growth factor-A predicts poor survival.* Cancer, 2010. **116**(24): p. 5676-85.
116. Purow, B.W., et al., *Expression of Notch-1 and its ligands, Delta-like-1 and Jagged-1, is critical for glioma cell survival and proliferation.* Cancer Res, 2005. **65**(6): p. 2353-63.
117. Li, J., et al., *Notch1 is an independent prognostic factor for patients with glioma.* J Surg Oncol, 2011. **103**(8): p. 813-7.
118. Santagata, S., et al., *JAGGED1 expression is associated with prostate cancer metastasis and recurrence.* Cancer Res, 2004. **64**(19): p. 6854-7.
119. Wang, Z., et al., *Down-regulation of Notch-1 and Jagged-1 inhibits prostate cancer cell growth, migration and invasion, and induces apoptosis via*

inactivation of Akt, mTOR, and NF-kappaB signaling pathways. J Cell Biochem, 2010. **109**(4): p. 726-36.
120. McAuliffe, S.M., et al., *Targeting Notch, a key pathway for ovarian cancer stem cells, sensitizes tumors to platinum therapy.* Proc Natl Acad Sci U S A, 2012. **109**(43): p. E2939-48.
121. South, A.P., R.J. Cho, and J.C. Aster, *The double-edged sword of Notch signaling in cancer.* Semin Cell Dev Biol, 2012. **23**(4): p. 458-64.
122. Egloff, A.M. and J.R. Grandis, *Molecular pathways: context-dependent approaches to Notch targeting as cancer therapy.* Clin Cancer Res, 2012. **18**(19): p. 5188-95.
123. Mizuma, M., et al., *The gamma secretase inhibitor MRK-003 attenuates pancreatic cancer growth in preclinical models.* Mol Cancer Ther, 2012. **11**(9): p. 1999-2009.
124. Kondratyev, M., et al., *Gamma-secretase inhibitors target tumor-initiating cells in a mouse model of ERBB2 breast cancer.* Oncogene, 2012. **31**(1): p. 93-103.
125. Maraver, A., et al., *Therapeutic effect of gamma-secretase inhibition in KrasG12V-driven non-small cell lung carcinoma by derepression of DUSP1 and inhibition of ERK.* Cancer Cell, 2012. **22**(2): p. 222-34.
126. Capaccione, K.M. and S.R. Pine, *The Notch signaling pathway as a mediator of tumor survival.* Carcinogenesis, 2013. **34**(7): p. 1420-30.
127. Strosberg, J.R., et al., *A phase II study of RO4929097 in metastatic colorectal cancer.* Eur J Cancer, 2012. **48**(7): p. 997-1003.
128. Wu, Y., et al., *Therapeutic antibody targeting of individual Notch receptors.* Nature, 2010. **464**(7291): p. 1052-7.
129. Kuhnert, F., J.R. Kirshner, and G. Thurston, *Dll4-Notch signaling as a therapeutic target in tumor angiogenesis.* Vasc Cell, 2011. **3**(1): p. 20.
130. Jenkins, D.W., et al., *MEDI0639: a novel therapeutic antibody targeting Dll4 modulates endothelial cell function and angiogenesis in vivo.* Mol Cancer Ther, 2012. **11**(8): p. 1650-60.
131. Liu, S.K., et al., *Delta-like ligand 4-notch blockade and tumor radiation response.* J Natl Cancer Inst, 2011. **103**(23): p. 1778-98.
132. Espinoza, I. and L. Miele, *Notch inhibitors for cancer treatment.* Pharmacol Ther, 2013. **139**(2): p. 95-110.
133. Ribatti, D., B. Nico, and E. Crivellato, *The role of pericytes in angiogenesis.* Int J Dev Biol, 2011. **55**(3): p. 261-8.
134. Armulik, A., G. Genove, and C. Betsholtz, *Pericytes: developmental, physiological, and pathological perspectives, problems, and promises.* Dev Cell, 2011. **21**(2): p. 193-215.
135. Bergers, G. and S. Song, *The role of pericytes in blood-vessel formation and maintenance.* Neuro Oncol, 2005. **7**(4): p. 452-64.
136. Armulik, A., A. Abramsson, and C. Betsholtz, *Endothelial/pericyte interactions.* Circ Res, 2005. **97**(6): p. 512-23.
137. Balabanov, R. and P. Dore-Duffy, *Role of the CNS microvascular pericyte in the blood-brain barrier.* J Neurosci Res, 1998. **53**(6): p. 637-44.
138. Gerhardt, H. and H. Semb, *Pericytes: gatekeepers in tumour cell metastasis?* J Mol Med (Berl), 2008. **86**(2): p. 135-44.
139. Paik, J.H., et al., *Sphingosine 1-phosphate receptor regulation of N-cadherin mediates vascular stabilization.* Genes Dev, 2004. **18**(19): p. 2392-403.

140. Tillet, E., et al., *N-cadherin deficiency impairs pericyte recruitment, and not endothelial differentiation or sprouting, in embryonic stem cell-derived angiogenesis.* Exp Cell Res, 2005. **310**(2): p. 392-400.
141. Manderfield, L.J., et al., *Notch activation of Jagged1 contributes to the assembly of the arterial wall.* Circulation, 2012. **125**(2): p. 314-23.
142. Patel, N.S., et al., *Up-regulation of endothelial delta-like 4 expression correlates with vessel maturation in bladder cancer.* Clin Cancer Res, 2006. **12**(16): p. 4836-44.
143. Scehnet, J.S., et al., *Inhibition of Dll4-mediated signaling induces proliferation of immature vessels and results in poor tissue perfusion.* Blood, 2007. **109**(11): p. 4753-60.
144. Helfrich, I., et al., *Resistance to antiangiogenic therapy is directed by vascular phenotype, vessel stabilization, and maturation in malignant melanoma.* J Exp Med, 2010. **207**(3): p. 491-503.
145. Baranowska-Kortylewicz, J., et al., *Effect of platelet-derived growth factor receptor-beta inhibition with STI571 on radioimmunotherapy.* Cancer Res, 2005. **65**(17): p. 7824-31.
146. Bergers, G., et al., *Benefits of targeting both pericytes and endothelial cells in the tumor vasculature with kinase inhibitors.* J Clin Invest, 2003. **111**(9): p. 1287-95.
147. Hainsworth, J.D., et al., *Treatment of advanced renal cell carcinoma with the combination bevacizumab/erlotinib/imatinib: a phase I/II trial.* Clin Genitourin Cancer, 2007. **5**(7): p. 427-32.
148. Erber, R., et al., *Combined inhibition of VEGF and PDGF signaling enforces tumor vessel regression by interfering with pericyte-mediated endothelial cell survival mechanisms.* FASEB J, 2004. **18**(2): p. 338-40.
149. Karlan, B.Y., et al., *Randomized, double-blind, placebo-controlled phase II study of AMG 386 combined with weekly paclitaxel in patients with recurrent ovarian cancer.* J Clin Oncol, 2012. **30**(4): p. 362-71.
150. Minami Y, S.T., Kawabe J, Ohsaki Y, *Accessory Cells in Tumor Angiogenesis — Tumor-Associated Pericytes*. 2013: Research Directions in Tumour Angiogenesis.
151. Nisancioglu, M.H., C. Betsholtz, and G. Genove, *The absence of pericytes does not increase the sensitivity of tumor vasculature to vascular endothelial growth factor-A blockade.* Cancer Res, 2010. **70**(12): p. 5109-15.
152. Lind, A.J., et al., *Angiopoietin 2 expression is related to histological grade, vascular density, metastases, and outcome in prostate cancer.* Prostate, 2005. **62**(4): p. 394-9.
153. Huang, H., et al., *Specifically targeting angiopoietin-2 inhibits angiogenesis, Tie2-expressing monocyte infiltration, and tumor growth.* Clin Cancer Res, 2011. **17**(5): p. 1001-11.
154. Mazzieri, R., et al., *Targeting the ANG2/TIE2 axis inhibits tumor growth and metastasis by impairing angiogenesis and disabling rebounds of proangiogenic myeloid cells.* Cancer Cell, 2011. **19**(4): p. 512-26.
155. Chae, S.S., et al., *Angiopoietin-2 interferes with anti-VEGFR2-induced vessel normalization and survival benefit in mice bearing gliomas.* Clin Cancer Res, 2010. **16**(14): p. 3618-27.

156. Ochiumi, T., et al., *Clinical significance of angiopoietin-2 expression at the deepest invasive tumor site of advanced colorectal carcinoma.* Int J Oncol, 2004. **24**(3): p. 539-47.
157. Hata, K., et al., *Expression of the angopoietin-1, angopoietin-2, Tie2, and vascular endothelial growth factor gene in epithelial ovarian cancer.* Gynecol Oncol, 2004. **93**(1): p. 215-22.
158. Brown, J.L., et al., *A human monoclonal anti-ANG2 antibody leads to broad antitumor activity in combination with VEGF inhibitors and chemotherapy agents in preclinical models.* Mol Cancer Ther, 2010. **9**(1): p. 145-56.
159. de Groot, J., et al., *Modulating antiangiogenic resistance by inhibiting the signal transducer and activator of transcription 3 pathway in glioblastoma.* Oncotarget, 2012. **3**(9): p. 1036-48.
160. Zhu, A.X., et al., *Efficacy, safety, and potential biomarkers of sunitinib monotherapy in advanced hepatocellular carcinoma: a phase II study.* J Clin Oncol, 2009. **27**(18): p. 3027-35.
161. Lo, C.W., et al., *IL-6 trans-signaling in formation and progression of malignant ascites in ovarian cancer.* Cancer Res. **71**(2): p. 424-34.
162. Podor, T.J., et al., *Human endothelial cells produce IL-6. Lack of responses to exogenous IL-6.* Ann N Y Acad Sci, 1989. **557**: p. 374-85; discussion 386-7.
163. Yao, J.S., et al., *Interleukin-6 triggers human cerebral endothelial cells proliferation and migration: the role for KDR and MMP-9.* Biochem Biophys Res Commun, 2006. **342**(4): p. 1396-404.
164. Fan, Y., et al., *Interleukin-6 stimulates circulating blood-derived endothelial progenitor cell angiogenesis in vitro.* J Cereb Blood Flow Metab, 2008. **28**(1): p. 90-8.
165. Cohen, T., et al., *Interleukin 6 induces the expression of vascular endothelial growth factor.* J Biol Chem, 1996. **271**(2): p. 736-41.
166. Angelo, L.S. and R. Kurzrock, *Vascular endothelial growth factor and its relationship to inflammatory mediators.* Clin Cancer Res, 2007. **13**(10): p. 2825-30.
167. Xu, Q., et al., *Targeting Stat3 blocks both HIF-1 and VEGF expression induced by multiple oncogenic growth signaling pathways.* Oncogene, 2005. **24**(36): p. 5552-60.
168. Kwon, K.A., et al., *Clinical significance of preoperative serum vascular endothelial growth factor, interleukin-6, and C-reactive protein level in colorectal cancer.* BMC Cancer, 2010. **10**: p. 203.
169. Willett, C.G., et al., *Efficacy, safety, and biomarkers of neoadjuvant bevacizumab, radiation therapy, and fluorouracil in rectal cancer: a multidisciplinary phase II study.* J Clin Oncol, 2009. **27**(18): p. 3020-6.
170. Feurino, L.W., et al., *IL-6 stimulates Th2 type cytokine secretion and upregulates VEGF and NRP-1 expression in pancreatic cancer cells.* Cancer Biol Ther, 2007. **6**(7): p. 1096-100.
171. Wei, L.H., et al., *Interleukin-6 promotes cervical tumor growth by VEGF-dependent angiogenesis via a STAT3 pathway.* Oncogene, 2003. **22**(10): p. 1517-27.
172. Porta, C., et al., *Changes in circulating pro-angiogenic cytokines, other than VEGF, before progression to sunitinib therapy in advanced renal cell carcinoma patients.* Oncology, 2013. **84**(2): p. 115-22.

173. Jat, P.S., et al., *Direct derivation of conditionally immortal cell lines from an H-2Kb-tsA58 transgenic mouse.* Proc Natl Acad Sci U S A, 1991. **88**(12): p. 5096-100.
174. D'Amico, G., et al., *Endothelial-Rac1 is not required for tumor angiogenesis unless alphavbeta3-integrin is absent.* PLoS One, 2010. **5**(3): p. e9766.
175. Nicosia, R.F., et al., *Paracrine regulation of angiogenesis by different cell types in the aorta ring model.* Int J Dev Biol, 2012. **55**(4-5): p. 447-53.
176. Baker, M., et al., *Use of the mouse aortic ring assay to study angiogenesis.* Nat Protoc, 2012. **7**(1): p. 89-104.
177. Nicosia, R.F., *The aortic ring model of angiogenesis: a quarter century of search and discovery.* J Cell Mol Med, 2009. **13**(10): p. 4113-36.
178. Gerhardt, H., et al., *VEGF guides angiogenic sprouting utilizing endothelial tip cell filopodia.* J Cell Biol, 2003. **161**(6): p. 1163-77.
179. Rymo, S.F., et al., *A two-way communication between microglial cells and angiogenic sprouts regulates angiogenesis in aortic ring cultures.* PLoS One, 2011. **6**(1): p. e15846.
180. Suzuki, Y., et al., *Transforming growth factor-beta induces vascular endothelial growth factor-C expression leading to lymphangiogenesis in rat unilateral ureteral obstruction.* Kidney Int, 2012. **81**(9): p. 865-79.
181. Kalishwaralal, K., et al., *Silver nanoparticles inhibit VEGF induced cell proliferation and migration in bovine retinal endothelial cells.* Colloids Surf B Biointerfaces, 2009. **73**(1): p. 51-7.
182. Xian, X., et al., *Pericytes limit tumor cell metastasis.* J Clin Invest, 2006. **116**(3): p. 642-51.
183. Cooke, V.G., et al., *Pericyte depletion results in hypoxia-associated epithelial-to-mesenchymal transition and metastasis mediated by met signaling pathway.* Cancer Cell, 2012. **21**(1): p. 66-81.
184. Kayakabe, K., et al., *Interleukin-6 promotes destabilized angiogenesis by modulating angiopoietin expression in rheumatoid arthritis.* Rheumatology (Oxford), 2012. **53**(299): p. 1-9.
185. Kulbe, H., et al., *A dynamic inflammatory cytokine network in the human ovarian cancer microenvironment.* Cancer Res, 2012. **72**(1): p. 66-75.
186. Schadler, K.L., et al., *Delta-like ligand 4 plays a critical role in pericyte/vascular smooth muscle cell formation during vasculogenesis and tumor vessel expansion in Ewing's sarcoma.* Clin Cancer Res, 2010. **16**(3): p. 848-56.
187. Gerhardt, H., *VEGF and endothelial guidance in angiogenic sprouting.* Organogenesis, 2008. **4**(4): p. 241-6.
188. Gerhardt, H., H. Wolburg, and C. Redies, *N-cadherin mediates pericytic-endothelial interaction during brain angiogenesis in the chicken.* Dev Dyn, 2000. **218**(3): p. 472-9.
189. Ledermann, J.A., *Randomised double-blind phase III trial of cediranib (AZD 2171) in relapsed platinum sensitive ovarian cancer: results of the ICON6 trial [abstract].* NCRO Cancer Conference,Liverpool, UK, 2013.
190. Sen, B., et al., *Sustained Src inhibition results in signal transducer and activator of transcription 3 (STAT3) activation and cancer cell survival via altered Janus-activated kinase-STAT3 binding.* Cancer Res, 2009. **69**(5): p. 1958-65.
191. McDonald, D.M. and P. Baluk, *Significance of blood vessel leakiness in cancer.* Cancer Res, 2002. **62**(18): p. 5381-5.

192. Dudley, A.C., *Tumor endothelial cells.* Cold Spring Harb Perspect Med, 2012. **2**(3): p. a006536.
193. Wang, X., et al., *Endothelial cells enhance prostate cancer metastasis via IL-6-->androgen receptor-->TGF-beta-->MMP-9 signals.* Mol Cancer Ther, 2013. **12**(6): p. 1026-37.
194. Richardson, W.D., et al., *NG2-glia as multipotent neural stem cells: fact or fantasy?* Neuron, 2011. **70**(4): p. 661-73.
195. Gertz, K., et al., *Essential role of interleukin-6 in post-stroke angiogenesis.* Brain, 2012. **135**(Pt 6): p. 1964-80.
196. Goel, S., et al., *Normalization of the vasculature for treatment of cancer and other diseases.* Physiol Rev, 2011. **91**(3): p. 1071-121.
197. Potente, M., H. Gerhardt, and P. Carmeliet, *Basic and therapeutic aspects of angiogenesis.* Cell, 2011. **146**(6): p. 873-87.
198. Liu, H., S. Kennard, and B. Lilly, *NOTCH3 expression is induced in mural cells through an autoregulatory loop that requires endothelial-expressed JAGGED1.* Circ Res, 2009. **104**(4): p. 466-75.
199. Cappellari, O., et al., *Dll4 and PDGF-BB convert committed skeletal myoblasts to pericytes without erasing their myogenic memory.* Dev Cell, 2013. **24**(6): p. 586-99.
200. Domcke, S., et al., *Evaluating cell lines as tumour models by comparison of genomic profiles.* Nat Commun, 2013. **4**: p. 2126.
201. Jain, R.K., et al., *Biomarkers of response and resistance to antiangiogenic therapy.* Nat Rev Clin Oncol, 2009. **6**(6): p. 327-38.
202. Stratman, A.N. and G.E. Davis, *Endothelial cell-pericyte interactions stimulate basement membrane matrix assembly: influence on vascular tube remodeling, maturation, and stabilization.* Microsc Microanal, 2012. **18**(1): p. 68-80.
203. Stratman, A.N., et al., *Pericyte recruitment during vasculogenic tube assembly stimulates endothelial basement membrane matrix formation.* Blood, 2009. **114**(24): p. 5091-101.
204. Waters, J.P., et al., *In vitro self-assembly of human pericyte-supported endothelial microvessels in three-dimensional coculture: a simple model for interrogating endothelial-pericyte interactions.* J Vasc Res, 2013. **50**(4): p. 324-31.
205. Stratman, A.N., et al., *Endothelial-derived PDGF-BB and HB-EGF coordinately regulate pericyte recruitment during vasculogenic tube assembly and stabilization.* Blood, 2010. **116**(22): p. 4720-30.
206. Scott, C.L., et al., *Patient-derived xenograft models to improve targeted therapy in epithelial ovarian cancer treatment.* Front Oncol, 2013. **3**: p. 295.
207. Cuadros, T., et al., *HAVCR/KIM-1 activates the IL-6/STAT-3 pathway in clear cell renal cell carcinoma and determines tumor progression and patient outcome.* Cancer Res, 2014. **74**(5): p. 1416-28.

1.